

Oil & Natural Gas Technology

DOE Award No.: DE-FE0005975

Final Research Performance Progress Report (Period ending 04/01/2013)

Measuring Fracture Density and Orientation in Unconventional Reservoirs Using Simple-Source Vertical Seismic Profiles

Project Period (February 2011 to April 2013)

Submitted by:
Bob A. Hardage

Signature

Bureau of Economic Geology
DUNS #:170230239
10100 Burnet Road
Austin, Texas 78758
e-mail: Bob.hardage@beg.utexas.edu
Phone number: (512) 471-0300

Prepared for:
United States Department of Energy
National Energy Technology Laboratory

Submission date: March, 2013



Office of Fossil Energy

Disclaimer

This report was prepared as an account of work sponsored by an agency of the United States Government. Neither the United States Government nor any agency thereof, nor any of their employees, makes any warranty, express or implied, or assumes any legal liability or responsibility for the accuracy, completeness, or usefulness of any information, apparatus, product, or process disclosed, or represents that its use would not infringe privately owned rights. Reference herein to any specific commercial product, process, or service by trade name, trademark, manufacturer, or otherwise does not necessarily constitute or imply its endorsement, recommendation, or favoring by the United States Government or any agency thereof. The views and opinions of authors expressed herein do not necessarily state or reflect those of the United States Government or any agency thereof.

Table of Contents

List of Figures	4
Abstract.....	6
Executive Summary	8
Chapter 1. Vertical-Force Sources and Direct-S Waves	10
Introduction	10
Vertical-Vibrator Sources and SV Shear Modes	10
Alford Rotation	15
Overview of Study Sites	16
Conclusions	17
Chapter 2. Data Processing	19
Introduction	19
Determining Natural Coordinates.....	19
Alford Rotation	21
S-Wave Splitting, Natural Coordinates, and Fracture Orientation	23
Orthogonal S-Wave Displacements	25
S-Wave Splitting and Fracture Density	27
Fracture Illumination	28
Transforming VSP Data to Wave-Mode Data	30
Removing Overburden Travel Time Differences.....	31
Improving Alford Rotation Accuracy with Gaussian Wavelets.....	33
Natural Coordinates within the Overburden	36
Estimating Fracture Attributes.....	37
Data Window Effects in Calculating S-Wave Anisotropy.....	44
Interpreting Alford Rotation Results	45
Conclusions	46
Chapter 3. VSP Analysis 1 – Marcellus Shale Prospect	48
Introduction	48
VSP Source-Receiver Geometry	48
Stratigraphy.....	50
Calibration Database	50
Examples of Raw Unprocessed VSP Data	52
Examples of Processed VSP Data.....	54
S-Wave Anisotropy and Fracture Density.....	59
Direct-Mode Velocities and Stress Directions	61
Conclusions	63
Chapter 4. VSP Analysis 2 – Tight Sandstone Prospect.....	64
Introduction	64

VSP Source-Receiver Geometry	64
Stratigraphy.....	65
Calibration Database	66
Examples of Raw Unprocessed VSP Data	67
Examples of Processed VSP Data.....	68
Redundancy Check.....	70
Non-Orthogonal Source Stations	77
Comparison with Calibration Data.....	81
Conclusions	82
Chapter 5. Concluding Remarks and Recommendations	83
Introduction	83
Observations.....	84
Recommendations	85
References	87
Glossary.....	90
Appendix A: Comparison of Direct-S Modes.....	91
Appendix B: VSP S-S Imaging with Vertical Vibrators	114

List of Figures

Figure 1.1. Vertical-force sources and direct SV radiation patterns	12
Figure 1.2. Map showing VSP study sites.....	16
Figure 2.1. Data coordinates.....	20
Figure 2.2. Alford rotation matrix.....	21
Figure 2.3. Application of Alford rotation	22
Figure 2.4. Laboratory measurement of S-wave splitting in fractures	24
Figure 2.5. Illuminating targets with orthogonal S vectors.....	26
Figure 2.6. Slow-S mode and fracture density	28
Figure 2.7. VSP source-receiver geometry	29
Figure 2.8. Orientation of VSP receivers.....	30
Figure 2.9. Example of direct-S wavefields.....	32
Figure 2.10. Generalized Gaussian wavelet	34
Figure 2.11. Replacing direct arrivals with Gaussian wavelets	35
Figure 2.12. Alford rotation of VSP data at receiver station 80	36
Figure 2.13. Alford rotation of VSP data at receiver station 60	37
Figure 2.14. Alford rotation of VSP data at receiver station 40	38
Figure 2.15. Alford rotation of VSP data at receiver station 20	38
Figure 2.16. Alford rotation of VSP data at receiver station 1	39
Figure 2.17. Display format used to illustrate data analyses.....	40
Figure 2.18. Expanded views of each term of Alford rotation.....	42, 43
Figure 2.19. Influence of window length on Alford rotation	45
Figure 3.1. Walk-around source stations	49
Figure 3.2. Positions of downhole receivers	49
Figure 3.3. Middle Devonian stratigraphy	50
Figure 3.4. Calibration well logs.....	51
Figure 3.5. Responses of vertical geophones.....	52
Figure 3.6. Responses of radial geophones	53
Figure 3.7. Responses of transverse geophones	53
Figure 3.8. Expanded views of direct-S modes.....	55
Figure 3.9.. Direct-P and direct-S modes.....	57
Figure 3.10. Average P-wave velocities.....	58
Figure 3.11. Average S-wave velocities.....	58
Figure 3.12. Polar plots of S velocities.....	59
Figure 3.13. S-wave anisotropy	60
Figure 3.14. Polar plot of S-wave anisotropy	61
Figure 3.15. Structure maps of Marcellus Shale	62
Figure 4.1. Source station geometry.....	65
Figure 4.2. Generalized stratigraphic column	66

Figure 4.3. VSP data produced at source station C	67
Figure 4.4. Map of source stations A and E	69
Figure 4.5. Map of source stations C and D	71
Figure 4.6. Direct-S modes from source stations C and D	72
Figure 4.7. Alford rotation of VSP data at receiver station 80	73
Figure 4.8. Alford rotation of VSP data at receiver station 60	74
Figure 4.9. Alford rotation of VSP data at receiver station 40	74
Figure 4.10. Alford rotation of VSP data at receiver station 20	75
Figure 4.11. Alford rotation of VSP data at receiver station 1	75
Figure 4.12. S-wave anisotropy for source stations C and D	76
Figure 4.13. Volumetric picture of S-wave anisotropy	77
Figure 4.14. Direct-S modes from stations B and DD	79
Figure 4.15. Alford rotation at receiver station 1	80
Figure 4.16. S-wave anisotropy for source stations B and DD	80
Figure 4.17. Comparison of anisotropy estimates	81

Appendix A

Figure 1. Maps of Devine Test Site	93
Figure 2. Well logs from Devine Test Site	94
Figure 3. VSP source-receiver geometry used at Devine Test Site	95
Figure 4. Map view of azimuth orientations of horizontal vibrator	97
Figure 5. Photo of horizontal vibrator	97
Figure 6. P and SV radiation from vertical-force source	98
Figure 7. Orienting VSP geophones to P, SR, and ST data space	101
Figure 8. Examples of test data	102
Figure 9. SR data from vertical and horizontal vibrators	105
Figure 10. ST data from vertical and horizontal vibrators	106
Figure 11. Overlays of direct-S data	107
Figure 12. SR and ST radiation patterns measured with test data	108
Figure 13. SR and ST radiation patterns measured by others	109

Appendix B

Figure 1. Long Offset VSP data	115
Figure 2. VSP transverse-S wavefield	116
Figure 3. Upgoing VSP transverse-S events	118
Figure 4. VSP transverse-S image	118

Abstract

The basic objective of this study was to demonstrate an easier and lower cost way to acquire shear (S) waves in vertical seismic profiling (VSP) programs. Our focus was to show the value of S waves produced directly at the point where a vertical vibrator applies its force vector to the earth. These shear modes will be referred to as **direct-S** waves to distinguish them from converted-S modes produced by downgoing compressional (**P**) waves at subsurface interfaces remote from a surface-source station. Converted-S modes generated at deep interfaces by energy exchange from P waves will be termed **P-SV** modes in this report.

There is strong interest in developing lower cost and more widely available S-wave VSP seismic sources because S-wave seismic data provide valuable fracture and stress information that is difficult, often impossible, to extract from P-wave data. Thus the generation of S-wave seismic data is essential for optimizing stress-dependent hydrofracturing operations in shale plays and for exploiting fractured unconventional-reservoir systems. Either direct-S waves or P-SV converted modes can be utilized in VSP programs when seismic-based stress and fracture information is needed. Our research objective was to provide new direct-S VSP seismic sources that can be used to exploit unconventional reservoirs.

Our research focused on three aspects of VSP S-wave source technology that are needed in order to expand the use of S-wave seismic data in the exploitation of unconventional reservoirs:

1. Increase the number of direct-S VSP sources that can be mobilized,
2. Lower the cost of direct-S VSP data acquisition, and
3. Provide S-wave VSP sources that can be utilized across a wider range of earth-surface conditions.

Regarding the first of these objectives, the only way that direct-S modes have been produced to date has been to deploy horizontal-force seismic sources. Horizontal-force sources can be classified as either horizontal vibrators or inclined-impact devices. Unfortunately, only a few horizontal-force sources are available within the U.S. and around the globe. In contrast, there are many vertical-force sources, with common examples being vertical vibrators, vertical impact devices, and shot-hole explosives. Thus, if it can be demonstrated that direct-S modes produced by vertical-force sources provide stress and fracture information equivalent to the information extracted from direct-S modes produced by horizontal-force sources, the number of direct-S VSP seismic sources will instantly increase many fold. Data examples presented in this report confirm vertical-force sources produce direct-S modes that are quite similar (we are tempted to say equivalent) to the direct-S modes produced by horizontal-force

sources. Thus we conclude our research has accomplished objective 1 above (increasing the number of direct-S sources).

By utilizing vertical-force VSP sources to produce direct-S waves, research objective 2 (lower-cost data acquisition), is also achieved because only one source, a vertical-force source, has to be deployed to a VSP well. Standard practice for acquiring direct-P and direct-S data in VSP projects has been to deploy two sources: a vertical-force source to generate direct-P modes and a horizontal-force source to generate direct-S modes. By utilizing direct-S modes produced by vertical-force sources, the cost of VSP data acquisition can be reduced by approximately 50-percent because the same source produces both direct-P and direct-S data.

With regard to research objective 3, neither type of horizontal-force source (horizontal vibrator or inclined-impact device) can be used in swamps, marshes, dense timber, or across severe topographic slopes. In contrast, shot-hole explosives can be used in all of these environments. Because vertical-force sources have been used primarily as P-wave sources for decades, and P-wave seismic data have been acquired in a wide range of earth-surface environments, it will be rare to find any earth-surface condition where a vertical-force source cannot be utilized to generate direct-S waves for VSP applications. Thus the extension of direct-S VSP data acquisition to vertical-force sources allows direct-S waves to be utilized in a much broader range of VSP operating environments than can be considered when direct-S data acquisition is constrained to the use of only horizontal-force sources.

Executive Summary

We explain in this report the basic theory of direct-S waves produced by vertical-force sources and provide real VSP data examples of these modes propagating away from surface-based vertical vibrators. The classic source used to produce direct-S modes is the horizontal vibrator. Our objective was to determine similarities and differences between direct-S modes produced by horizontal vibrators and vertical vibrators. We include as an appendix to this report a comparison between direct-S wavefields generated by a vertical vibrator and by a horizontal vibrator positioned at the same offset surface coordinates and recorded by the same array of downhole geophones. It is rare to find offset VSP data that allow such one-to-one comparisons of horizontal-vibrator and vertical-vibrator wavefields. These wavefield comparisons indicate that the radial-S and transverse-S modes produced by these two sources are essentially identical except for the fact that vertical-vibrator data have a wider frequency spectrum.

We analyzed offset VSP data generated by vertical vibrators at two sites. Our effort at the first site was to take advantage of the excellent azimuth sampling of the walkaround VSP (WAR VSP) data available at this shale-gas prospect to calculate and compare the direct-S and direct-P radiation patterns produced by a vertical vibrator. We also used these WAR VSP data to calculate azimuth dependency of radial-S and transverse-S velocities and then converted these azimuth-dependent velocities to S-wave anisotropy values. S-wave anisotropy determined in this way agreed with S-wave anisotropy measured by a dipole-sonic log in the VSP well. This data equivalence indicates direct-S modes produced by vertical vibrators have valuable applications and should be utilized much more than they have to date, which to our observation has been to completely ignore the presence of these modes.

We used data at the second site (a tight sandstone prospect) to demonstrate how the downgoing direct-S modes produced by a vertical vibrator can be used to estimate S-wave anisotropy, which is the standard calculation done by shale-gas operators to establish qualitative (not quantitative) indications of spatial distributions of fracture density around a VSP well. We believe the results are realistic indications of fracture density and that our analysis technique can be reliably applied to vertical-vibrator direct-S modes by others.

Although we are comfortable in recommending the use of direct-S modes produced by vertical vibrators for determining “sweet spots” of fracture density, we do not recommend that these direct-S modes be used to estimate fracture orientation. Our attempts to determine fracture orientation with vertical-vibrator direct-S modes led to ambiguous results.

We also include as a second appendix, examples of S-S VSP images made from direct-S modes produced by a vertical vibrator. Although these VSP images are high-quality, we have no companion horizontal-vibrator VSP data from which S-S images can be made for comparison with the vertical-vibrator images. We include this second

appendix to emphasize that in addition to the S-wave applications provided by vertical vibrators that are described throughout this report, vertical vibrators also create direct-S modes that can be used to construct valuable images of geologic conditions around a well.

Chapter 1

Vertical-Force Sources and Direct-S Waves

Introduction

A common feature of unconventional reservoir systems is that most reservoir units have embedded fracture systems that need to be understood to properly position exploitation wells. Thus a remote seismic technology that can visualize the internal architecture of unconventional reservoirs and predict fracture orientation and fracture density will be invaluable for exploiting tight sandstones, shale-gas units, and other unconventional resource plays.

Investigations by others have demonstrated shear (S) waves are more responsive to fractures than are compressional (P) waves (Lynn, 2004a, 2004b; Thomsen, 1995). Based on this knowledge, operators across unconventional-resource plays need an effective, low-cost way to illuminate reservoir systems with surface-generated S waves so well placements in fracture systems can be optimized.

This report describes a vertical seismic profiling (VSP) technology in which S waves are produced with a vertical vibrator that applies a vertical force to the earth. The technology utilizes S modes created directly at the point where a vibrator source applies its vertical force to the Earth's surface, which is an important distinction to current practices of: (1) using sources that apply a horizontal force to the earth to produce S waves, or (2) using converted-S modes produced at remote subsurface interfaces by downgoing P wavefields. Because the S modes we analyze are produced directly at the point where a vertical vibrator baseplate contacts the earth, we call the wave modes **direct-S** modes.

The procedure described in this report removes the common assumption that the only way to create a downgoing S mode with a vertical-force source is to use interfaces above a target to produce downgoing P-to-SV converted modes that continue downward to illuminate a targeted interval. An important feature of the expanded use of vertical-force seismic sources is that these sources allow fracture properties to be estimated several tens of meters away from a VSP receiver well rather than being limited to a 1-meter distance from a borehole as is the case for a dipole sonic log.

Vertical-Vibrator Sources and SV Shear Modes

To generate S waves, standard practice is to use a source that applies a horizontal force to the earth surface. Such sources (horizontal vibrators or inclined impacts) are limited in number and cannot be deployed in surface

conditions such as swamps, marshes, rugged mountains, or heavy timber. We deviate from the constraint of using horizontal-force sources to produce direct-S waves and demonstrate how direct-S modes can be extracted from wavefields produced by vertical-force sources. The S-wave strategy described here involves S waves produced directly at the application point of a vertical displacement force, not the traditional converted P-SV mode produced at distant subsurface impedance interfaces. Because vertical-force seismic sources are abundant and can be used across almost any surface terrain, they are more useful than horizontal-force sources for evaluating unconventional reservoirs with S-wave data in many basins.

The basic wave physics of our source concept has been discussed by Miller and Pursey (1954) and White (1983) and is illustrated on Figure 1.1. These investigators explain that when a vertical force is applied to a homogeneous elastic half-space more SV energy is generated than P energy. This principle can be demonstrated on Figure 1.1a and 1.1b by drawing a radial line from the origin (where force F is applied) at any arbitrary takeoff angle relative to vertical. The distances from the origin to the point where that line intersects the P and SV radiation-amplitude surfaces on the figure define the strengths of the P and SV wave modes propagating in that takeoff angle direction. Inspection of Figure 1.1 shows that for takeoff angles within 15° (approximately) of vertical, this theoretical model indicates a P mode has greater amplitude than an SV mode. However, at takeoff angles exceeding approximately 15° from vertical, the model shows SV modes have greater amplitudes than P modes. This robust SV radiation occurs for media having Poisson ratios outside the numerical range used in these two models (0.44 and 0.33). Our objective is to take advantage of this large amount of S-wave energy radiating away from the point where a vertical-force source applies its force vector to the earth.

It is important to consider the direct-SV radiation illustrated in Figures 1.1a and 1.1b in 3D seismic propagation space. This 3D view can be created by rotating either of these 2D patterns a full 360 degrees around the vertical axis of the applied force vector. An example of the resulting 3D SV radiation created by this full azimuth rotation is illustrated on Figure 1.1c. The P-wave mode is eliminated in this 3D view because our purpose is to focus on only the radiated SV energy. A 90-degree sector of the radiation pattern is removed to allow a view of the interior of the expanding S-wave illumination.

Four receiver stations labeled R_A , R_B , R_C , and R_D are shown at 90-degree azimuth increments around vertical-force station VFS on Figures 1.1c and 1.1d. As shown on Figure 1.1d, regardless of where a receiver station is located relative to the source station, a vertical-force source causes SV vectors to be in the vertical plane passing through the source and receiver and also SV displacement vectors to be normal to the plane passing between source and receiver. For example, shear displacements 2 and 4 produce radial-S responses at receivers R_A and R_C . Similarly, shear displacements 1 and 3

produce radial-S data at receivers R_B and R_D . In our work, we simply apply the principle of reciprocity that allows source and receiver stations to be exchanged in this diagram. This application of the reciprocity principle results in a central VSP receiver array being at position VFS and vertical vibrators being at positions R_A , R_B , R_C , and R_D .

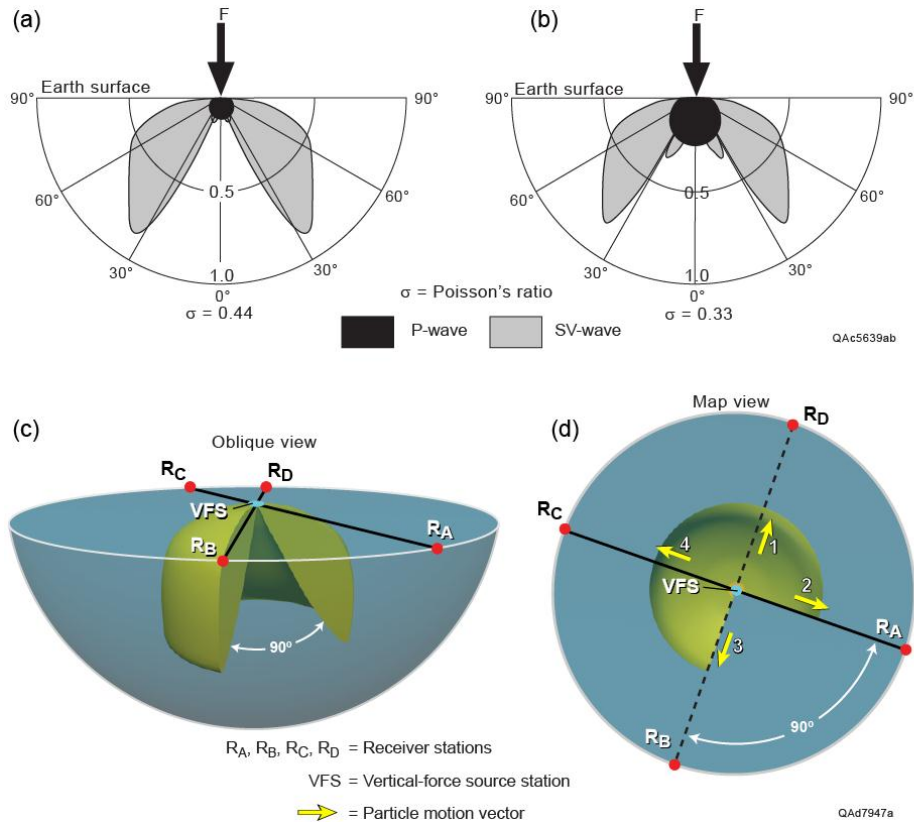


Figure 1.1. Section views of P and S radiation patterns produced by a vertical-force source for (a) a soft Earth and (b) a hard Earth. (c) An oblique view of the SV radiation in 3D space. The P-wave lobe is omitted to allow consideration of only the SV pattern (d) Map view of SV displacement vectors and source and receiver stations. VFS is the vertical-force source. R_A , R_B , R_C , and R_D are receiver stations. 1, 2, 3, and 4 are SV displacement vectors.

As investigators continued to observe S waves radiating away from vibrator source stations, numerous physical mechanisms were proposed to explain why S waves were present. Popular assumptions have been that there has to be a subsurface interface local to a source station that causes P-to-SV mode conversion to occur almost at the source position, or that there must be a step-like variation in topography local to the source station that creates a P-to-SV mode conversion close to the source location. Although these conditions do create converted SV modes, none of these assumptions are necessary. The basic physics is that an SV shear mode is produced directly at the point of application of a vertical force to the Earth without the presence of local interfaces or local topographic variations (Fig. 1.1).

Geyer and Martner (1969) were among the first to recognize that a shot-hole explosive (another type of vertical-force source) produces S-wave energy. These authors came to this conclusion because they deviated from common industry practice of deploying only single-component vertical geophones during the decade of the 1960's (when they did their work), and used surface-based three-component (3C) geophones to record reflection data produced by shot-hole explosives. Because their data were analog recordings, not digital recordings, they were not able to process the data and develop a robust theory. Interpretation results in their paper are shown only as marked reflection events on paper wiggle-trace records produced as camera layouts. Their evidence of direct-S modes radiating away from vertical-force source stations was based on the responses of surface-based 3C geophones because VSP data acquisition was not practiced in the U.S. during the 1960's.

Three papers published in the 1980's deserve citation and comment. The first paper, by Helbig and Mesdag (1982), is a theoretical study that summarizes the potential of S-wave technology. What is noteworthy about this classic paper is that it points out SV shear energy is produced by a vertical vibrator, a vertical impact, and an explosion in a half space, which covers the full range of vertical-force sources that can be used in VSP data acquisition. The material in this paper is theoretical, and no real data are exhibited. A second paper by Fertig (1984) in this 1980's decade emphasized shot-hole explosives produce S-wave energy. However, this paper teaches that S energy is not produced directly at the explosion point, but at the free surface above a buried explosive at the earth-air interface. The claim that a free surface is required in order for a subsurface explosion to generate SV energy resulted from the numerical modeling used in this paper. Although it is true that an explosive creates an SV mode at the free surface above a buried shot, the principle that an SV mode can be produced only at a free surface is a matter of debate. The third paper in the 1980's decade, by Mazzotti, et al. (1989), appears to be the first published example demonstrating an S-wave reflection profile can be created from data produced by a vertical vibrator. However, the authors assumed S energy is produced by mode conversion reasonably close to the source point, not directly at the source station. None of these three papers from the 1980's involve VSP technology.

It is not surprising that nothing can be found in geophysical literature even in the 1980's that documents the fact vertical vibrators produce S-wave modes that can be utilized in VSP studies. The principal investigator for this DOE study (Hardage) published the first English-language book on vertical seismic profiling in 1983, followed by a second edition in 1985 (Hardage, 1983; 1985). When writing these books in the 1980's, the principal investigator could find no published examples of S-wave VSP studies to include in the book except for a small number of VSP efforts that used true S-wave sources (horizontal-force sources) to generate S waves.

Four papers were published in the 1990's that begin to establish the VSP concepts that are utilized in this report. The earliest of the four papers (O'Brien, 1992) presents conclusive evidence that a downgoing SV mode is produced directly at the position of a surface-positioned vertical vibrator. This documentation is a fundamental thesis of our study. However, the only use made of these SV data was to measure S-wave velocity (V_S). No S-wave images were made, and no effort was made to investigate applications to fracture properties as is done in our study. The second paper (Sun and Jones, 1993) documents a downgoing SV wave is produced at the surface coordinates occupied by two bumper-to-bumper vertical vibrators. These authors promote the idea that the SV waves are the result of operating these vibrators with sweeps that were 180-degrees out of phase. However, this counter-phase operation of a vibrator pair is not required to produce an SV wave. Our report will demonstrate robust S waves are produced by a single vertical vibrator, as described on Figure 1.1. The third paper of this decade (Luschen, 1994) illustrated a shot-hole explosive generates SV waves, but the data used in this study were deep crustal reflections recorded by surface-based receivers, not VSP data. Even so, the physics illustrated by these surface-recorded data support the fundamental thesis of our study that a vertical-force source produces usable SV shear data. The fourth paper (Yokoi, 1996) presents both theoretical models and actual data that illustrate a vertical impact produces downgoing S waves. However, the author proposes that a fundamental requirement for generating the SV waves is that there needs to be a step-like change in the surface topography in the immediate vicinity of the surface impact. Our position is that a topographic discontinuity local to a source station will indeed create an SV mode, but a vertical impact will also produce a downgoing SV wave when there is no local discontinuity close to the point of impact.

The most pertinent papers occur after year 2000. Four papers published between 2002 and 2007 will be summarized. The first (Daley, 2002) is a theoretical analysis of P and S radiation from a shot-hole explosive. According to the model described in this paper, a shot-hole explosive produces a downgoing S wave only because there is a P reflection from the free surface above the shot. As stated in the preceding comments about the Fertig (1984), our position is that this free-surface requirement is not mandatory for S-wave generation.

Zhou et al. (2005) and Zhao et al. (2005) presented companion VSP research papers at the 2005 Annual Meeting of the Society of Exploration Geophysicists in which they illustrated SV waves are produced directly at vertical-vibrator source stations. The value of these papers is that the authors used these SV modes to create images local to the VSP well. Following these papers, Yang et al. (2007) presented compelling evidence that downgoing S waves exist in VSP data generated by both vertical vibrators and shot-hole explosives. These investigators then used these VSP S-wave data to construct geological images local to the receiver well. None of these papers imply these S-

wave modes can be used for fracture studies, which is the objective of our investigation.

Alford Rotation

Our analysis of VSP data will utilize Alford rotation. The theory and concepts of Alford rotation are described in Chapter 2. Detailed illustrations and discussions of Alford rotation principles and applications are presented in subsequent chapters. For the present, Alford rotation will be considered only as a mathematical transformation of S-wave seismic data acquired across a fractured rock area to a new coordinate system that allows natural coordinate axes to be defined, fracture orientation to be estimated, and fast-S and slow-S modes to be analyzed. The purpose of these introductory remarks is to summarize what previous investigators have assumed when applying Alford rotation to seismic data and to document the types of applications where Alford rotation has been applied.

R.M. Alford introduced his method for rotating S-wave data coordinate space so that S-wave data are simplified to fast and slow modes that propagate along principal axes at the 1986 Annual Meeting of the Society of Exploration Geophysicists (Alford, 1986). This paper was followed by United States patents (Alford, 1989; Alford et al., 1989). Following these descriptions of how to determine the principal axes along which fast and slow S modes propagate, numerous other investigators began to use and apply Alford rotation methods in S-wave applications (Angerer, et al., 2002; Dellinger and Nolte, 1997; Dellinger, et al., 2001; Hou and Marfurt, 2002; Liu, et al., 2003; Michaud and Snieder, 2004; Mueller, 1991; Winterstein and Meadows, 1991; Winterstein and De, 2001; Zeng and Macbeth, 1993).

Collectively these papers describe assumptions related to data to which Alford rotation can be applied, as well as data effects that occur when the axes of S-wave data space have been rotated to azimuths corresponding to principal axes for fast-S and slow-S mode propagation. Principal observations are:

1. Alford rotation applies when S-wave travel paths are vertical (Dellinger, et al., 2001; Mueller, 1991).
2. To utilize Alford rotation, S-wave source displacements must be orthogonal, receivers must likewise be orthogonal, and sources and receivers must be aligned with each other (Dellinger, et al., 2001).
3. Principal earth axes must be oriented in the same azimuths at all depths over which Alford rotation is applied (Dellinger, et al. 2001).
4. When S-wave data are rotated to azimuths corresponding to principal axes for S-wave propagation, the off-diagonal terms of the Alford rotation matrix must reach zero, or minimum, values (Hou and Marfurt, 2002; Liu,

et al., 2003; Michaud and Snieder, 2004; Winterstein and Meadows, 1991; Winterstein and De, 2001; Zeng and Macbeth, 1993).

Regarding observation #1, Zeng and Macbeth (1993) propose their method of coordinate rotation is valid when travel paths deviate as much as 20 degrees from vertical. In our study, VSP source-to-receiver travel paths will deviate even more than 20 degrees from vertical.

Regarding observation #4, many investigators determine when off-diagonal terms of an Alford rotation matrix reach near-zero minima by visual inspection of Alford rotation results. When a significant amount of S-wave data has to be analyzed, rapid and versatile graphical display options must be used to inspect the large volume of Alford rotation output.

Overview of Study Sites

To demonstrate the value of direct-S modes produced by vertical-force sources, data from two vertical-vibrator VSP surveys were analyzed in this study. The locations where the two VSP data sets were acquired are defined on Figure 1.2. These VSP data sets were acquired in different types of unconventional resource plays to demonstrate that direct-S modes provide valuable fracture and stress information for a wide range of unconventional reservoir systems.



Figure 1.2. U.S. map showing the three study sites used in this project.

Conclusions

Vertical-force sources, particularly vertical vibrators, produce a rich amount of SV shear energy directly at the point where their vertical force vectors are applied to the earth. To date, geophysicists have not utilized these direct-S modes effectively. Vertical-force sources have been used to generate compressional-wave (P-wave) VSP data since the 1950's. However, direct-SV modes produced by these sources appear to have been ignored in VSP studies until approximately year 1992 when it was demonstrated that S modes produced directly at vertical-vibrator source stations could be used to determine S-wave velocities. In 2005, a small number of VSP studies appeared in the literature in which investigators expanded the use of direct-SV modes produced by vertical-force sources to construct S-wave images around a VSP receiver well. No evidence was found that S modes produced directly at the point where a vertical-force VSP source applies its force vector to the earth have ever been used to analyze fracture systems, which is the objective of this project.

The research we describe in this report will show that direct-S modes produced by vertical-force sources have great value in VSP applications. Our longer range objective is to extend VSP applications of these direct-S modes to surface-positioned receivers. Although we limit our study to VSP data generated by vertical vibrators, the principles we document apply to any type of vertical-force source. The same concepts we illustrate can also be implemented if a vertical-impact source, a shot-hole explosive source, or a mud-pit air gun is used in a VSP program.

Correct insights into the fundamental physics that a vertical-force source produces robust SV shear waves directly at a source station appear occasionally in geophysical literature. Examples are Miller and Pursey (1954), Helbig and Mesdag (1982), and Mazzotti, et al. (1989). However, none of these papers apply this physics to VSP data acquisition.

We credit the first VSP paper to focus on the concept that vertical vibrators produce robust SV data to O'Brien (1992). However, the papers that best illustrate the concept of direct S-wave VSP data are those published much later by Zhao, et al. (2005), Zhou, et al. (2005), and Liu, et al. (2007). An additional paper of value is one by Li et al. (2007) that illustrates SV data produced directly at shot-holes can be used to make impressive SV images along a 2D profile. Although the emphasis of this paper is surface-based data, not VSP data, the motivation to use shot-hole explosives to produce direct-source SV data came from the authors analyzing VSP data generated by shot-hole explosives.

Although SV waves produced by vertical-vibrator VSP data have been used to make S-wave images local to a well, we found no evidence that these SV waves have ever been used to analyze fracture systems. We conclude that our objectives of: (1) extracting direct-source SV shear modes from vertical-vibrator

VSP data, and (2) analyzing those S-wave data to estimate fracture orientation and fracture density in shale-gas and tight-sandstone gas plays are novel and unique.

Although a few VSP investigators began to utilize direct-source S modes in the decade of 2000 to 2009, there is no published evidence that any investigations have used these S modes to determine fracture attributes. We conclude our project has the potential to expand VSP technology so that simple vertical-force sources can be used to apply S-wave data to geological problems, including fracture analysis.

The Alford rotation studies we reviewed confirmed that the manner in which we will apply Alford rotation in analyzing VSP direct-source S waves will push the limits of applicability of the algorithm. If we can verify that our violations of some of the popular constraints applied in the use of Alford rotation still allow valid fracture attribute to be determined, this project will allow wider use of Alford rotation concepts in future S-wave studies.

Chapter 2

Data Processing

Introduction

There are two important aspects of the technology that is described in this report. The first is the fundamental principle that robust S waves are produced directly at the point where a vertical-force seismic source applies its force vector to the earth. We refer to these S waves as **direct-S** modes. This concept of direct-S modes produced by vertical-force sources is introduced in Chapter 1 and will be repeated throughout the remainder of this report. The second aspect to emphasize is the data-processing philosophy that is applied to these direct-S modes to extract stress-sensitive and fracture-sensitive information. The data-processing strategy we use to analyze fracture and stress attributes in vertical-force VSP data is discussed in this chapter.

Vertical-force seismic sources can be segregated into three categories: vertical vibrators, vertical-impact devices, or shot-hole explosives. We limit our analyses of vertical-force VSP data to only vertical-vibrator sources because vertical vibrators are the dominate type of source used in onshore VSP work.

Determining Natural Coordinates

Several coordinate systems are used to describe concepts involved in acquiring, processing, and applying multicomponent seismic data. Three coordinate systems often encountered are depicted on Figure 2.1. The map view on this figure shows a seismic source station and a receiver station positioned on the earth's surface above a fracture system. When acquiring 3D multicomponent seismic data, a common practice is to deploy source lines orthogonal to receiver lines. In geophysical terminology, when this type of orthogonal source-receiver geometry is used, the direction in which receiver lines are deployed is called *inline*. The direction orthogonal to inline (the source line direction) is called *crossline*. The inline/crossline directions used on Figure 2.1 are indicated by axes having subscripts **i** (for inline) and **x** (for crossline). Together, these two axes—inline and crossline—define a seismic *data-acquisition coordinate system*. Axes other than orthogonal inline and crossline directions may be used to acquire seismic data. However, to simplify discussion in this report, orthogonal inline and crossline terminology will be used to describe seismic data-acquisition geometry.

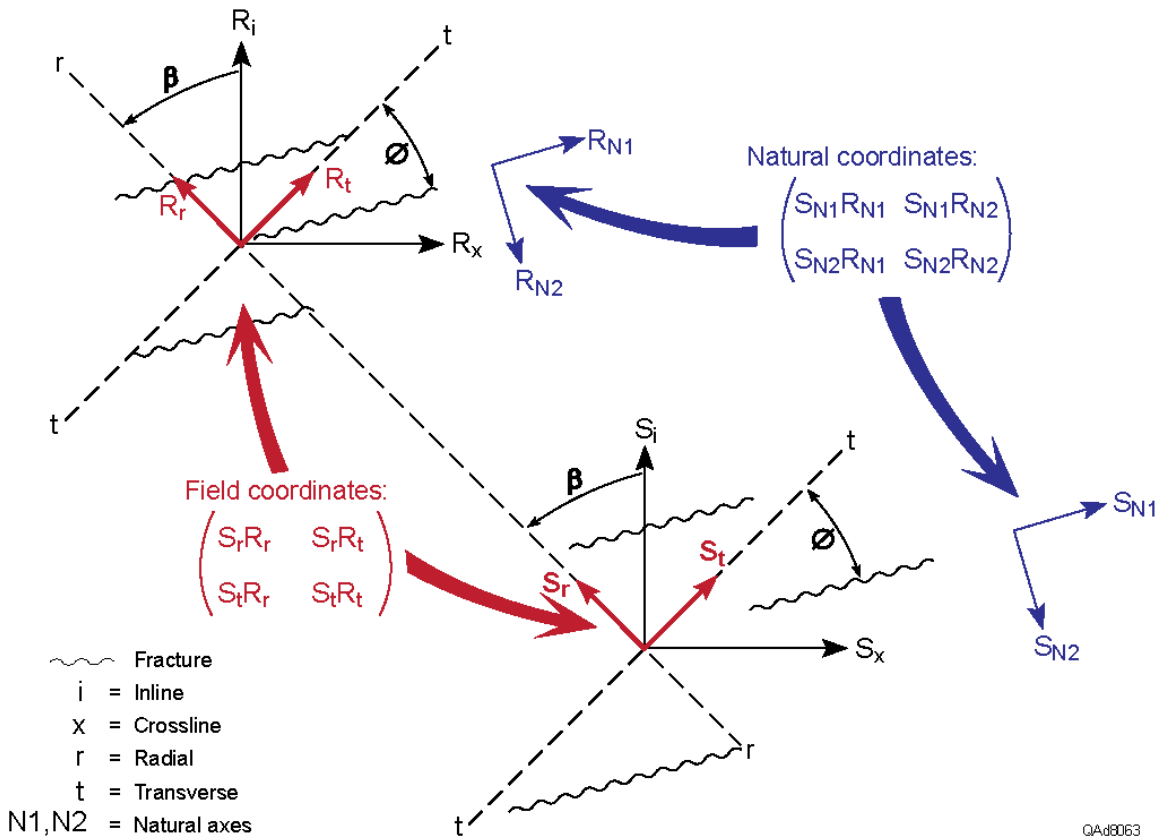


Figure 2.1. Vectors and quantities labeled **R** relate to a receiver station. Vectors and quantities labeled **S** relate to a source station. This map view illustrates three orthogonal-axis coordinate systems encountered when using multicomponent seismic technology to analyze fracture systems. The first coordinate system is an *inline* and *crossline* geometry used to deploy sources and receivers for data acquisition (subscripts **i** and **x**). The second coordinate system is a *radial-transverse* system created when processing data (subscripts **r** and **t**). The third coordinate system is the *natural coordinate* system that needs to be determined to interpret fracture properties (subscripts **N1** and **N2**).

During seismic data processing, data are usually transformed to a second orthogonal-azimuth coordinate system referred to as *radial/transverse*. For the source-receiver pair drawn on Figure 2.1, this coordinate transformation is achieved by mathematically rotating inline and crossline axes by angle β so one axis is in the vertical plane passing through this selected source station and receiver station. The coordinate axis rotated into this vertical plane is the radial axis for this particular source-receiver pair. The axis normal to this vertical plane is the transverse axis for the same source-receiver pair. Angle β differs for each source-receiver pair and is calculated from GPS coordinates defining locations of all source and receiver stations across a survey area. On Figure 2.1, radial and transverse axes are identified by axes labeled with subscripts **r** (for radial) and **t** (for transverse). Together, these two orthogonal axes—radial and transverse—define a seismic *data-processing coordinate system*.

The third coordinate system will be called *natural coordinates* in this report. Natural coordinates align with principal anisotropy axes of the earth. For this reason, these axes are referred to as *principal axes* in some technical papers. For the fracture system depicted on Figure 2.1, the principal anisotropy within the earth is a system of aligned fractures. The challenge of utilizing multicomponent data in fracture analysis is to rotate radial and transverse data-processing axes to natural coordinate axes. On Figure 2.1, natural coordinate axes and natural coordinate data terms are identified by subscripts **N1** and **N2**. Together, these two axes—natural coordinate axis N1 and natural coordinate axis N2—define a seismic *data-interpretation coordinate system*.

Receiver R identified on Figure 2.1 can be on the earth surface or in the subsurface. In this study, the receiver is in the subsurface deployed as a sensor station in a downhole VSP receiver array.

Alford Rotation

The Alford Rotation procedure for estimating orientations of natural coordinate axes was described publically as an oral presentation at the 56th Annual Meeting of the Society of Exploration Geophysicists (SEG). The Expanded Abstract of that SEG presentation (Alford, 1986) is one of the more widely cited references in geophysical literature, illustrating some SEG Expanded Abstracts are as valuable for preserving geophysical research developments as are full-length journal papers. A detailed explanation of the logic and physics embedded in the coordinate transformation procedure was later published as U.S. Patent 4,803,666 (Alford, et al., 1989).

$$\begin{array}{ccc}
 \text{Natural} & & \text{Field} \\
 \text{coordinate space?} & & \text{coordinates} \\
 \begin{pmatrix} S_A R_A & S_A R_B \\ S_B R_A & S_B R_B \end{pmatrix} & = & \begin{pmatrix} \text{M rotations of field} \\ \text{coordinate axes by } (\Delta\theta) \end{pmatrix} \begin{pmatrix} S_r R_r & S_r R_t \\ S_t R_r & S_t R_t \end{pmatrix}
 \end{array}$$

Matrix terms undergo polarity reversals and have minimal values when rotated axes A and B align with natural-coordinate axes N1 and N2.

QAd8065

Figure 2.2. The Alford Rotation procedure used to define natural coordinate data space. **S** is a source displacement vector; **R** is a receiver orientation vector. Subscripts **r** and **t** define radial/transverse coordinate space (or data-processing data space). Subscripts **A** and **B** define axes rotated from radial and transverse axes by azimuths that successively increase by small increments of $\Delta\theta$. When this coordinate rotation aligns axes **A** and **B** with natural coordinate axes **N1** and **N2** (Fig. 2.1), the terms in the left-hand-side matrix undergo polarity reversals.

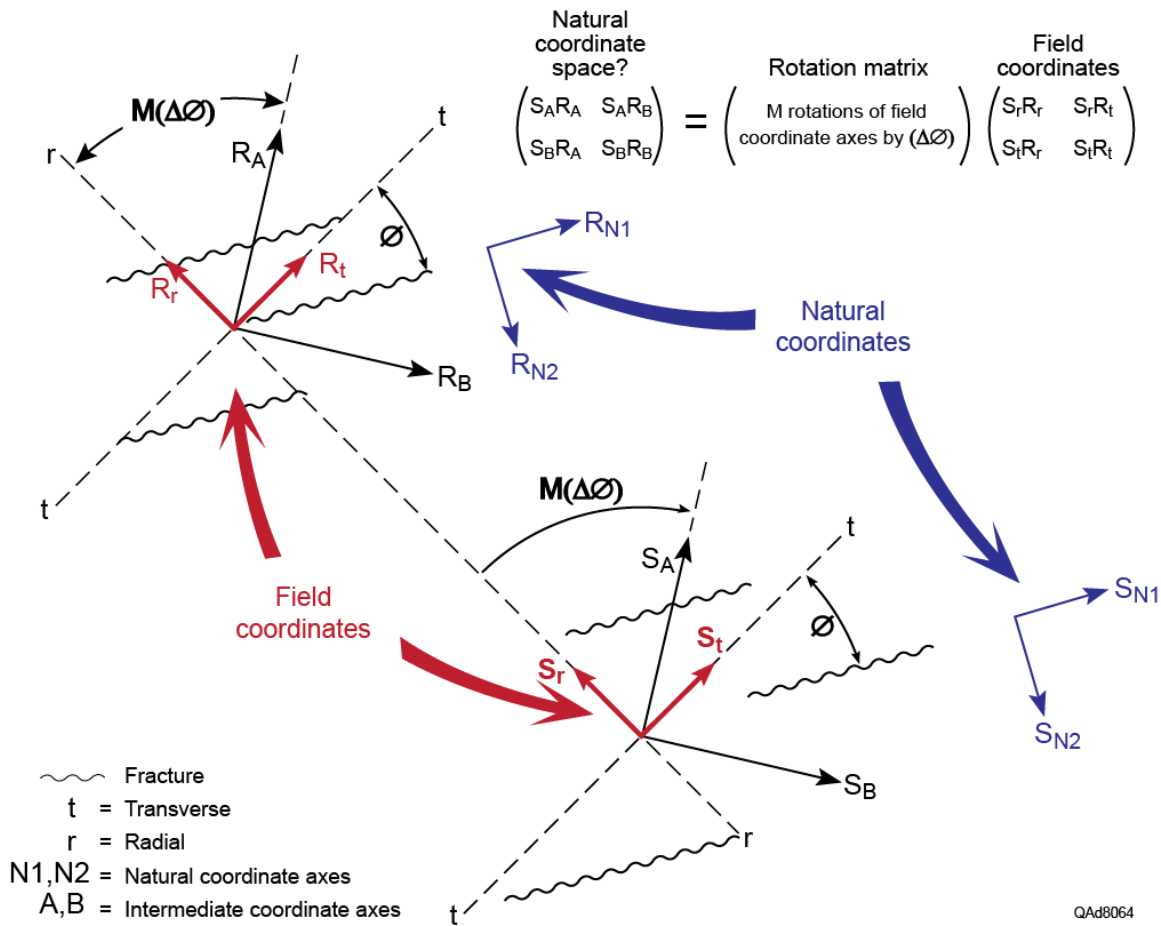


Figure 2.3. Graphical description of the Alford Rotation procedure described on Figure 2.2. Axes with subscripts **A** and **B** have been rotated from radial/transverse axes by **M** azimuth increments of $\Delta\phi$. At each new rotated coordinate position, the left-hand-side matrix above is calculated and saved. When this calculation is done over a 360° azimuth range, all matrices are examined to find which azimuth rotation causes terms of the left-side matrix to undergo polarity reversals. When a polarity reversal occurs, axis **A** or **B** should be aligned with natural coordinate axis **N1** or **N2**. Quantities using label **R** are associated with a receiver station, and quantities labeled **S** are associated with a source station.

When a fracture target is illuminated with orthogonal S-wave displacement vectors, Alford rotation techniques can be used to estimate natural coordinate axes oriented parallel and orthogonal to fracture trends. The mathematics of Alford rotation is illustrated on Figures 2.2 and 2.3. The right-hand-side matrix of the equation displayed on these figures (labeled “Field coordinates”) defines data components created by orthogonal S-wave source displacements and recorded by orthogonal S-wave sensors. Radial and transverse data (subscripts **r** and **t**) are used in the right-side matrix on Figures 2.2 and 2.3, but the calculation procedure can utilize inline and crossline data, or data defined by any orthogonal field-coordinate axes. Common assumptions when applying Alford rotation are

that a fracture system has to be illuminated with orthogonal S-wave vectors, and that the earth response has to be recorded with orthogonal S-wave sensor elements.

The target-illuminating data (“Field coordinates” matrix) are repeatedly transformed to a new coordinate system (left-side matrix of Figures 2.2 and 2.3), in which axes are rotated in small azimuth increments of $\Delta\Phi$. This calculation is typically done over an azimuth range of 360° at small increments of 1, 5, or 10 degrees of azimuth, depending on the preferences of a data processor. For each new choice of azimuth, the left-side matrix of Figure 2.2 defines the azimuth orientation of a “possible” natural coordinate system having one axis parallel to a fracture trend and one axis orthogonal to that trend. If $\Delta\phi = 1$ degree, these 360 possible choices for the orientation of a natural coordinate system are analyzed to determine which azimuth value causes terms of the left-hand-side matrix to undergo polarity reversals. The rotation angle at which a matrix term exhibits a phase reversal defines the azimuth of a natural coordinate axis. This polarity-reversal physics is discussed in the following section.

S-Wave Splitting, Natural Coordinates, and Fracture Orientation

The experimental data illustrated on Figure 2.4 were generated using a cylindrical core sample and small piezoceramic dipole sources and receivers to simulate S-wave propagation through a fracture system. This fractured rock sample has a dominating natural-coordinate system. One natural-coordinate axis (**N1**) is parallel to the aligned fractures; the second natural-coordinate axis (**N2**) is perpendicular to the fractures. A piezoceramic element attached to one end of the sample created an illuminating horizontal-source vector polarized at angle Φ relative to aligned fractures. The force vector created by this source element simulates an S-wave source displacement vector oriented at angle Φ relative to natural-coordinate axis **N1**. The wavelets plotted around the circumference of the test sample define data recorded by an S-wave piezoceramic sensor attached to the opposite end of the test sample. These wavelets represent what a rotating VSP geophone would record if that geophone was positioned inside a fractured reservoir.

The notation S_1 and S_2 used on the figure correspond, respectively, to fast-S and slow-S modes. These data illustrate the principle that a single S-wave displacement vector creates two S-wave modes in a fractured medium. One mode has its particle-displacement vector oriented along natural-coordinate axis **N1** (parallel to fractures). The second mode has its particle-displacement vector oriented along natural-coordinate axis **N2** (perpendicular to fractures).

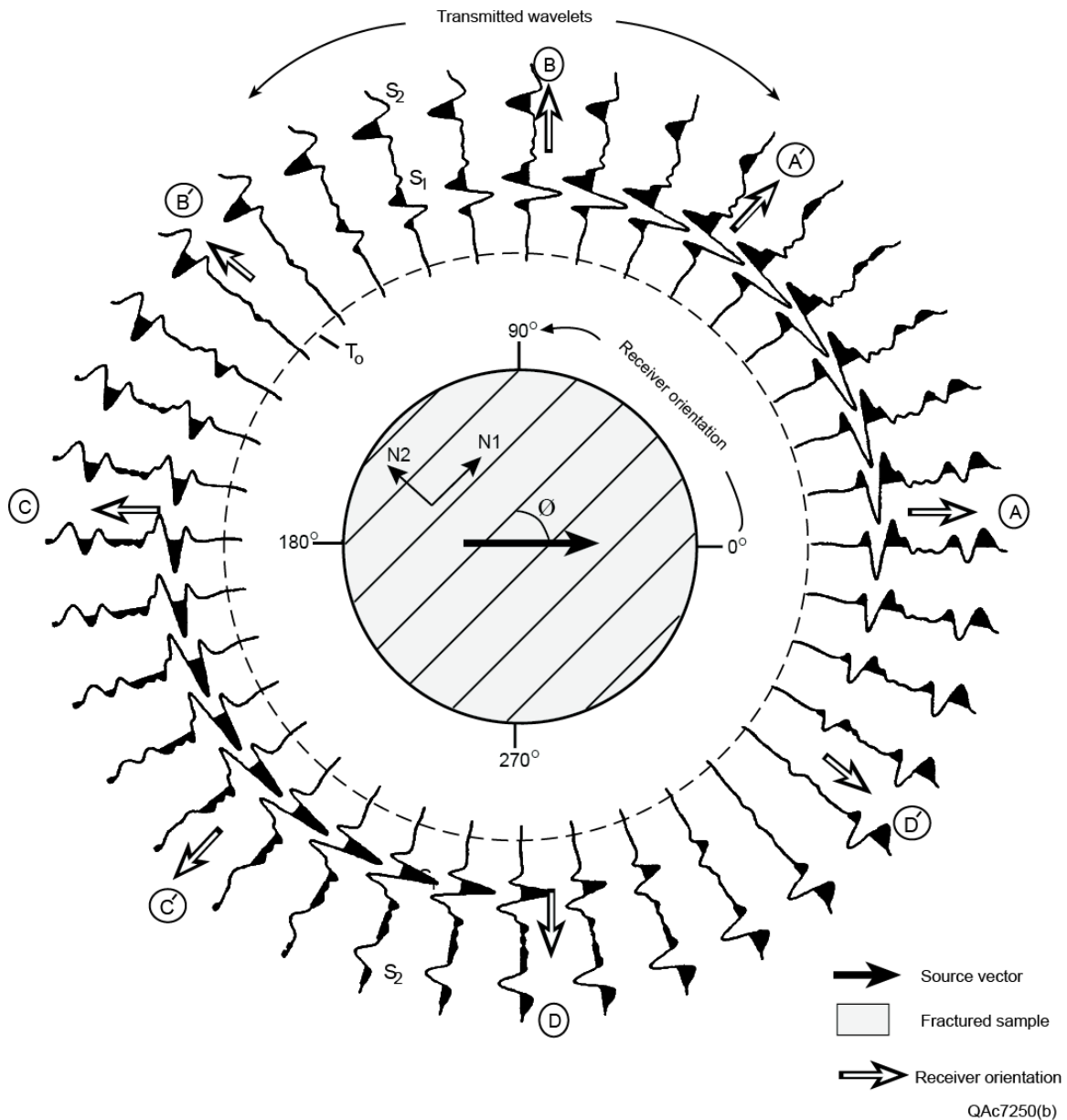


Figure 2.4. End-on view of a fractured test sample from the source end. The source vector is polarized at an angle ϕ relative to the azimuth of the fracture planes. As the source remains fixed, a receiver at the opposite end of the sample is rotated 360 degrees at angular increments of 10 degrees relative to the orientation of the positive-polarity of the S-wave source vector. These test data show that only a fast-S mode (S_1) propagates parallel to fracture planes (responses **A'** and **C'**), and only a slow-S mode (S_2) propagates perpendicular to the fracture planes (responses **B'** and **D'**). A mixture of fast-S and slow-S is observed at all other azimuth orientations. A line connecting **A'** and **C'** is one natural coordinate axis (**N1**). A line connecting **B'** and **D'** is the second natural coordinate axis (**N2**). Amplitude and phase behaviors of S_1 and S_2 wavelets are affected by the continually changing angle between the vector orientations of the positive-polarity ends of the source and receiver elements. Modified from Sondergeld and Rai (1992).

The wavefields that propagate through the medium are combinations of S_1 and S_2 modes. Wavelets A, B, C, D are the responses observed when the receiver is either parallel to or orthogonal to the illuminating S-wave source vector. These four wavelets contain both S_1 and S_2 arrivals. The length of the propagation path through the sample is such that the differences in S_1 and S_2 travel times cause S_1 and S_2 wavelets to not overlap. In real seismic data when a fracture interval is thin and the difference in S_1 and S_2 travel times is not large, the response will be a complicated waveform representing the sum of partially overlapping S_1 and S_2 wavelets.

The wavelets at positions A', B', C', D' illustrate important S-wave physics. Only a S_1 mode propagates parallel to the fracture planes (responses A' and C'). Only a S_2 mode propagates perpendicular to the fracture planes (responses B' and D'). The propagation directions of these pure- S_1 and pure- S_2 wavelets define natural coordinate axes **N1** and **N2** illustrated on Figures 2.1 through 2.3. This S_1 and S_2 wave physics is what we attempt to replicate with the orthogonal-azimuth VSP data analyzed in this report in order to estimate fracture orientation across reservoir intervals.

Note S_2 wavelets undergo a phase reversal and have minimum values when their azimuth polarization direction rotates across the N1 natural coordinate axis parallel to fractures (defined as a line passing through A' and C'). Likewise S_1 wavelets exhibit phase reversals and minimum values when their polarization direction rotates across the N2 natural coordinate axis that is perpendicular to fractures (defined as a line passing through B' and D'). These phase reversals are the phenomena that occur in the terms of the Alford rotation matrix (Figs. 2.2 and 2.3) when a data-space axis rotation sweeps past a real-earth natural coordinate axis.

The data on Figure 2.4 were created by a single S-wave displacement vector. In contrast, the data used in Alford rotation (Fig. 2.2) involve two S-wave displacement vectors that are orthogonal to each other.

Orthogonal S-Wave Displacements

The S-wave data-acquisition and data-processing coordinate systems discussed to this point are based on orthogonal coordinate axes (Figs. 2.1q and 2.3). Similarly, the Alford rotation algorithm used to determine the orientations of natural-coordinate axes assumes S-wave data are produced by orthogonal S-wave source displacements (Fig. 2.3). Several options can be used to illuminate a fracture interval with orthogonal S-wave displacement vectors. All options require that 3-component geophones be used to record the data. From a source perspective, our methodology introduces a source option (orthogonal-azimuth vertical vibrators) that does not appear to be used across the oil and gas industry. The source strategy commonly used to evaluate fracture systems is to

create crossed-dipole sources by orienting horizontal vibrators orthogonal to each other (Figs. 2.5a and 2.5c). S-wave data acquired with this orthogonal horizontal-vibrator method appear to be quite effective for fracture analysis.

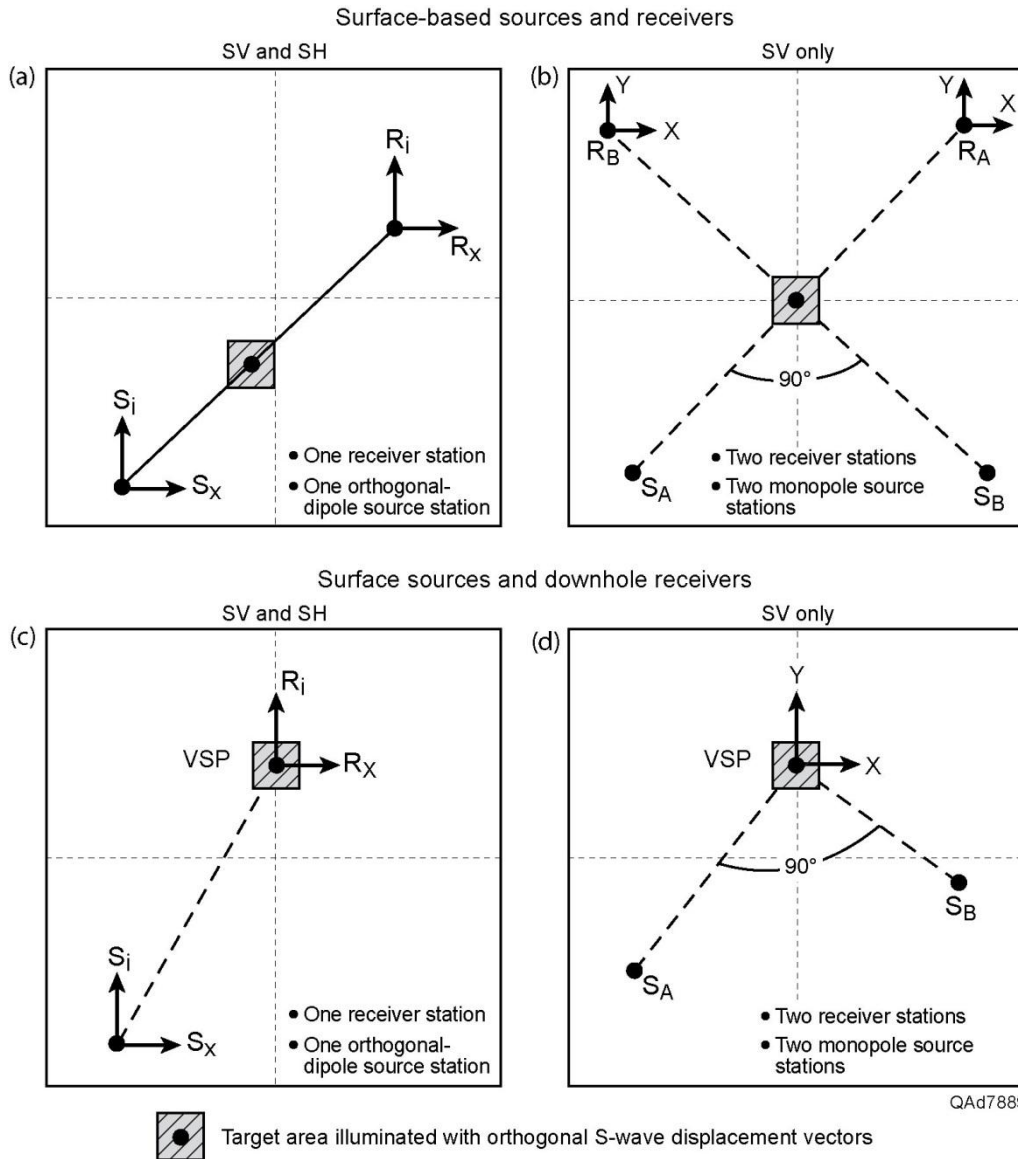


Figure 2.5. Options for illuminating targets with orthogonal S-wave displacement vectors. Options (a) and (c) use orthogonal horizontal-force sources (crossed dipoles) such as horizontal vibrators. Wave modes produced by these cross-dipole sources are termed **SV** and **SH** at the top of panels (a) and (c). Options (b) and (d) use vertical-force sources. The wave mode radiating from each vertical-vibrator source is termed **SV only** at the top of panels (b) and (d). Option (d) is the method evaluated in this report.

In contrast to this common practice of using horizontal vibrators, the source concept used in this study is based on the assumption that results equivalent to those achieved with crossed-dipole sources can be achieved with

simpler vertical-vibrator sources if these vibrator sources are deployed at source-to-receiver azimuths that differ by 90 degrees (Figs. 2.5b and 2.5d). Our study is limited to vertical seismic profiling data (Fig. 2.5d). In this application, one SV shear mode generated by a vertical vibrator, as defined on Figure 1.1a and 1.1b, propagates in the vertical plane passing through source station SP_A and the VSP receiver, and a second SV mode propagates in the vertical plane passing through source station SP_B and the VSP receiver (Fig. 2.5d). The result is orthogonal S-wave illumination of fracture intervals local to VSP receivers similar to that achieved with crossed-dipole horizontal vibrators.

S-Wave Splitting and Fracture Density

The model illustrated on Figure 2.6 simulates a seismic profile traversing an earth system consisting of lateral blocks of anisotropic rock bounded on each end by blocks of isotropic rock. Anisotropic conditions in blocks B, C, and D are caused by aligned fractures which have different fracture density (FD) and fracture azimuth (Φ) from block to block.

Fast-S velocity in a fractured medium tends to be the same as it is in an unfractured sample of that same medium. Fast-S velocity may decrease by a small amount if fracture density is sufficient to alter bulk density; otherwise, it is reasonably correct to assume fast-S velocity has the same magnitude in fractured rock as it has in non-fractured sections of the same rock. This invariant nature of S_1 velocity is identified by velocity parameter V_S shown by the horizontal dashed line connecting blocks A and E on the lower portion of Figure 2.6.

In contrast, slow-S velocity has the generalized behavior diagrammed below the earth model. As fracture density FD increases, slow-S velocity tends to decrease. The magnitude by which slow-S velocity decreases is a qualitative, not quantitative, indicator of fracture density. Slow-S velocity behavior can be used to predict fracture density in a quantitative manner only if fracture density can be independently determined at several calibration points across seismic image space and correlated with slow-S velocities at the same coordinates. Establishing such calibration is difficult to accomplish because extensive core analysis is required. However, using slow-S velocity behavior as only a qualitative predictor of fracture density is still important for understanding fracture distributions across areas imaged with multicomponent seismic data. Variations in fracture azimuth affect only the polarization direction of the slow-S mode, not the magnitude of slow-S velocity. Our use of orthogonal-azimuth VSP data to estimate relative fracture density within fractured reservoirs is based on the fracture-induced S_2 time delay illustrated on Figure 2.6.

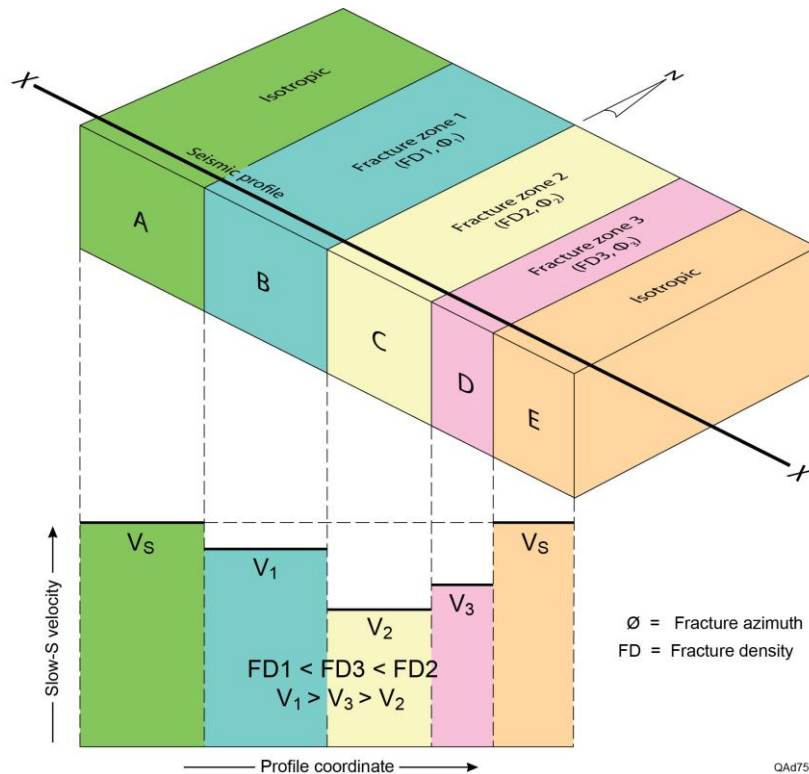


Figure 2.6. Relationship between slow-S velocity and fracture density (**FD**). As fracture density increases, S_2 velocity decreases. In contrast, fast-S velocity and P-wave velocity do not change, or change by only minor amounts across fractured Blocks **B** through **D**. In isotropic Blocks **A** and **E**, there is no S-wave splitting and only one S-wave velocity V_s . In all Blocks (**A** through **E**), fast-S velocity = V_s , the velocity in the nonfractured rock. Mineralogy, porosity, and pore fluid do not change across the profile. The only earth properties that vary from block to block are fracture density and fracture orientation.

Fracture Illumination

In theory, Alford rotation should be applied to orthogonal S-wave displacements that involve only zero-offset geometry between sources and receivers. In this study, we violate these constraints in two respects:

1. S-displacement vectors are only approximately orthogonal, and sometimes greatly differ from orthogonal, and
2. Source-to-receiver offsets are significant, being of the order of the depth to a targeted unconventional reservoir..

In our VSP field technique, unconventional reservoirs are illuminated with quasi-orthogonal S-wave displacement vectors—a fundamental requirement for determining fracture properties. The illumination procedure involves a simple deployment of vertical-vibrator source stations around the well at azimuths that differ by approximately 90 degrees (Fig. 2.5d). Downgoing SV modes produced

directly at the point of application of a vertical force at two orthogonal-azimuth source stations illuminate targets with quasi-orthogonal S displacement vectors, which allow Alford rotation to be applied to determine natural-coordinate azimuths. By recording orthogonal-source SV modes at VSP receiver stations spaced a few meters apart and performing Alford rotations of data recorded at each of these receiver stations (Fig. 2.7), fracture orientation and fracture density can be mapped across either thin or thick intervals of a reservoir system. At each subsurface receiver station, the orientation of fast-S polarization defines fracture orientation local to the receiver position, and time delays between slow-S and fast-S modes indicate relative fracture density between receiver stations.

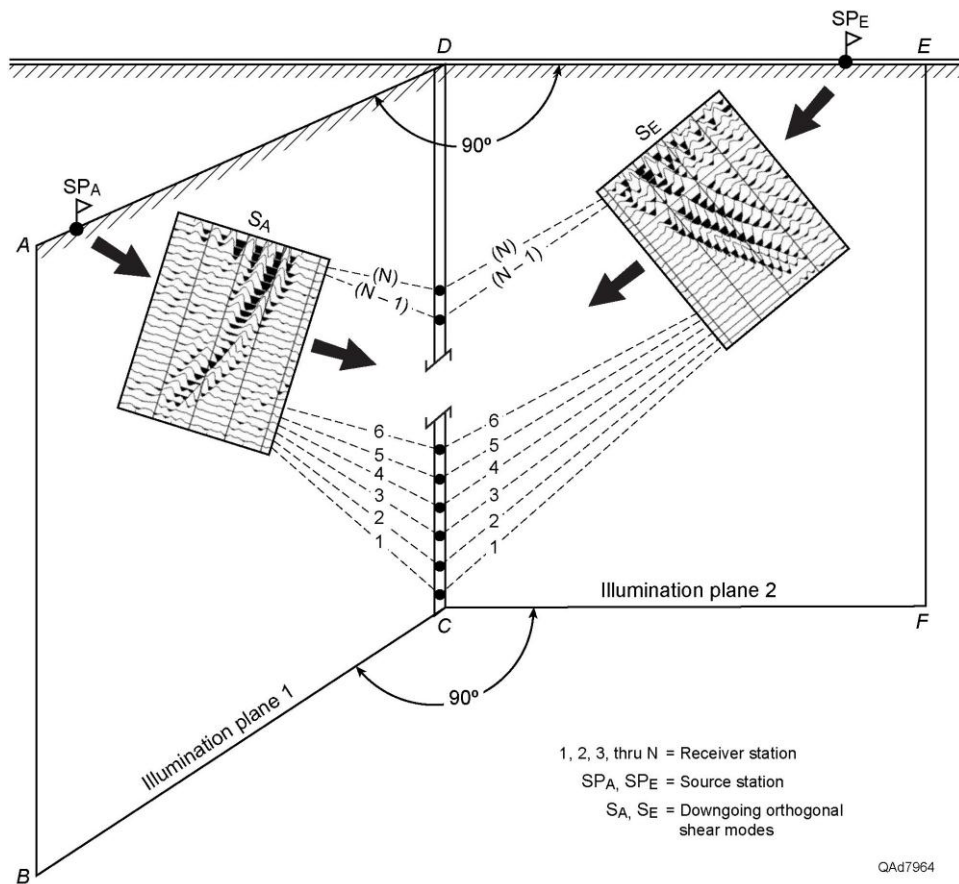


Figure 2.7. The concept of measuring fracture properties at closely spaced intervals across a reservoir system. The azimuths from receiver well **CD** to source stations **SPA** and **SPE** differ by 90 degrees. The wavefields in **Illumination plane 1** and **Illumination plane 2** are, respectively, SV wavefields produced directly at the points where vertical vibrator sources at source stations **SPA** and **SPE** apply force vectors to the earth. These orthogonal S displacements are recorded by a vertical array of **N** 3-component receivers.

Transforming VSP Test Data to Wave-Mode Data

In a vertical receiver well, azimuth orientations of X,Y horizontal geophones differ at each downhole station because sensor packages are deployed on twisted-wire cable that rotates as it spools off a cable reel. As a result, sensors rotate by different amounts when they reach different deployment depths. Phase shifts and amplitude variations introduced into horizontal-sensor data by station-to-station variations in receiver orientation do not allow individual events or distinct wave modes to be recognized, particularly S-wave events that dominate horizontal-sensor response. Receivers must be mathematically oriented to consistent azimuths and to proper inclinations to define downgoing and upgoing P and S modes.

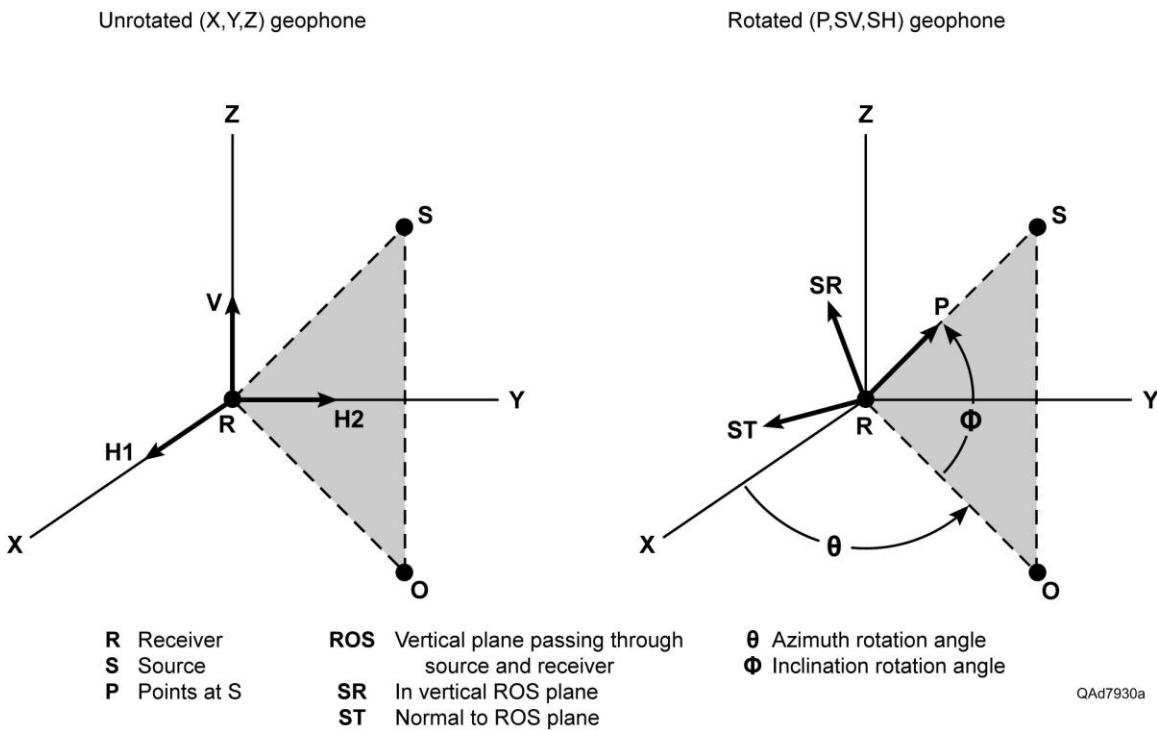


Figure 2.8. Reorientation of X, Y, Z receivers to P, SR, and ST receivers.

Transformations of borehole receivers from in situ X, Y, Z orientations to a data space where receivers are oriented to emphasize P, radial-shear (SR), and transverse-shear (ST) events have been practiced in VSP technology for several decades. A graphical description of the transformation of receivers from X, Y, Z data space to P, SR, ST data space is shown on Figure 2.8. Azimuth rotation angle θ and inclination angle Φ have to be determined at each receiver station so that P-wave displacement vectors are aligned along raypath RS, SV displacement vectors are confined to vertical plane ROS, and SH displacement vectors are orthogonal to plane ROS. Any downgoing direct-S wavefield that is

used as illustrated on Figure 2.7 must first be rotated to radial and transverse coordinate space as described on Figure 2.8

Removing Overburden Travel Time Differences

Downgoing S wavefields produced at two orthogonal-azimuth offset source stations may arrive at the shallowest station of a downhole vertical-receiver array at different times if they travel different distances from their respective surface-source stations. The S first-arrival wavelets from source stations SP_A and SP_E (Fig. 2.7) may also undergo different S-wave splitting before they come to this common receiver station because wavefields from the two different offset sources travel through a different overburden to reach the VSP receivers. These source-dependent overburden effects must be removed to analyze S-wave propagation across a targeted unconventional reservoir.

Overburden-induced travel-time differences were eliminated in our data analyses by applying static time shifts to align radial and transverse components of each S wavefield at a common time datum at the topmost station of the vertical receiver array. An example of static time shifts applied to direct-S data produced at two vertical-vibrator source stations positioned at significantly different azimuth and offset coordinates is illustrated on Figure 2.9b. In this example, the vertical array of VSP receivers consisted of 80 stations spaced at intervals of 50 ft, which created a vertical array spanning 4,000 ft of a major unconventional reservoir. In this example, the first-arrival times of radial and transverse S wavefields from the two far-offset, orthogonal-azimuth source stations are adjusted to time datum T at receiver station 80 (Fig. 2.9b), the shallowest receiver station in the vertical array. The receiver-station numbers decrease with increasing depth, with station 1 being the deepest receiver station.

The source stations where the data in Figure 2.9 were generated are labeled SP_A and SP_E for ease of reference to the data-acquisition geometry illustrated in Figure 2.7. Exact time coordinates are eliminated on the displays to ensure confidentiality of the data.

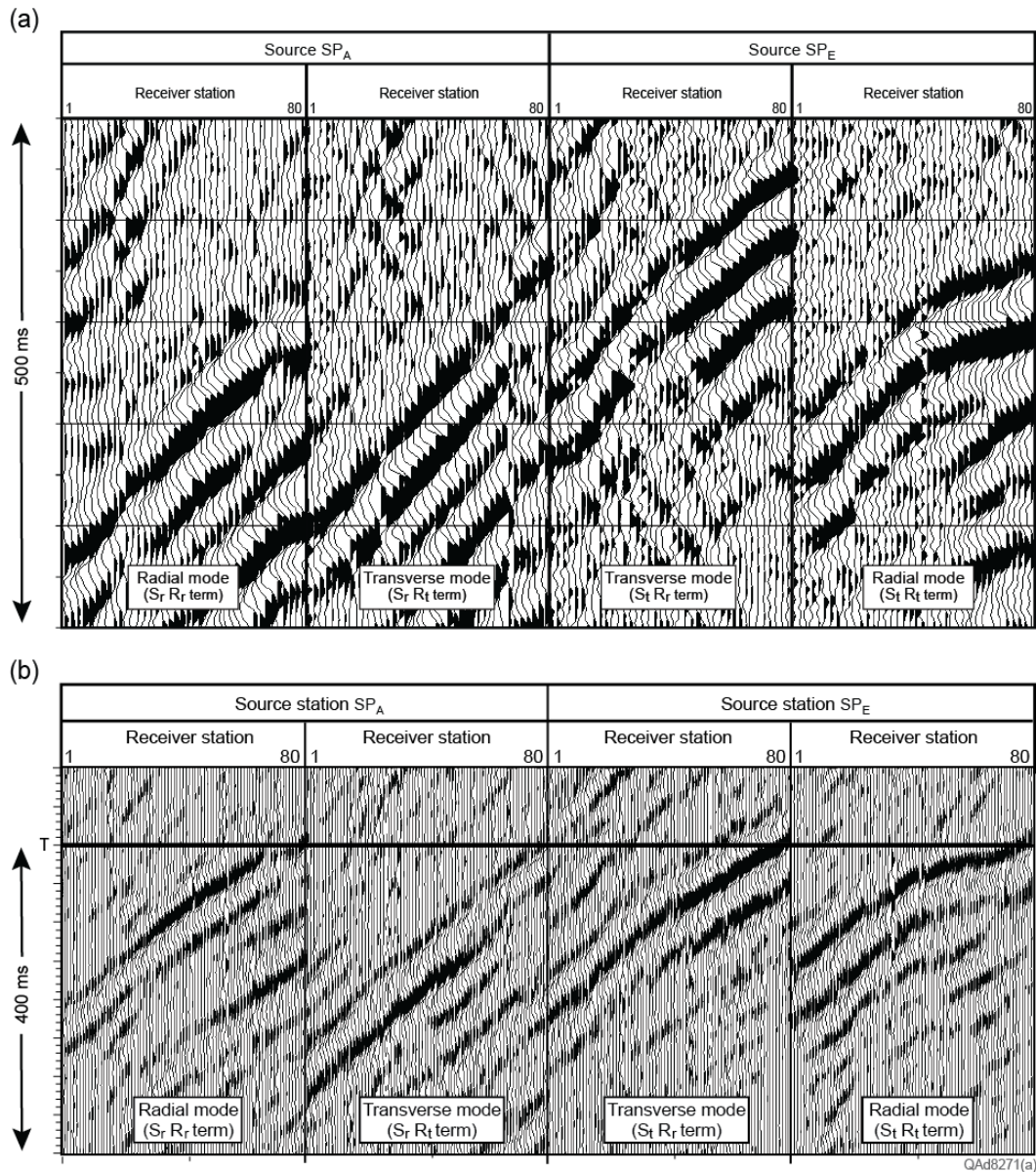


Figure 2.9. (a) Radial and transverse direct-S wavefields produced by two far-offset, orthogonal-azimuth vertical vibrators. (b) Wavefields after shifting the arrival times at receiver station 80 to a fixed time datum T to remove the effects of travel time differences through the overburden. Labels $S_r R_r$, $S_r R_t$, $S_t R_r$, $S_t R_t$ placed on the data panels correspond to matrix element terms used in the right-hand-side matrix of the Alford rotation equation (Fig. 2.2).

Improving Alford Rotation Accuracy with Gaussian Wavelets

More accurate estimates of natural-coordinate axis azimuths and wavelet travel times can be made by simplifying the data used in Alford rotation calculations. We found Alford rotation results were easier to interpret when short, compact SV wavelets were analyzed rather than longer SV-wave data traces that have complex wavelet properties.

Two attributes of SV wavelets that affect natural-coordinate calculations are: (1) wave shape, and (2) wavelet arrival time. The term *wave shape* includes all amplitude and phase characteristics of an SV wavelet. In order to apply Alford rotation analysis across thin 50-ft intervals between adjacent VSP receiver stations, we implemented two assumptions that not only simplified calculations, but more importantly, improved the accuracy of estimations of S_1 and S_2 travel times over short travel paths. These assumptions were:

1. S-wavelet arrival times dominate the results of Alford rotation more than do S-wavelet wave shapes, and
2. Alford rotation results are simpler and more accurate if simple mathematical wavelets are substituted for real-data S wavelets.

Our implementation of assumption 1 was to do precise arrival-time picking of direct-S first-arrival wavelets. Our implementation of assumption 2 was to replace all direct-S arrivals with a Gaussian wavelet, specifically with a 30-Hz Gaussian function. A generalized Gaussian function is shown on Figure 2.10 to illustrate the simple waveform character of the Gaussian function we used.

Alford rotation tests were done using a constant-amplitude Gaussian wavelet at each VSP receiver station and also by adjusting the amplitude of the Gaussian wavelet at each station to the amplitude of the real-data first arrival at that station. We found no difference in the estimated azimuths of natural-coordinate axes, or in estimates of S_2 time delay, when Alford Rotation was done using constant-amplitude Gaussian wavelets or true-amplitude Gaussian wavelets. An example of replacing real-data first-arrival wavelets with simpler Gaussian wavelets is illustrated on Figure 2.11.

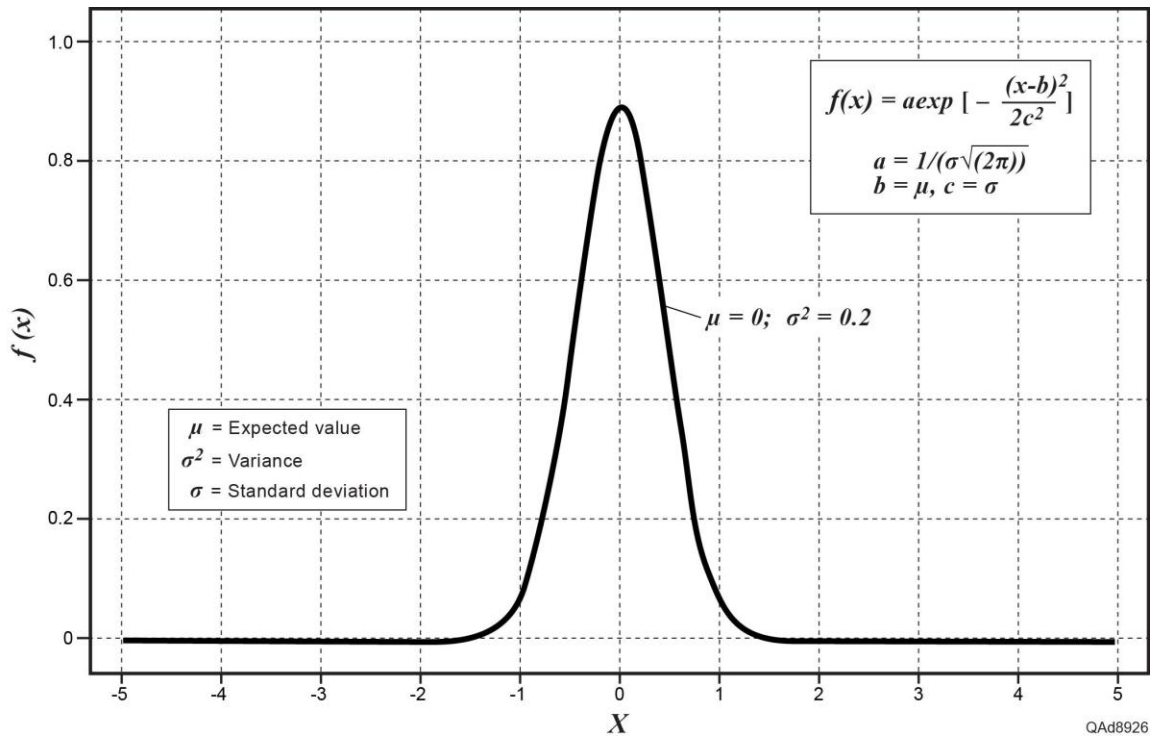


Figure 2.10. Generalized Gaussian function. A function of this type, with a central frequency of 30 Hz, was substituted for each S-wave first arrival to simplify Alford rotation analysis.

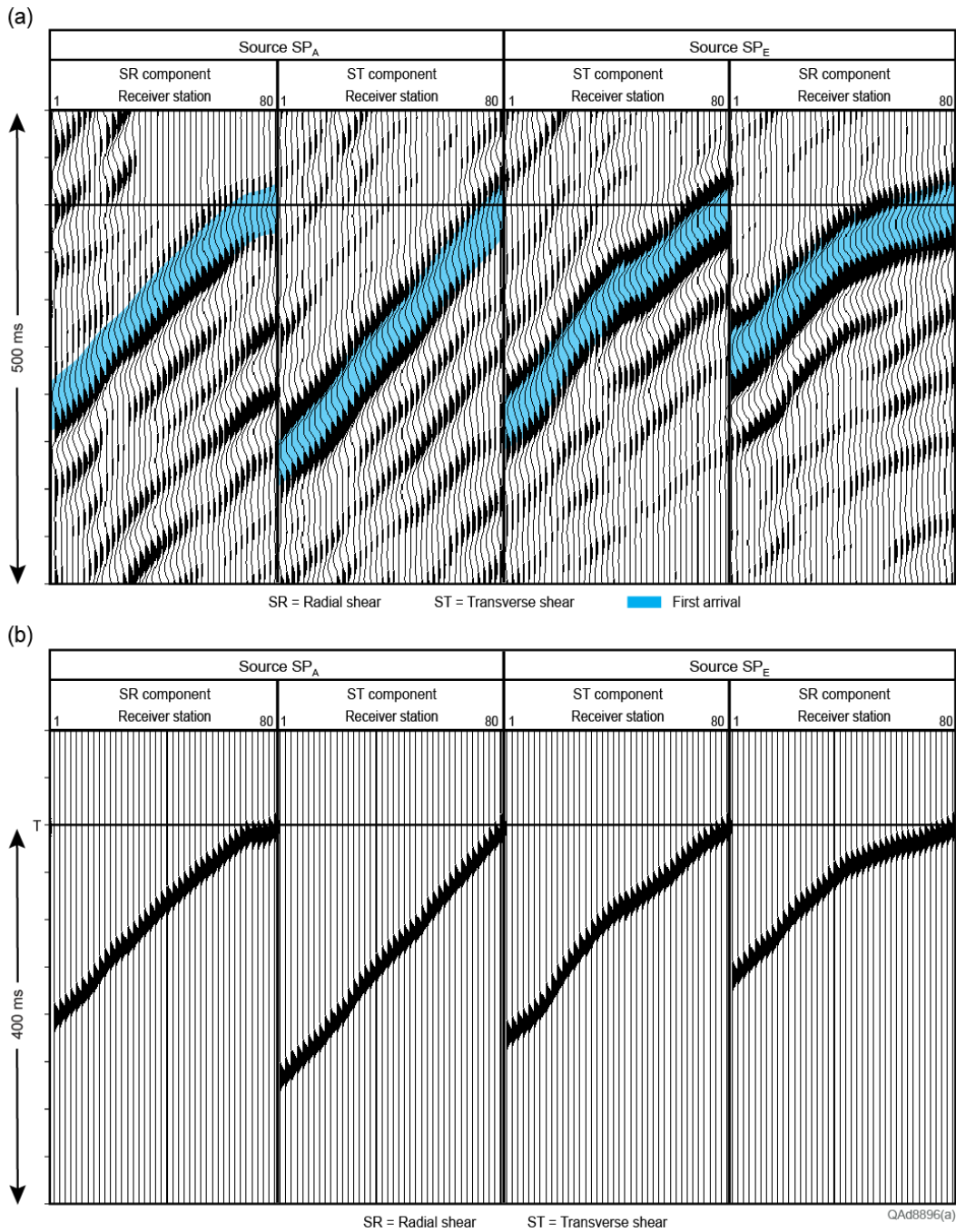


Figure 2.11. (a) Direct-S first arrivals generated at the two source stations introduced on Figure 2.9b (highlighted wavelet troughs). (b) Replacement 30-Hz Gaussian functions used for Alford rotation analysis. These Gaussian wavelets are centered on precisely determined first-arrival times of the shaded troughs shown in (a).

Natural Coordinates within the Overburden

The azimuths of natural-coordinate axes in the overburden above this unconventional reservoir can be estimated by performing an Alford rotation of the four wavelets from Figure 2.11b that are positioned at receiver station 80 at the top of the reservoir interval. These wavelets are the direct-S wavefields as they exit from the overburden. This rotation analysis is shown as Figure 2.12. Each data panel shows the four data-rotation elements of the left-hand-side matrix of Figure 2.2 for 10-degree axis rotations from 0 to 360 degrees. Natural-coordinate azimuths within the overburden are positioned where phase reversals occur in matrix terms S_{AR_A} , S_{AR_B} , S_{BR_A} , and S_{BR_B} (Figs. 2.2 and 2.3). These phase reversals imply the axes are oriented at azimuths of 50 and 140 degrees counterclockwise from the vertical plane passing through the VSP well and source station SP_A . The azimuth-dependent wavelet character displayed on Figure 2.12 is equivalent to the lab measured azimuth-dependent wavelet character shown on Figure 2.4. Note the wavelets in Figure 2.12 undergo a polarity reversal when a natural-coordinate axis is crossed just as did the wavelets in the laboratory experiment illustrated on Figure 2.4.

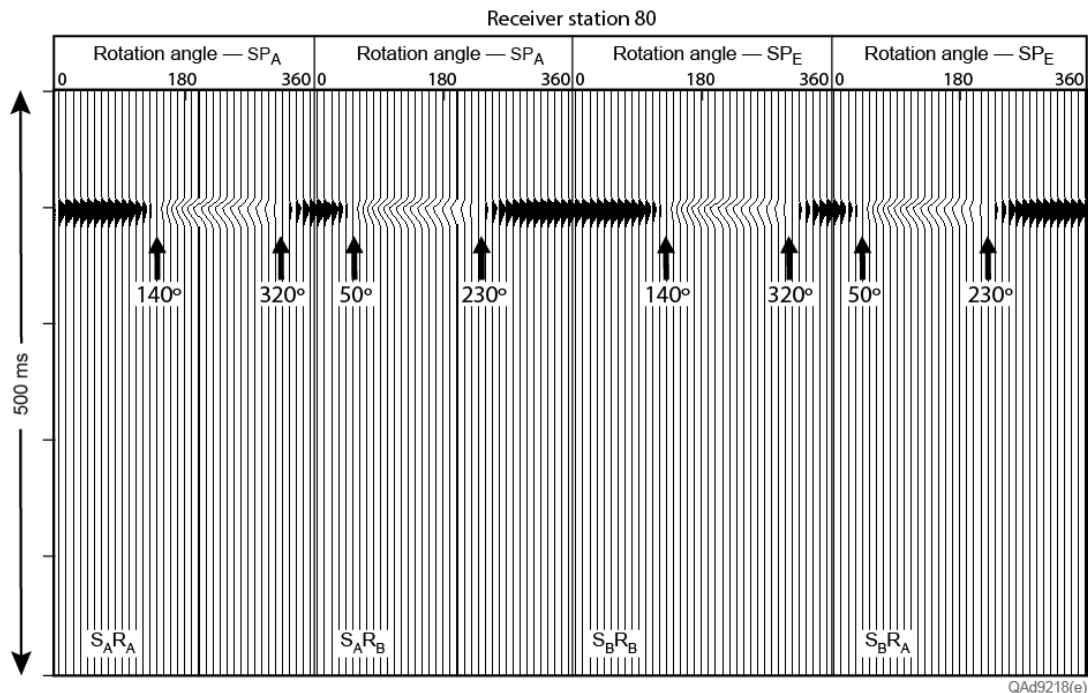


Figure 2.12. Alford rotation of direct-S wavelets at VSP receiver station 80 at the top of the reservoir interval. Radial and transverse data input to the Alford rotation procedure are defined by two orthogonal vertical planes. One plane passes through receiver 80 and vertical vibrator source station SP_A (Fig. 2.7), and the second plane passes through receiver 80 and source station SP_E (Fig. 2.7). These radial and transverse input-data axes are rotated in 10-degree azimuth increments to locate natural coordinate axes. At this receiver depth, direct-S wavefields are just emerging from the overburden and beginning to enter the reservoir interval. Alford rotation analysis implies the natural earth coordinates in the overburden above receiver station 80 are oriented 50 degrees and 140 degrees counterclockwise from the azimuth to source station SP_A .

Estimating Fracture Attributes

Alford rotation calculations at every twentieth VSP receiver station (intervals of 1,000 ft) across this reservoir section are displayed as Figures 2.13 through 2.16 to illustrate how fracture orientation and S-wave anisotropy (fracture density) are estimated within thick stratigraphic intervals (thickness spanned by 20 receiver stations = 1000 ft). In chapter 4, the procedure described here will be applied to thin 50-ft intervals between successive VSP receiver stations. The following calculations use the direct-S wavelets displayed on Figure 2.11b at receiver stations 60, 40, 20, and 1.

In each Alford rotation analysis, wavelets are projected onto new coordinate axes rotated counterclockwise from the two orthogonal receiver-source planes in increments of 10 azimuth degrees. One plane passes through each VSP receiver station and source station SP_A (Fig. 2.7); the other plane passes through each VSP receiver station and source station SP_E (Fig. 2.7). This coordinate transformation is done as coordinate axes rotate counterclockwise away from these two orthogonal source-receiver planes over a 360-degree range. Natural coordinate axes N1 and N2 are labeled on each figure. Note the similarity between these wavelets after they propagate through a fractured interval and the wavelet polarities and time delays exhibited on Figure 2.4 after lab-generated wavelets propagate through a simulated fractured medium.

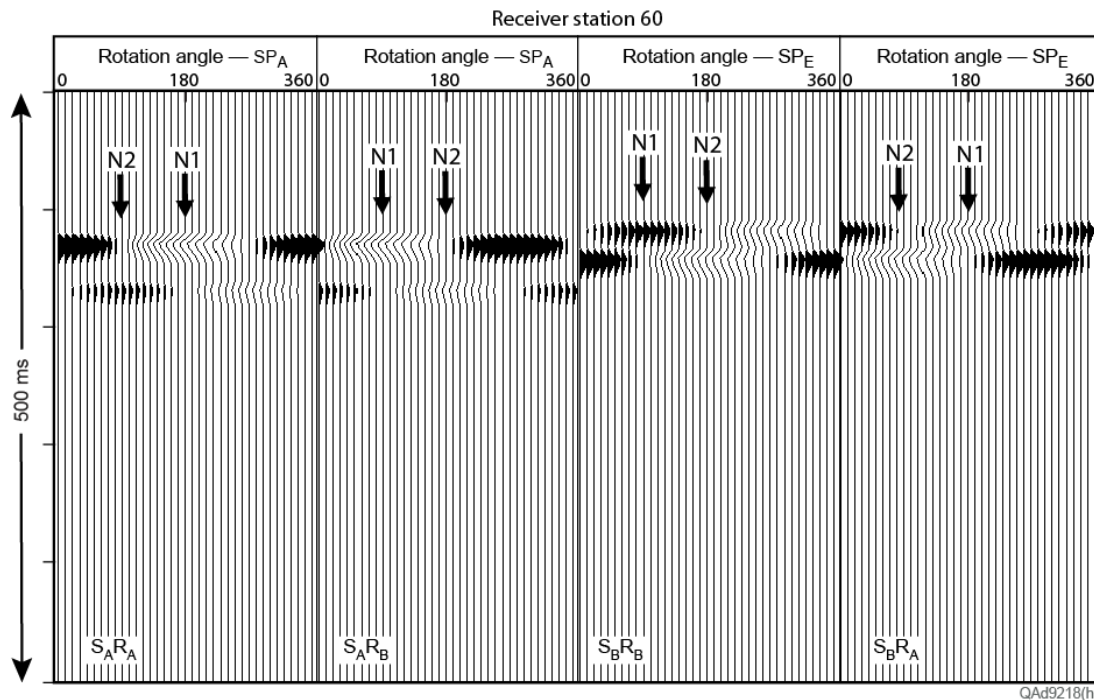


Figure 2.13. Alford rotation at receiver station 60 (1000 ft below receiver 80 of Figure 2.12) using direct-S wavelets propagating from source stations SP_A and SP_E (Fig. 2.7). N1 and N2 = azimuths of natural coordinate axes measured counterclockwise from source station SP_A .

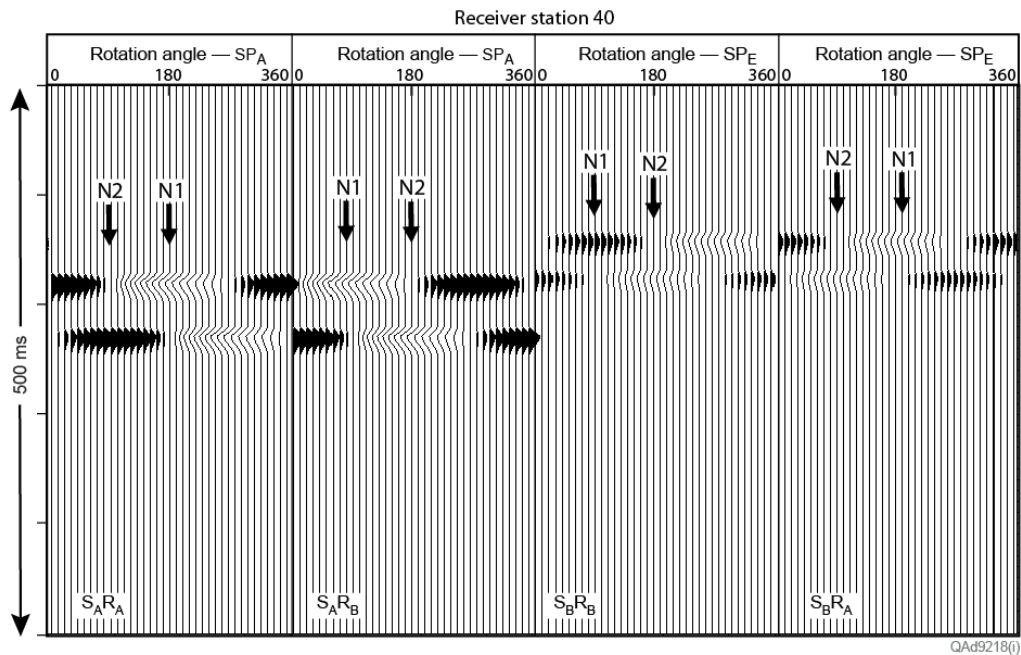


Figure 2.14. Alford rotation at receiver station 40 (1000 ft deeper than receiver 60, Fig. 2.13) using direct-S wavelets propagating from source stations SP_A and SP_E (Fig. 2.7). N1 and N2 = azimuths of natural coordinate axes measured counterclockwise from source station SP_A .

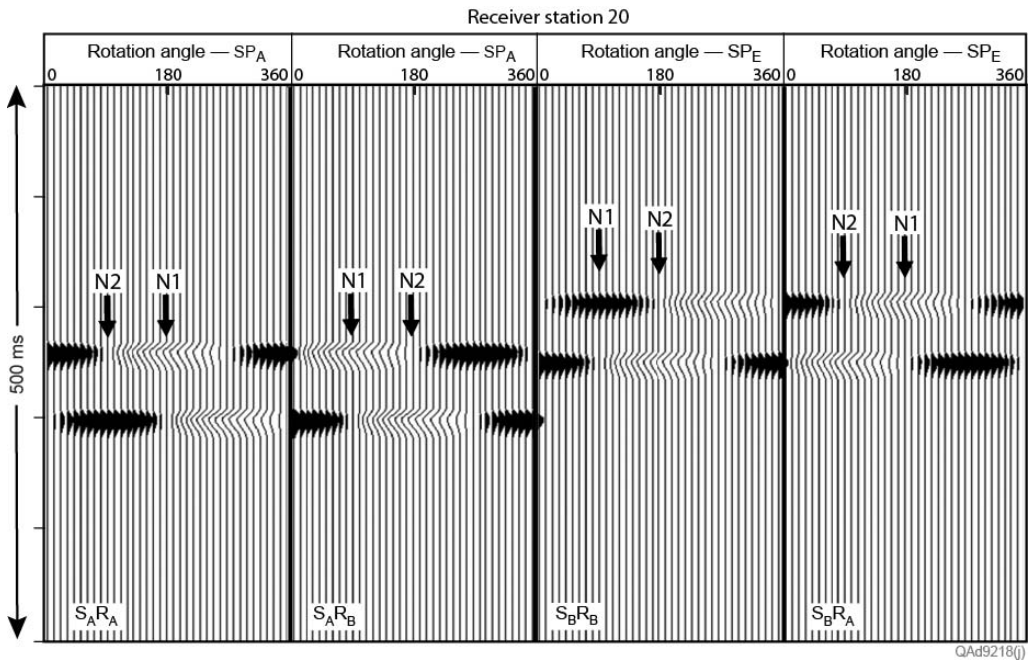


Figure 2.15. Alford rotation at receiver station 20 (1000 ft deeper than receiver 40, Fig. 2.14) using direct-S wavelets propagating from source stations SP_A and SP_E (Fig. 2.7). N1 and N2 = azimuths of natural coordinate axes measured counterclockwise from source station SP_A .

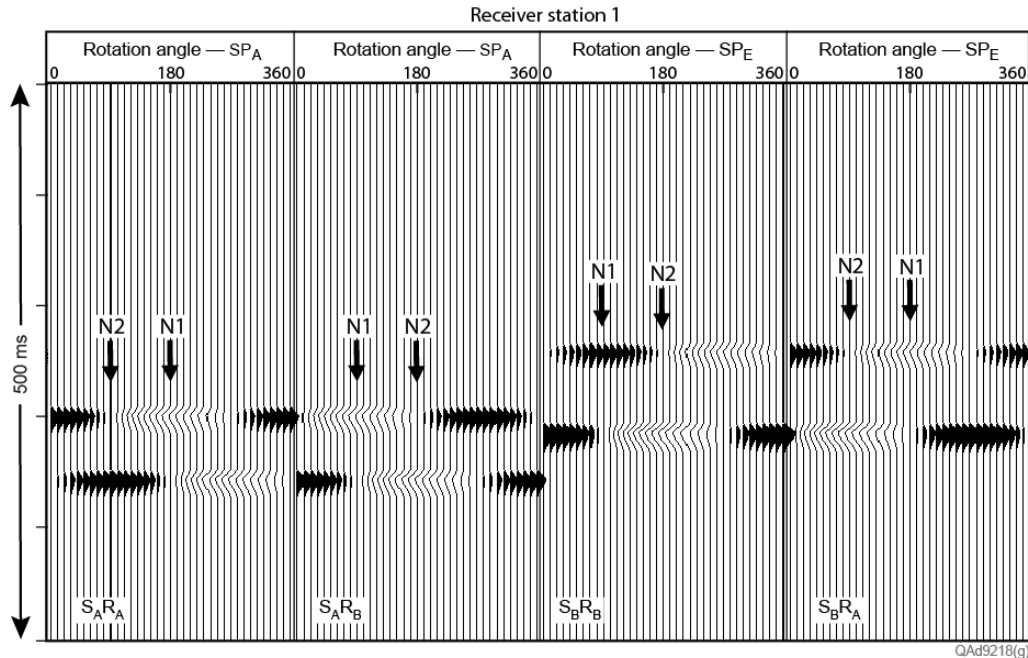


Figure 2.16. Alford rotation at receiver station 1 (1000 ft deeper than receiver 20, Fig. 2.15) using direct-S wavelets propagating from source stations SP_A and SP_E (Fig. 2.7). N1 and N2 = azimuths of natural coordinate axes measured counterclockwise from source station SP_A .

Fracture Orientation

Azimuths of natural coordinate axes N1 and N2 determined at receiver stations 60, 40, 20, and 1 remained fixed at 111 degrees and 21 degrees from North, respectively. The azimuth of axis N1 indicates fracture orientation stays fixed at 111 degrees from North across the entire extent of this reservoir interval.

Fracture Density

Fracture density within an interval is assumed to be proportional to S_2 time delay across that interval as illustrated on Figure 2.6. Alford Rotation analyses were done at all 80 VSP receiver stations of this VSP data set which allowed S_2 time delays to be determined at intervals of 50 ft across the 4000-ft of unconventional reservoirs penetrated by this VSP well.

The format used to display S_2 time delays is illustrated on Figure 2.17. At each VSP receiver depth, the azimuth behavior of slow-S and fast-S modes exhibited by each of the four matrix terms involved in an Alford rotation are calculated in the manner exhibited on Figures 2.13 through 2.16. The Alford rotation data panel calculated at receiver station 40 when data from source stations SP_A and SP_E are analyzed is shown as Figure 2.17c. The 37 traces of wavelet data on each panel of Figure 2.17c (0 to 360-degree analyses at

10-degree increments) are squashed into a narrow data display. Each of these four squash plots is then positioned at its correct time coordinates at the depth position of receiver 40 on separate time-vs.-depth plots as shown by the data-flow arrows. When this procedure is repeated at all 80 receiver stations, the result is the four depth-dependent estimates of S_2 time delay show as Figures 2.17a, b, d, and e. This display format of fast-S and slow-S mode propagation is a convenient way to summarize S_2 time delays along travel paths from a source station to each 50-ft depth increment of reservoir facies penetrated by a VSP well.

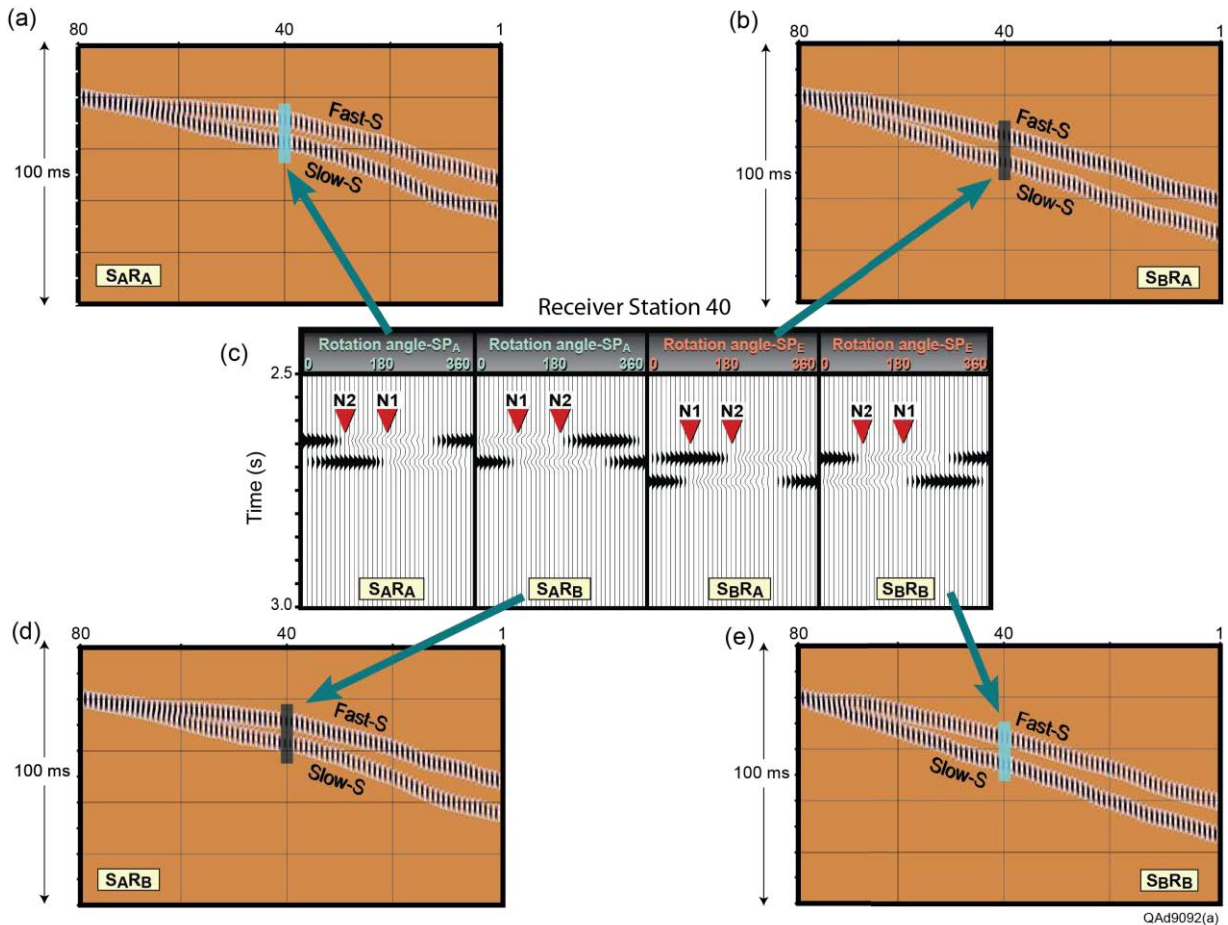


Figure 2.17. Display format used to show S_2 time delays determined at all 80 VSP receiver stations when vertical-vibrator direct-SV modes are produced at source stations SP_A and SP_E (Fig. 2.7). (a) Time-depth plot of S_1 and S_2 modes associated with the S_{1R} term of an Alford rotation. (b) Time-depth plot of S_1 and S_2 modes associated with the S_{1R} term of an Alford rotation. (c) The 4-term Alford rotation matrix calculated at receiver station 40. S_1 and S_2 wavelets on each of the four data panels of this display are converted to narrow squash plots and positioned at station coordinate 40 on the surrounding displays as shown by the data-flow arrows extending to (a), (b), (d), and (e) and the respective color bars on these plots. (d) Time-depth plot of S_1 and S_2 modes associated with the S_{1R} term of an Alford rotation. (e) Time-depth plot of S_1 and S_2 modes associated with the S_{1R} term of an Alford rotation. Note the similarity of (a) to (d) and of (b) to (e).

The time-depth plots exhibited as Figures 2.17a, b, d, and e are shown as larger displays on Figure 2.18. Using these larger data plots, it is easier to see that the time-depth behaviors of the S_1 and S_2 modes associated with the S_rR_r and S_rR_t matrix terms (Figs. 2.18a, 2.18b) are identical. These identical behaviors occur because these two terms describe S_2 time delays along the same travel paths, these being travel paths from source station SP_A to each receiver station in the 4000-ft vertical array in the VSP well.

The time-depth behaviors of the S_1 and S_2 modes associated with the S_tR_r and S_tR_t matrix terms (Figs. 2.18c, 2.18d) are also identical because they, like the S_rR_r and S_rR_t matrix terms, describe S_2 time delays along identical travel paths. However, in this case the travel paths are from source station SP_E to each VSP receiver station, not from source station SP_A .

S_2 time delays defined by S_tR_r and S_tR_t matrix terms (Figs. 2.18c, 2.18d) differ from S_2 time delays exhibited by S_rR_r and S_rR_t matrix terms (Figs. 2.18a, 2.18b) because the travel paths from source station SP_E propagate through a different part of the reservoir system than do travel paths from source station SP_A . Thus an advantage of this application of Alford rotation analysis is that it provides estimates of fracture density (S_2 time delays) through different portions of a fracture system penetrated by a VSP well. The two distinct sections of the reservoir that are probed depend on where the two vertical-vibrator source stations are positioned.

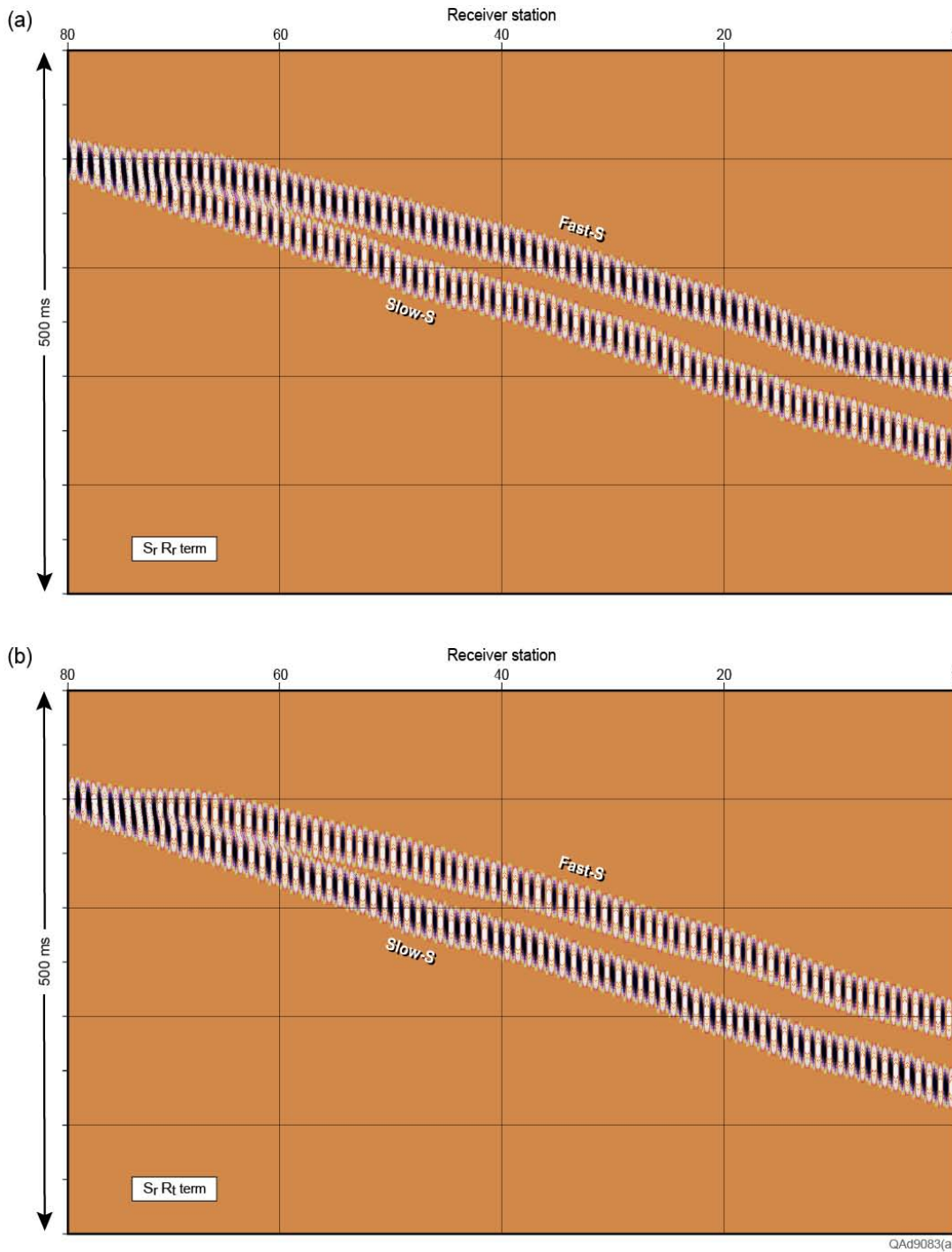
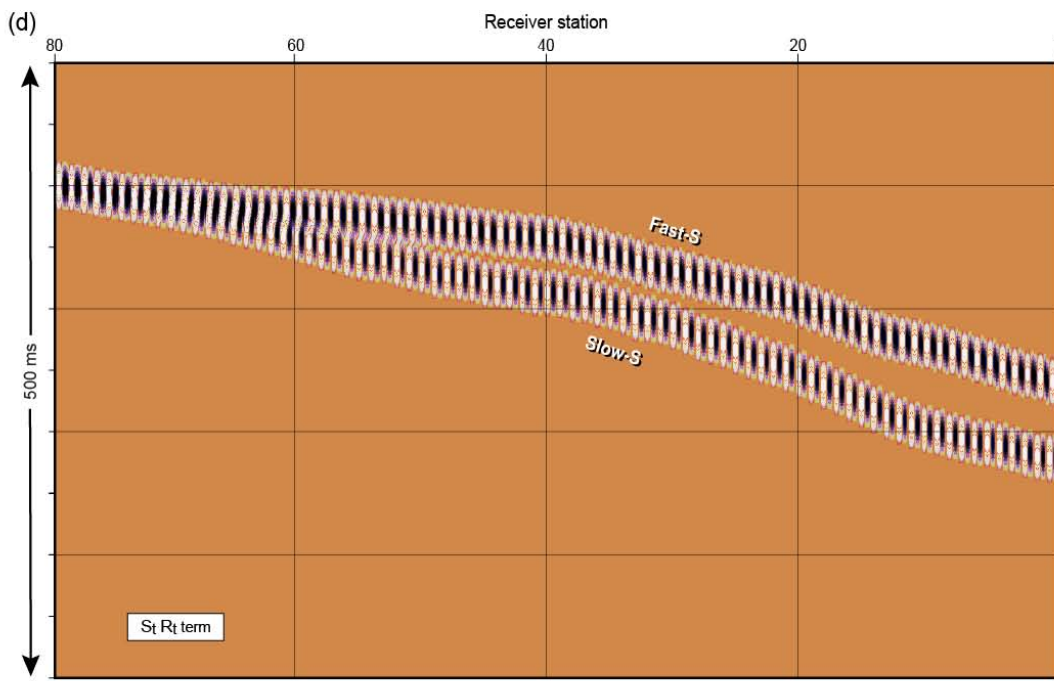
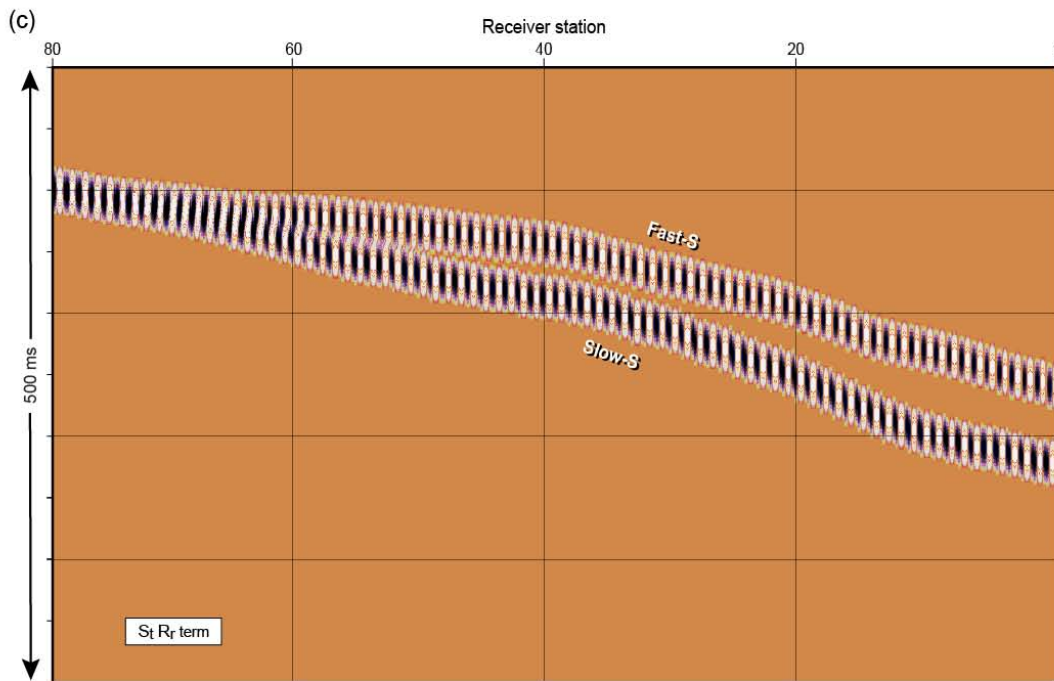


Figure 2.18. Time-depth plots of fast-S and slow-S modes along selected travel paths through a thick fractured reservoir. Fast-S and slow-S arrivals times are extracted from the four terms of the Alford rotation performed at each receiver depth. (a) Travel paths from source station SP_E to all 80 VSP radial receivers (matrix term $S_r R_r$). (b) Travel paths from source station SP_E to all 80 VSP transverse receivers (matrix term $S_r R_t$).



QAd9085(a)

Figure 2.18, cont. (c) Travel paths from source station SP_A to all 80 VSP radial receivers (matrix term $S_t R_r$). (d) Travel paths from source station SP_A to all 80 VSP transverse receivers (matrix term $S_t R_t$).

Data Window Effects in Calculating S-Wave Anisotropy

The differences in fast-S and slow-S arrival times are rather easy to evaluate in Figures 2.12 through 2.18 because compact Gaussian wavelets are used to display S_1 and S_2 travel time coordinates. The use of short, simple waveforms as representations of S_1 and S_2 wavelets is quite important for extracting optimal S-wave anisotropy information from Alford rotation results. S-wave modes produced by an orthogonal-source pair will be used to illustrate how window length and wavelet shape affect calculations of S-wave anisotropy. These comparisons are illustrated on Figure 2.19. The data show compelling evidence that fast-S and slow-S modes are difficult to recognize when the input data to an Alford rotation calculation are long sequences of peaks and troughs. For example, S-wave anisotropy calculated for 500-ms real-data windows is impossible to interpret (right panel in Figure 2.19c). Likewise, it is not possible to interpret polarity reversals in Alford-rotation matrix terms to determine natural coordinate azimuths (center panel of Figure 2.19c).

When the input data to an Alford rotation calculation are restricted to short real-data windows that span S-wave first arrivals, it is possible to recognize polarity reversals in matrix terms (center panel of Figure 2.19b). Thus azimuths of natural coordinate axes can be estimated. However, it is still not possible to measure S-wave anisotropy with confidence and reliability (right panel of Figure 2.19b). The important principle is that azimuths of natural coordinate axes as well as S_2 time delays can be best measured when the input data to an Alford-rotation analysis are short, simple, mathematical wavelets such as Gaussian wavelets (Fig. 2.19a).

Thus window lengths used in Alford rotation analyses have profound effects on the ease and confidence with which calculation results can be interpreted. Short, compact, simple wavelets confined to narrow data windows should always be used in Alford rotation analyses if possible.

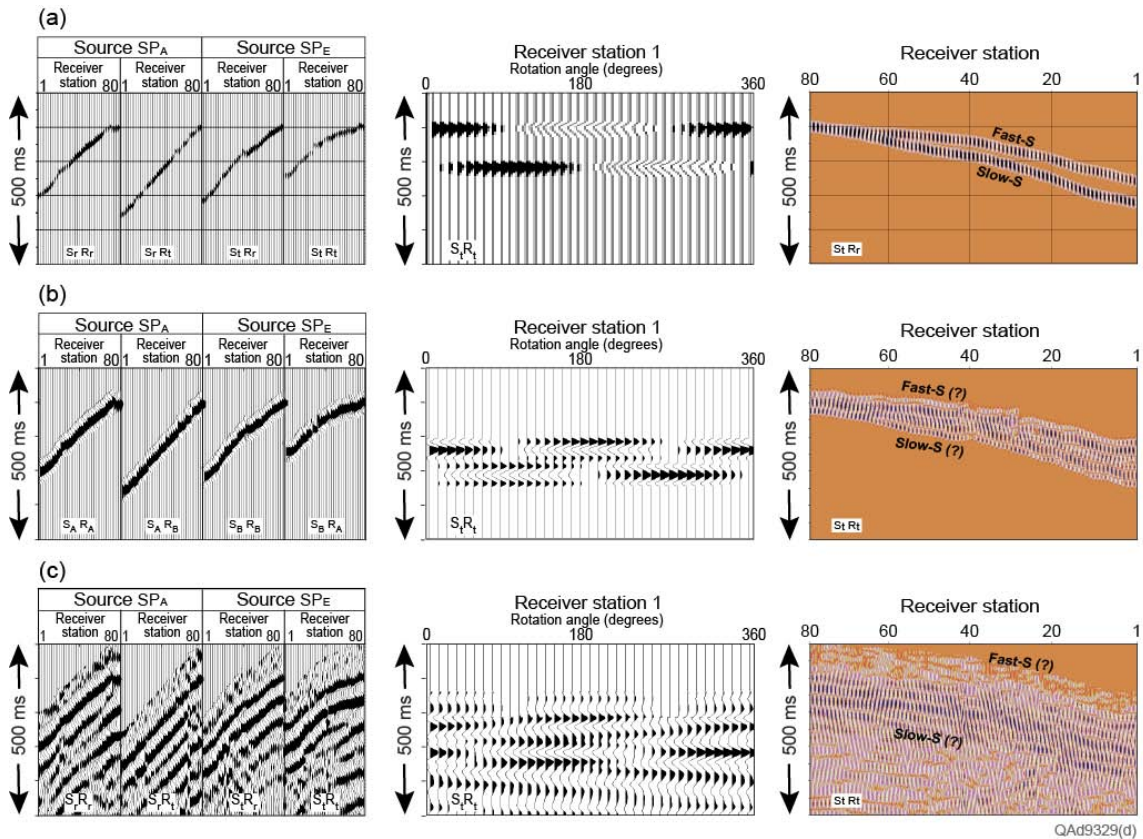


Figure 2.19. Influences of window length and wavelet shape on Alford-rotation calculations of fracture attributes. (a) Short data window and simple mathematical wavelet shape (Gaussian wavelet). (b) Longer data window and actual first-arrival wavelets. (c) 500-ms data windows immediately following S-wave first arrivals. The azimuths where data polarity reversals occur are easy to see in (a), reasonably obvious in (b), but impossible to interpret in (c). Examination of the right-side column of panels shows S-wave anisotropy can be easily measured in (a) but cannot be interpreted in (b) or (c).

Interpreting Alford Rotation Results

The Alford rotation results displayed as Figures 2.12 through 2.16 define two attributes of the direct-S modes that propagate in the fractured tight sandstone reservoirs where these VSP data were acquired:

1. The time delays between radial-S and transverse-S modes as these two modes propagate through the layered, fractured section where the VSP data were acquired. The time delays between radial-S and transverse-S modes are assumed to be reasonable proxies of the time delays between the fast-S and slow-S modes that could be estimated with Alford rotation if the VSP data had been generated by orthogonal horizontal vibrators positioned at a single source station rather than by two vertical vibrators positioned at two different stations whose azimuths from the VSP well differed by 90 degrees.

2. The azimuths in which natural coordinate axes of the fracture system are oriented. These azimuth estimations imply the natural coordinate axes in the overburden have orientations of 50-degrees and 140-degrees counterclockwise from source station SPA (Fig.2.12) and then change to azimuth orientations of 0-degrees and 90-degrees through the entire 4000-ft thickness of reservoir section (Figs. 2.13 to 2.16).

The fundamental purpose of the Alford rotation procedure was to determine the azimuths of the natural coordinate axes within the fractured interval. To establish confidence in the reliability of the fracture orientations (the azimuth of the N1 natural coordinate axis labeled on Figures 2.13 to 2.16), redundancy calculations involving VSP data generated at different choices of orthogonal vertical-vibrator stations need to be compared. These comparisons are made in Chapter 3. These redundancy checks indicate fracture orientation cannot be determined with direct-S modes produced by vertical vibrators. This conclusion will be discussed in Chapter 3.

The time delays between the radial-S and transverse-S modes could be taken directly from the measured first-arrival times of the two modes at a receiver station rather than using an Alford rotation analysis to show the travel time difference of radial-S and transverse-S modes. However, we found it useful to convert Alford rotation results such as those shown on the individual panels of Figures 2.13 to 2.16 to be shown in squash-plot form at all 80 receiver stations. This technique is described in Figure 2.17. We found expanded views of the squash plots (Fig. 2.18) provided easy-to-understand indicators of fracture intensity (S-wave anisotropy) around the VSP well.

Conclusions

A logical data-processing procedure has been developed to analyze direct-S modes generated by vertical vibrators and recorded by downhole VSP receivers. The fundamental data-processing step is the application of the Alford rotation algorithm to direct-S first arrivals. We show that Alford rotation results are easier to analyze and interpret when two simple steps are taken:

1. Limit the data analysis to a narrow window centered on the first arrivals of the downgoing direct-S wavefields, and
2. Replace the complex shape of each direct-S first arrival wavelet with a simple-shape Gaussian wavelet.

Alford rotation results calculated in this manner yield data that allow valuable visualization of fracture intensity (fracture density) around a VSP well and also indicate the azimuth orientations of fracture orientation. To do a thorough

research investigation, in Chapter 3 we will do Alford rotation analyses using several different pairs of orthogonally positioned vertical vibrators to confirm if these repeated analyses produce consistent estimates of fracture orientation.

Chapter 3

VSP Analysis 1 – Marcellus Shale Prospect

Introduction

VSP data presented in this chapter were acquired in a well drilled to evaluate a Marcellus Shale prospect in northeast Pennsylvania. The exact coordinates of the VSP well, the well name, and its API number will not be provided to protect the business interest of the operator who allowed the data to be used for this study. The general location of the well is labeled on the map shown as Figure 1.2 of Chapter 1.

VSP Source-Receiver Geometry

An extensive walkaround (WAR) VSP program was implemented at this study site. Data from 70 WAR VSP stations were analyzed. A map of these WAR vertical-vibrator stations is shown as Figure 3.1. These source stations allow VSP data to be studied at azimuth increments of approximately 5 degrees around the VSP well.

A vertical array of sixteen 3-component geophones recorded these WAR VSP data. Receiver stations were separated by 50 ft to create an 800-ft vertical array. This vertical array was positioned so that it was centered on the Marcellus Shale interval as illustrated on Figure 3.2. While recording the data generated at all of the 70 WAR source stations, the vertical array was not moved, nor was any geophone in the array unlocked.

Comparing the source offset distances (Fig. 3.1) with the geophone depths (Fig. 3.2) shows that some of these VSP data were generated at offsets that exceed receiver depth. Thus direct-P and direct-S raypaths arrive at receiver stations at significant slant-path angles. This source-receiver geometry deviates significantly from the zero-offset, vertical travel-path conditions that are assumed for S-wave data used in Alford rotation analyses (Chapter 2).

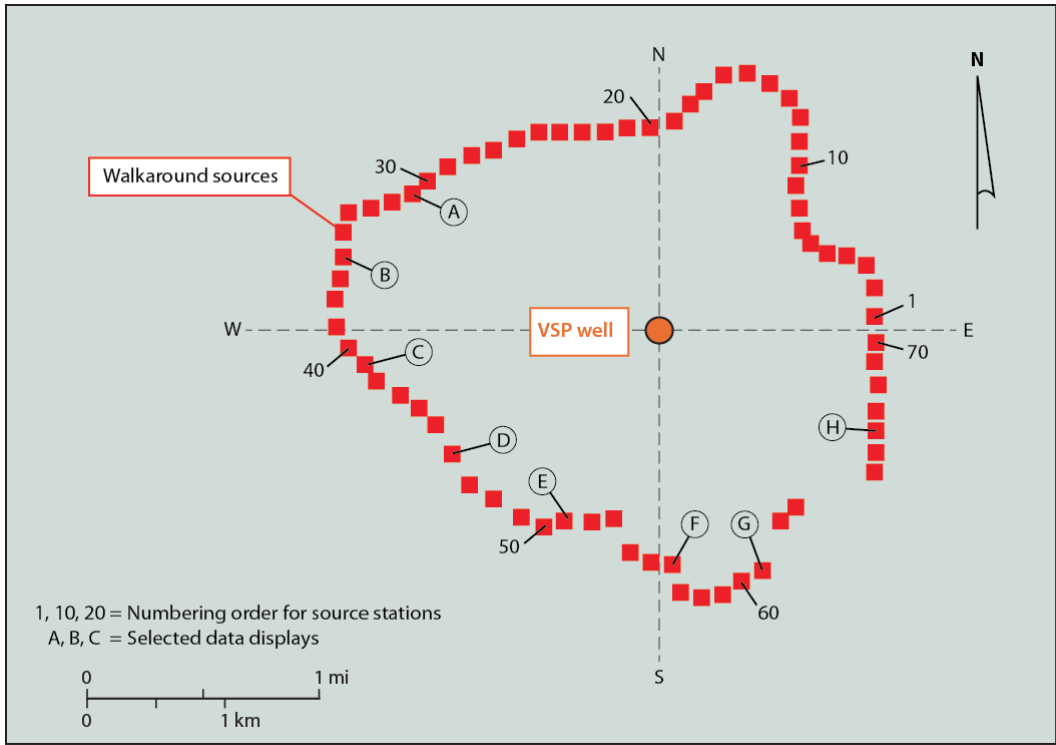


Figure 3.1. Walkaround source stations 1 through 70 occupied by vertical vibrators. Data generated at stations A through H are displayed later on Figure 3.8

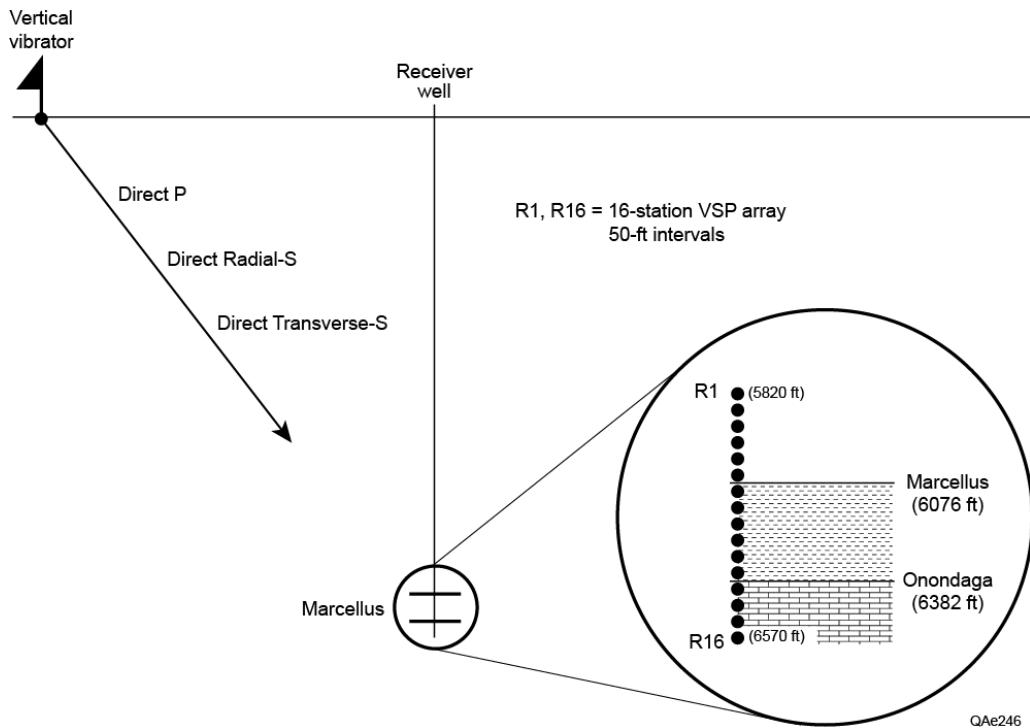
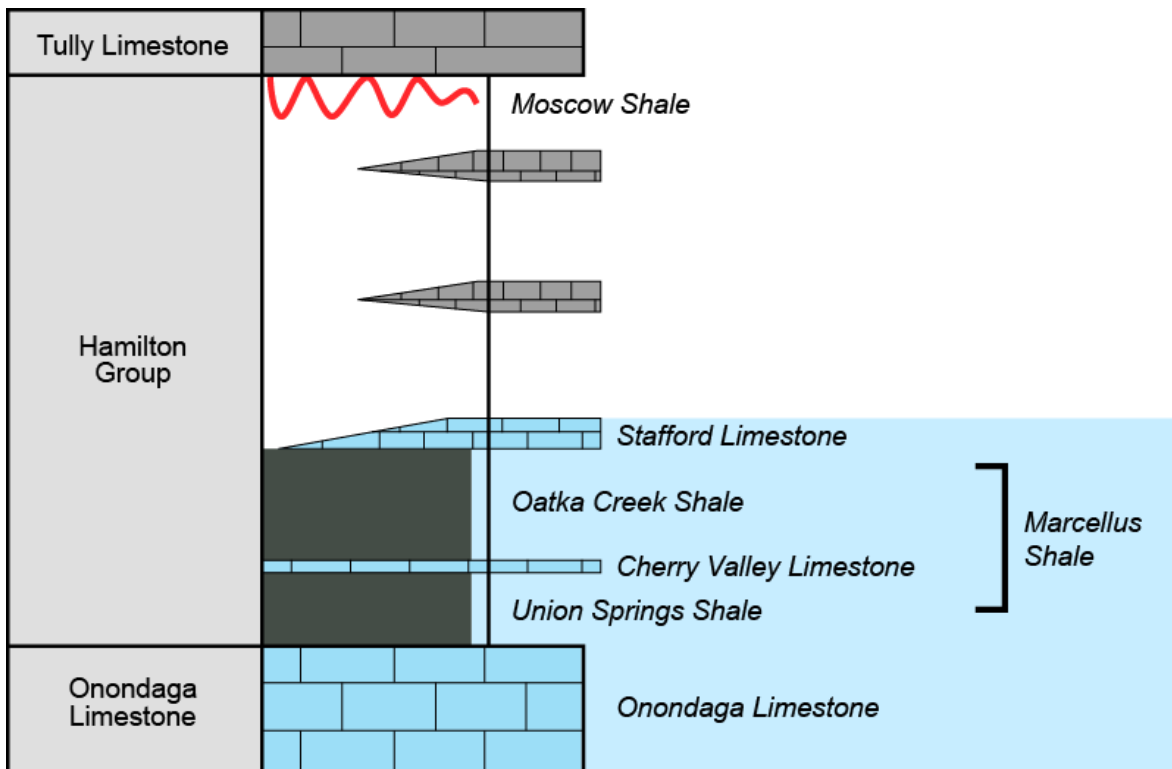


Figure 3.2. Positions of downhole receivers that recorded direct-P and direct-S modes produced at the WAR VSP stations.

Stratigraphic Column

The Marcellus Shale is a Middle Devonian black shale deposited across the Appalachian Basin and is a member of the Hamilton Group, a dominant part of the Middle Devonian rocks within this basin. A generalized stratigraphic column of Middle Devonian units local to this VSP well is displayed as Figure 3.3. The Tully Limestone is a strong seismic reflector at the top of the Hamilton Group. Some people use the downgoing P-SV converted mode produced at the Tully to study VSP S-wave attributes across the deeper Marcellus interval. An intriguing aspect of the Marcellus Shale is that it is an orthorhombic rock. The entire Marcellus Shale interval is fractured by two systems of vertical joints that are orthogonal to each other. These orthogonal joint sets, combined with the layered nature of the shale, create a classic orthorhombic medium.



QAd9571

Figure 3.3. Middle Devonian stratigraphy in New York and Northern Pennsylvania. The Tully Limestone and the Marcellus Shale create high-amplitude P and S reflections that dominate the seismic response across the Hamilton Group. Modified from Lash, 2007.

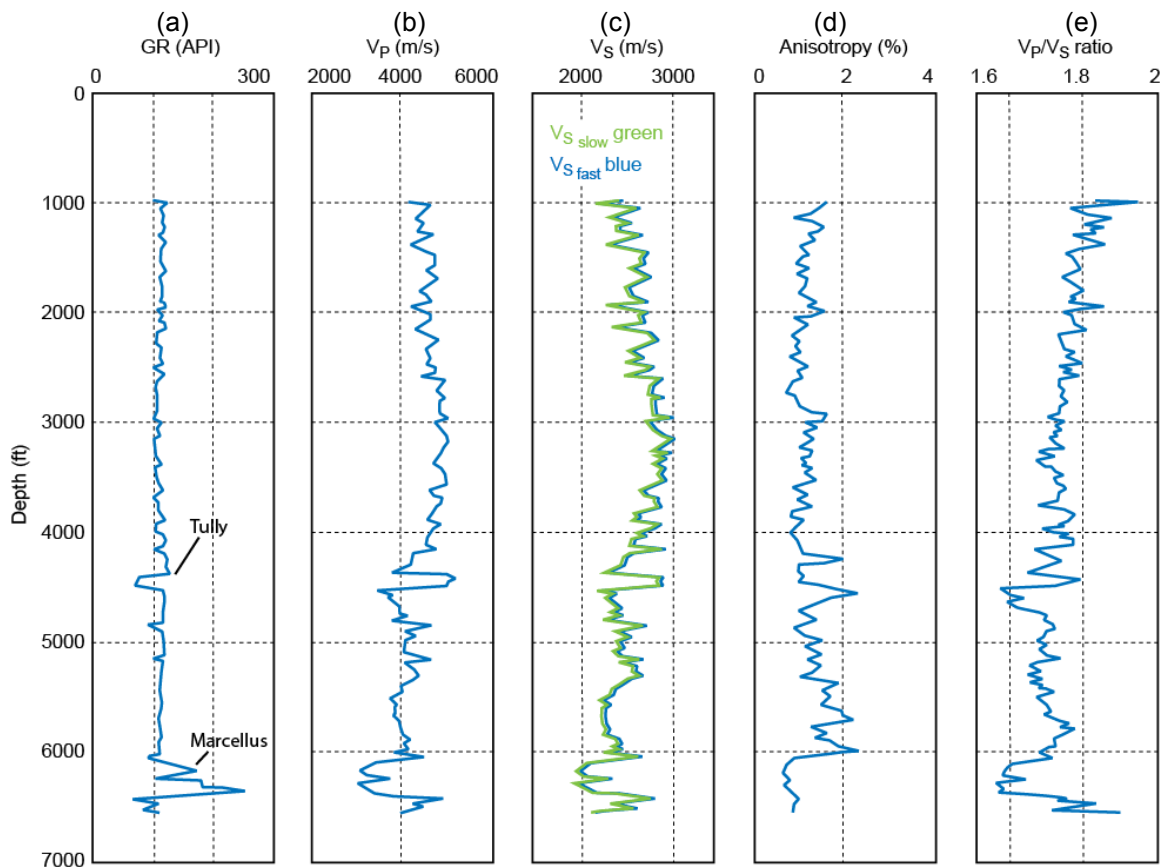
Calibration Database

Gamma-ray (GR) and velocity logs acquired in our VSP study well are displayed on Figure 3.4. The low-GR/high-velocity interval response between

4400 and 4500 ft (1341 and 1372 m) is the Tully Limestone. The high-GR/low-velocity interval response between 6100 and 6500 ft (1859 and 1981 m) is the Marcellus Shale. Fast-S and slow-S velocities calculated from dipole sonic log data by a well-log contractor show only minor differences across the entire well depth (Fig. 3.4c). The anisotropy curve plotted on Figure 3.4d is a measure of the difference between slow-S velocity [$V_S(\text{slow})$] and fast-S velocity [$V_S(\text{fast})$] calculated as,

$$(3.1) \quad \text{ANISO} = \{ [V_S(\text{fast}) - V_S(\text{slow})] / V_S(\text{slow}) \} \times 100.$$

In this equation, ANISO is the S-wave velocity anisotropy value plotted on Figure 3.4d. The anisotropy calculated for the entire logged interval is only 1 to 2 percent. This is a low value of S-wave anisotropy, particularly for a shale rock, and is a surprising result for an orthorhombic medium such as the Marcellus Shale. The importance of this log-based estimate of S-wave anisotropy is that it provides an independent calibration of S-wave anisotropy that can be used to judge the value of S-wave anisotropy estimated from direct-S modes produced by vertical vibrators. This comparison is made later in this chapter.



QAd8328

Figure 3.4. (a) Gamma-ray, (b) V_P , and (c) V_S velocity logs acquired in the VSP well. Both fast-S and slow-S velocities are shown on (c) and are used to calculate S-wave anisotropy (d). The V_P/V_S velocity ratio (e) is based on fast-S velocity.

Examples of Raw Unprocessed VSP Data

Raw unprocessed VSP data generated at all 70 WAR source stations are displayed on Figures 3.5 through 3.7. In preparing these displays, vertical geophones were not inclined to align with downgoing P displacement vectors, thus the vertical-geophone data in Figure 3.5 show not only direct-P arrivals (at approximately 0.6 s) but also direct-SV arrivals (at approximately 1.0 to 1.1 s). This option for orienting vertical geophones was used to illustrate the arrival time relationships between direct-P and direct-SV modes, and to emphasize the fact that amplitudes of direct-SV modes are usually more robust than amplitudes of their companion direct-P modes. In contrast, horizontal geophone H1 at each receiver station was inclined in the vertical plane passing through the receiver station and the source station (Fig. 3.6) so that it aligned with downgoing SV displacement vectors. Consequently the data in Figure 3.6 show robust direct-SV arrivals but only hints of the direct-P arrivals. Horizontal geophone H2 at each receiver station was oriented perpendicular to the vertical plane passing through the source and receiver stations (Fig. 3.7). This rotation procedure for the two horizontal geophones is illustrated on Figure 2.8 of Chapter 2. Each data strip in Figures 3.5 through 3.7 has 16 data traces that show the response of the 16-station receiver array (Fig. 3.2) to each individual source of the 70 source-station walkaround VSP

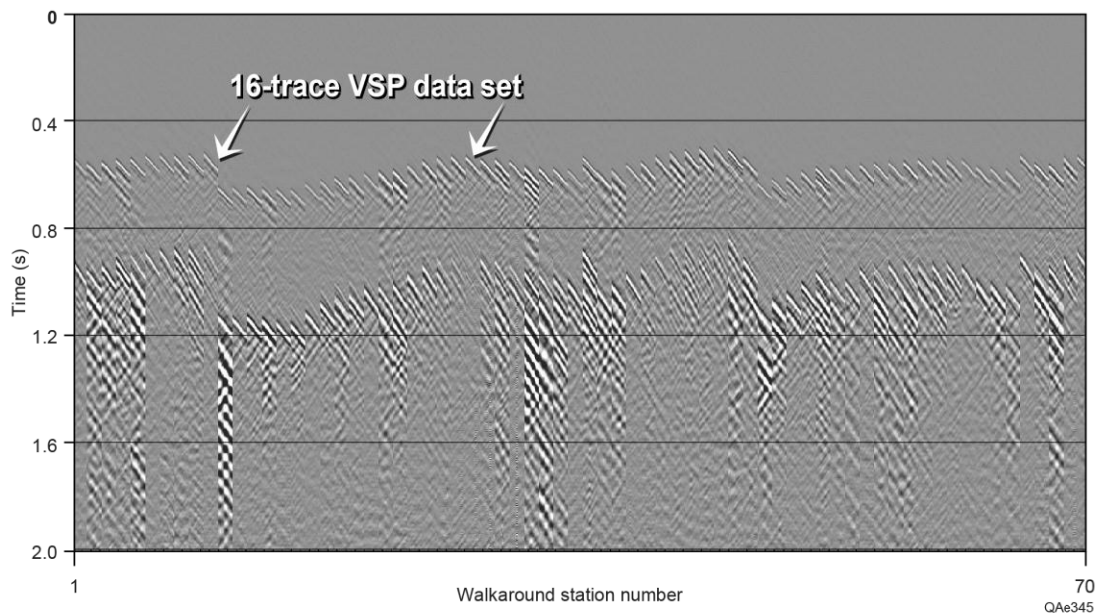


Figure 3.5. Responses of untilted vertical geophones for all 70 WAR VSP source stations. The sensor array consisted of 16 receiver stations spanning 5820 to 6570 ft. Each of the 70 data strips contains the 16-trace output of the unrotated vertical geophones.

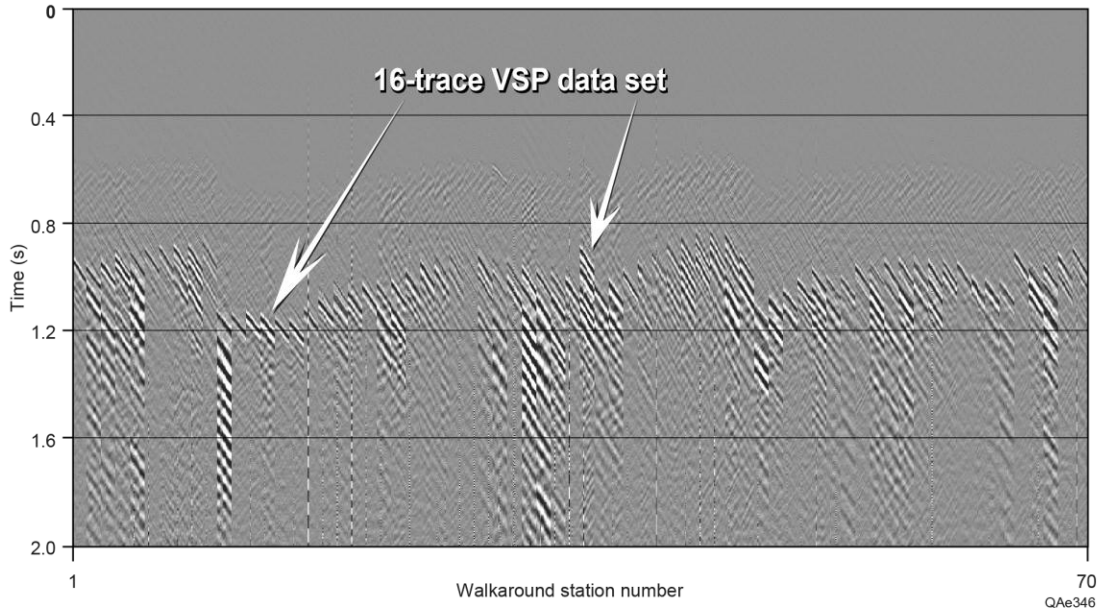


Figure 3.6. Responses of rotated and tilted radial-horizontal geophones for all 70 walk-around source stations. The sensor array consisted of 16 receiver stations spanning 5820 to 6570 ft. Each of the 70 data strips contains the 16-trace output of the rotated radial geophones.

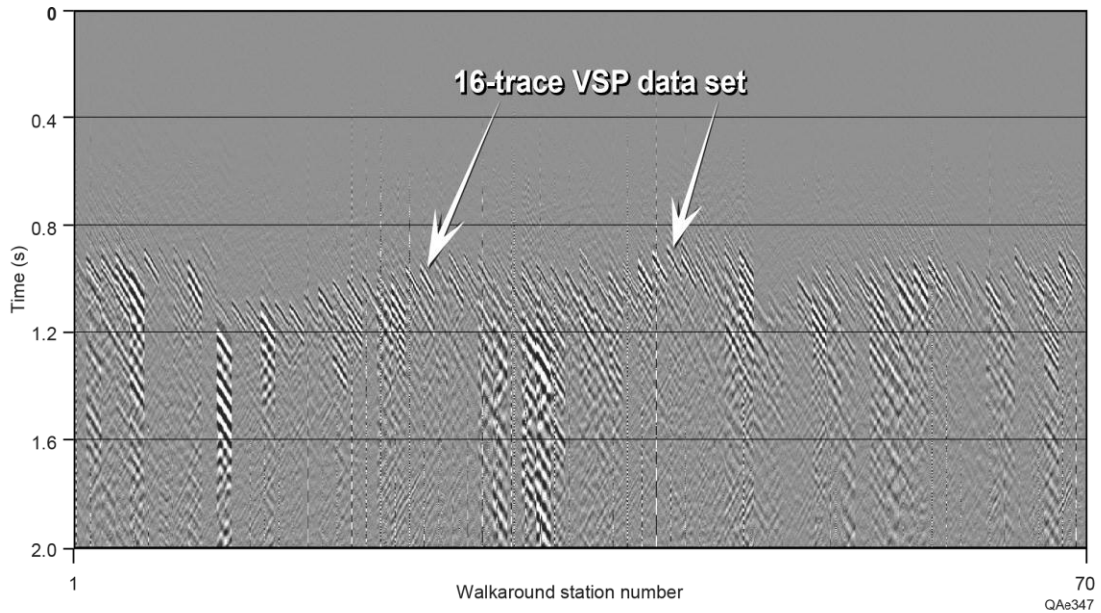


Figure 3.7. Responses of rotated transverse-horizontal geophones for all 70 walk-around source stations. The sensor array consisted of 16 receiver stations spanning 5820 to 6570 ft. Each of the 70 data strips contains the 16-trace output of the rotated transverse geophones.

The scale of these displays does not allow the quality of these WAR VSP data to be appreciated. Expanded displays of direct-S modes propagating from several vertical-vibrator source stations are presented as Figure 3.8 to illustrate the high signal-to-noise character of these particular VSP data. Source station locations A through H labeled on the data strips are defined on the map shown as Figure 3.1. Each data strip in Figure 3.8 displays the 16 data traces recorded by the 16-station receiver array for each of these eight selected source stations.

In these displays, events that slope down to the right are downgoing events. Events that slope down to the left are upgoing events. When 3-component VSP geophones are properly rotated in azimuth and in inclination (Figure 2.8 of Chapter 2), upgoing SV reflections and downgoing P events appear on the same geophone. Examples of this data-acquisition principle are labeled on the *rotated vertical geophone* response displayed on Figure 3.8a. Downgoing SV events and upgoing P reflections also both appear on the same geophone, the *rotated radial geophone*, as shown by the labeling on Figure 3.8b. Downgoing and upgoing SH events appear on only the *rotated transverse geophone* (Fig. 3.8c).

Examples of Processed VSP Data

Equation 3.1 defines S-wave anisotropy in terms of fast-S and slow-S velocities. The velocities $V_S(\text{fast})$ and $V_S(\text{slow})$ used in this equation can be interval velocities, rms velocities, or average velocities across a fractured interval. In our investigation, we opted to calculate average velocities of direct-S modes across the Marcellus interval in order to estimate S-wave anisotropy within the Marcellus Shale. Spatial variations of S-wave anisotropy determined in this manner are assumed to indicate spatial variations in fracture density within the Marcellus.

In order to calculate accurate values of S-wave average velocities, it is essential to interpret a consistent phase of the VSP first-arrival wavelets that propagate from each vertical-vibrator source station. The time coordinates of these consistent wavelet phases define accurate travel times of direct-S modes from source to receiver, which in turn yield accurate estimates of average S-wave velocities from all source stations. Examples of direct-P and direct-S modes arriving at the shallowest VSP receiver station are displayed as Figure 3.9. Data are shown for all 70 WAR source stations. The direct-P first-arrival wavelets (Fig. 3.9a) have a stable waveshape, and it is not difficult to interpret a consistent wavelet phase to represent each direct-P arrival time. The interpreted arrival time for each P-wave wavelet is marked with a tic mark.

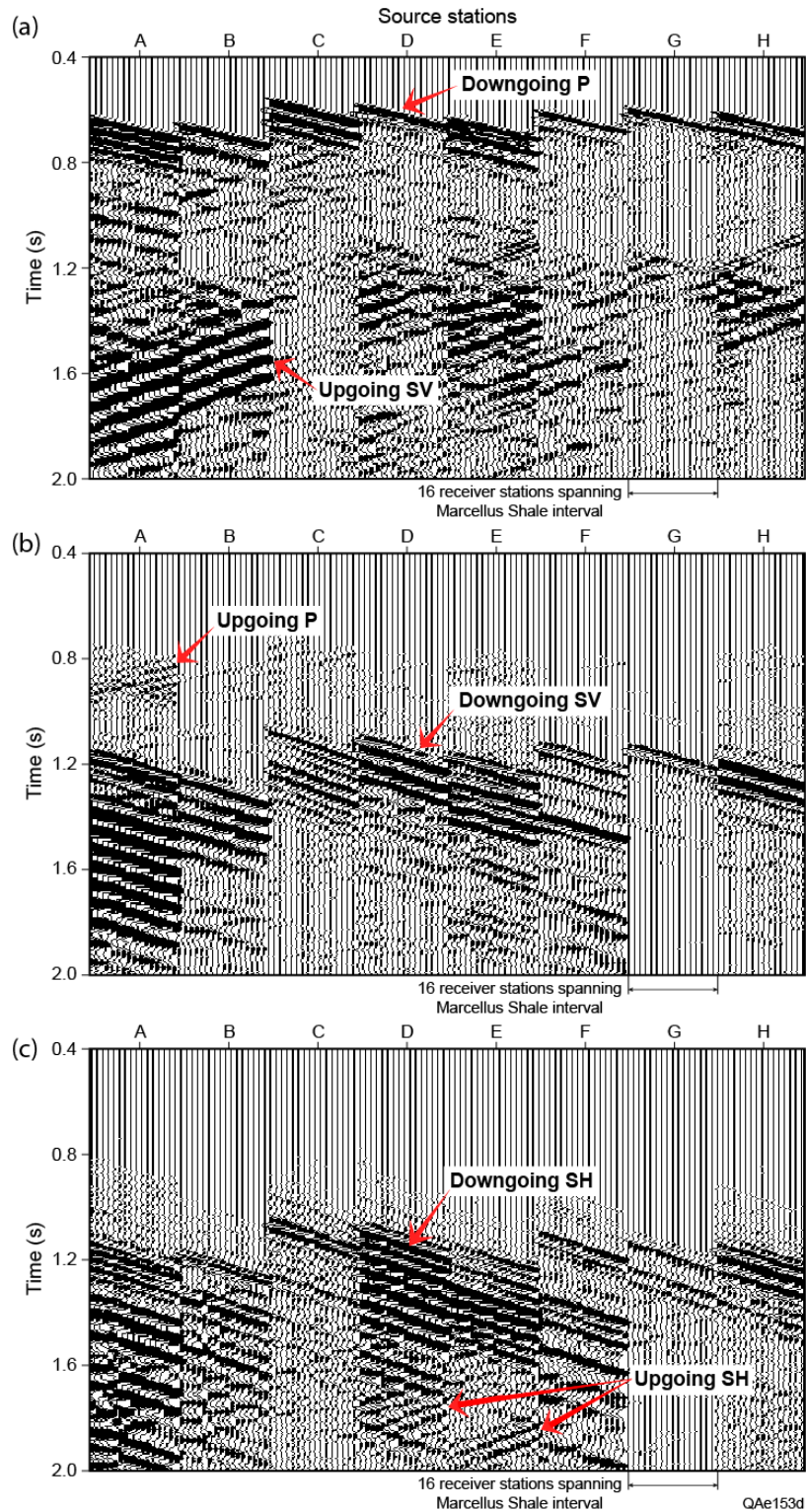


Figure 3.8. Expanded views of direct modes from eight source stations. (a) Data from rotated and tilted vertical geophones. (b) Data from rotated and tilted radial geophones. (c) Data from rotated transverse geophones. Source stations A through H are labeled on Figure 3.1. In each data strip, the first (leftmost) trace is recorded at the shallowest receiver station, and last (rightmost) trace is data recorded at the deepest receiver station.

The waveshapes of the first arrivals of the direct-S modes exhibited on Figures 3.9b and 3.9c are not as stable as the direct-P first arrivals and vary from source station to source station. The wavelet phase that was chosen as a consistent S-wave arrival time is marked with tic marks.

To calculate average P and S velocities, we assumed source-to-receiver travel paths were straight, not refracted or curved. This assumption is not literally true but should yield sufficiently accurate estimates of average velocities. The straight-line distance from a surface source to a downhole receiver is calculated by simple trigonometry. The time coordinates of the tic marks shown on Figures 3.9a and 3.9b are combined with this straight travel-path distance to yield estimates of P and S average velocities. P-wave average velocities calculated in this manner are displayed as Figure 3.10, and the average velocities of direct-S modes are shown on Figure 3.11. The latter display combines velocities determined from the transverse-S direct mode and from the radial-S direct mode. This combined-velocity display format shows that transverse-S velocities are faster than radial-S velocities in almost every azimuth direction.

The display scales used on these figures allow the 16 average-velocity estimates calculated across the 16-station receiver array to be seen as individual data points. In general, the velocity estimated at the shallowest receiver, whether V_P or V_S velocity, is faster than the same wave-mode velocity estimated at the deepest receiver. This behavior is caused by the large decrease in V_P and V_S velocities across the Marcellus Shale interval (Fig. 3.4b and 3.4c). The slow interval velocity within the Marcellus Shale causes average V_P velocity calculated across the VSP receiver array to decrease by approximately $400 \text{ m/s} \pm 50 \text{ m/s}$. The average V_S velocity decreases by approximately $200 \text{ m/s} \pm 50 \text{ m/s}$ across the 16-station array.

These SV and SH average velocities are displayed in map view on Figure 3.12 using a polar-grid format to illustrate the azimuth dependency of the velocities. At the expanded scale used in these polar-grid displays, the 16 data points calculated across the 16-station receiver array meld into a single blurred data point for the azimuth pointing to each of the 70 WAR source stations.

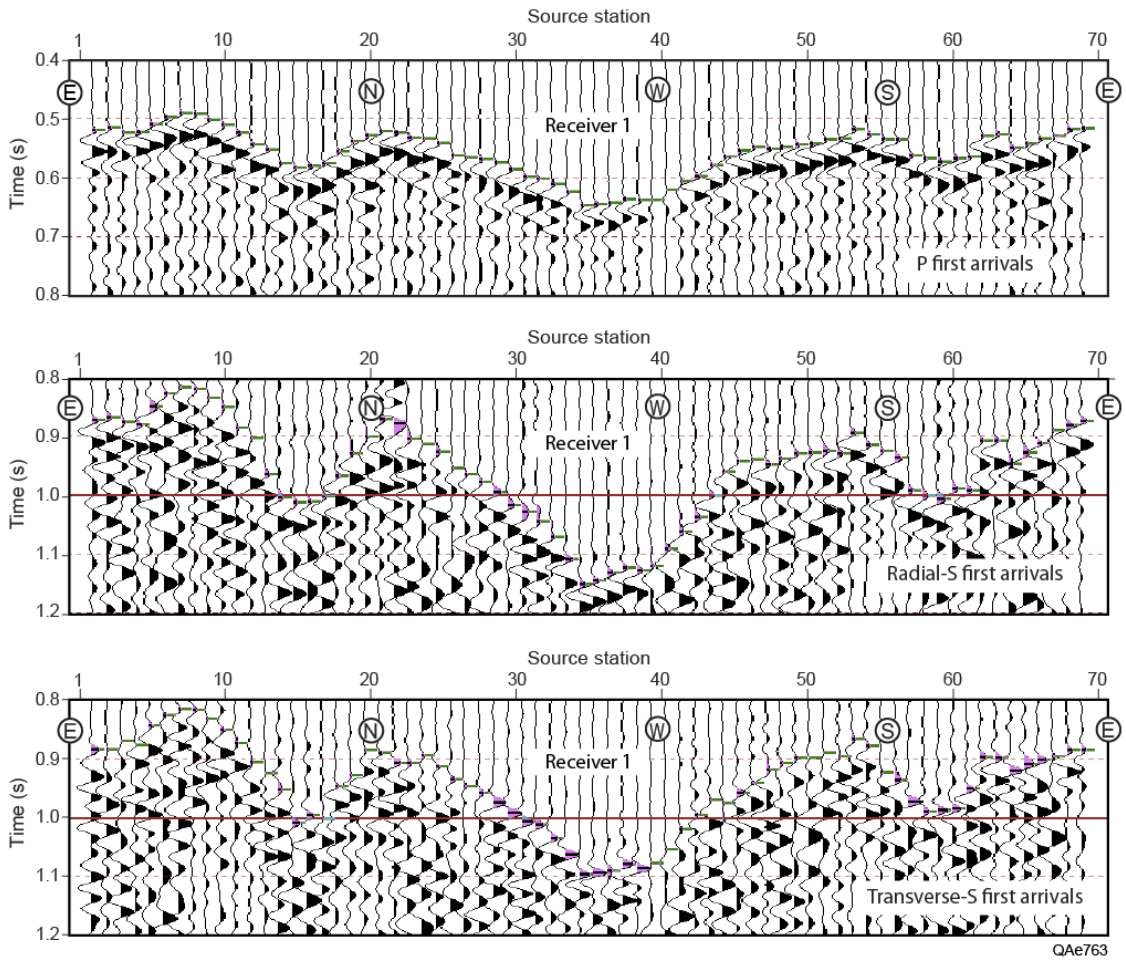


Figure 3.9 (a) Direct-P mode generated at all 70 WAR vertical-vibrator source stations and recorded by the tilted vertical geophone at downhole receiver station 1. (b) Direct-S mode generated at all 70 WAR vertical-vibrator source stations and recorded by the rotated and tilted radial geophone at downhole receiver station 1. (c) Direct-S mode generated at all 70 WAR vertical-vibrator source stations and recorded by the rotated transverse geophone at downhole receiver station 1.

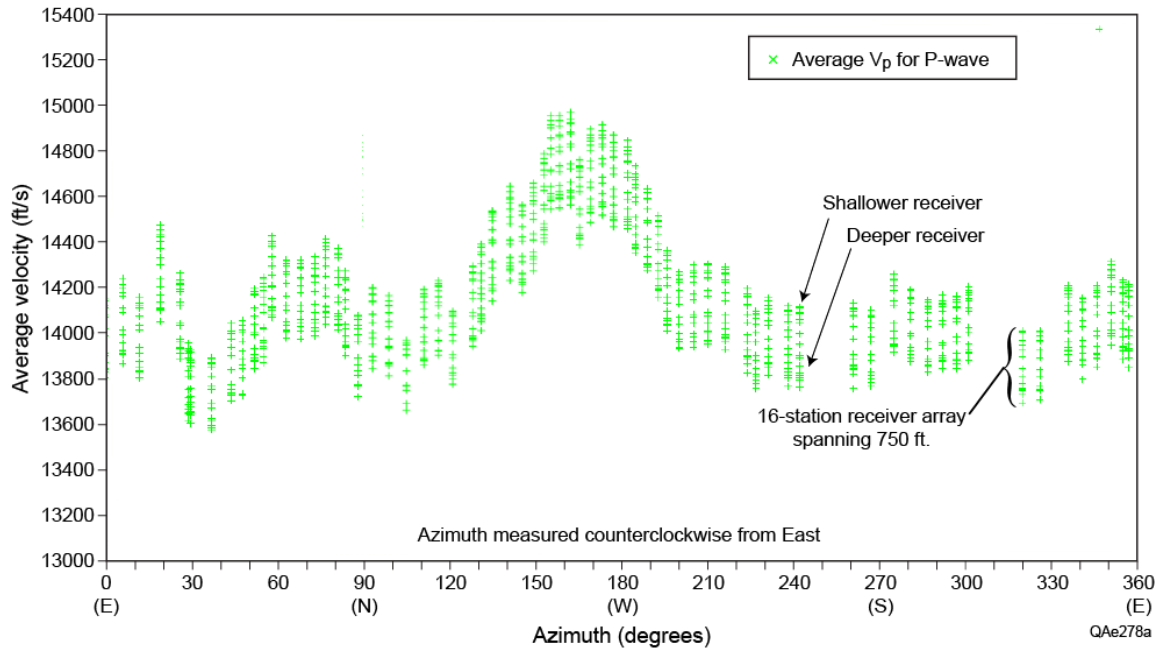


Figure 3.10. Average P-wave velocities calculated for each source station and each receiver station and displayed as functions of azimuth.

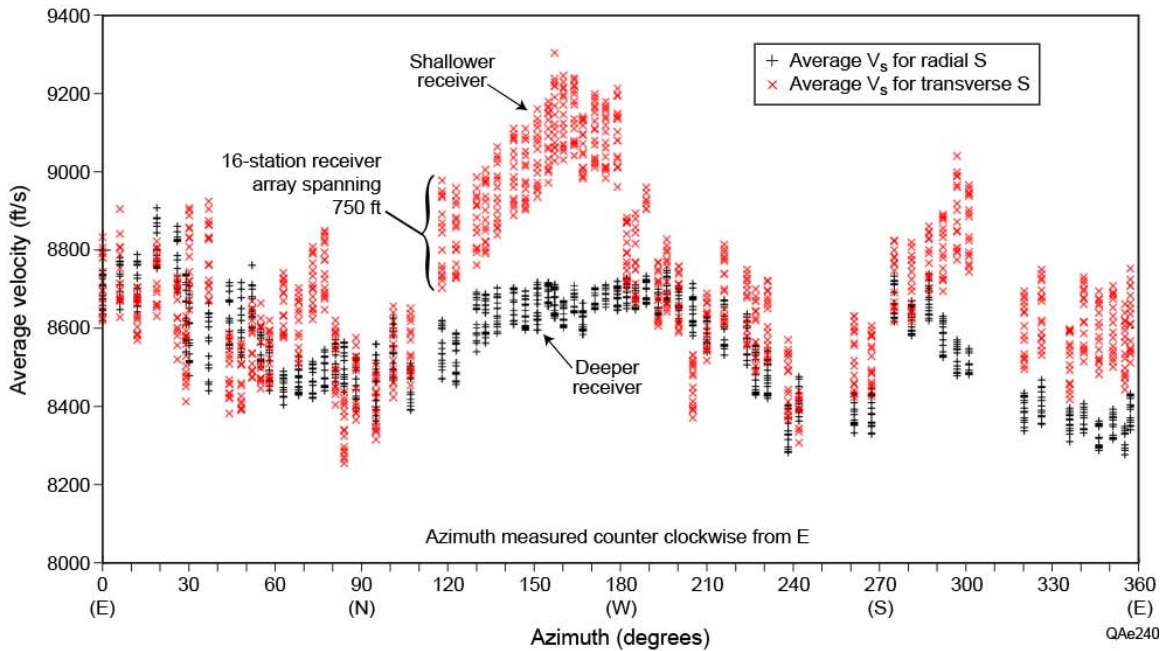


Figure 3.11. Average radial-S and transverse-S velocities calculated for each source station and each receiver station and displayed as functions of azimuth.

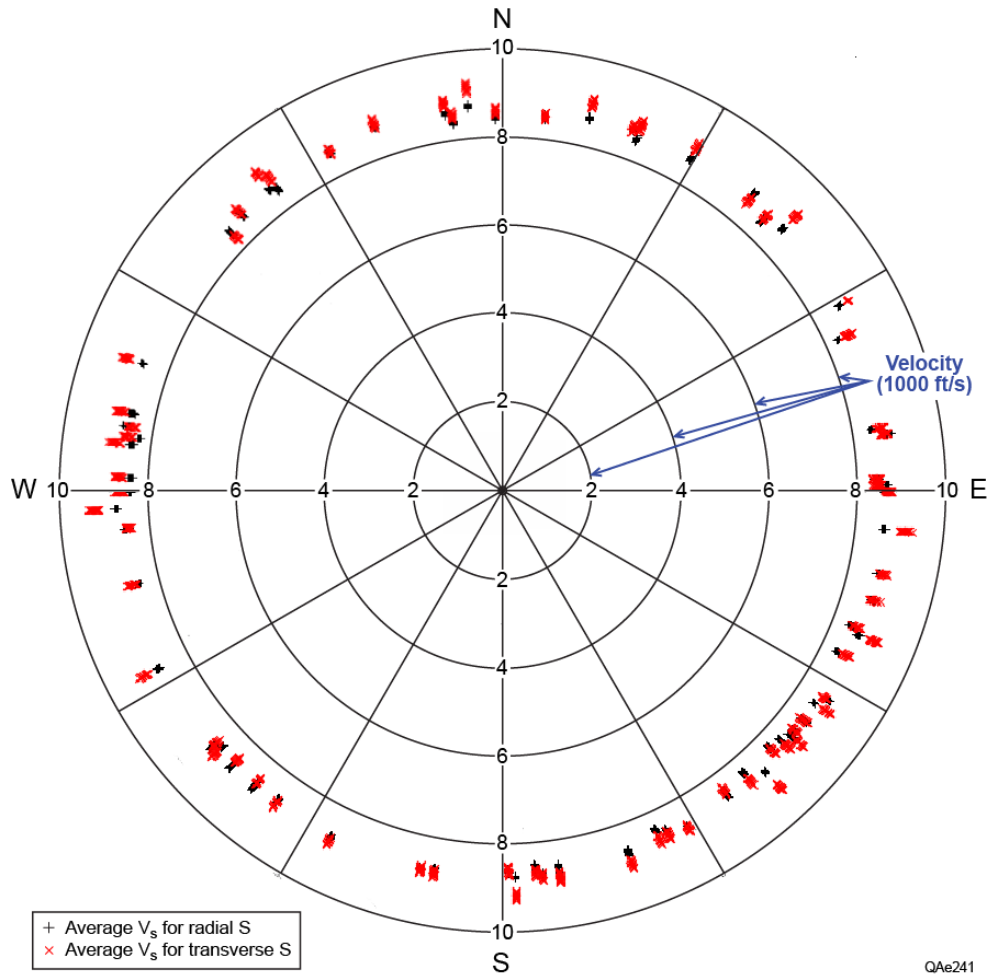


Figure 3.12. Average radial-S and transverse-S velocities displayed in polar-grid format.

S-Wave Anisotropy and Fracture Density

The fundamental principle of seismic estimation of fracture density is illustrated on Figure 2.6 (Chapter 2), which shows that the velocity of the slow-S mode decreases as fracture density increases. Said another way, fracture intensity increases as S-wave anisotropy increases, with S-wave anisotropy being calculated using Equation 3.1. The S-wave velocities displayed on Figures 3.11 and 3.12 illustrate the azimuth behavior of fast-S and slow-S velocities at this Marcellus Shale study site. As stated earlier, transverse-S velocities are faster than radial-S velocities in almost all azimuth directions at this prospect. When the separation between the velocities of the two S modes increases, the classic interpretation of the rock property that causes this velocity separation is that fracture intensity increases along the raypath the two S-modes have traveled.

To utilize S-wave anisotropy in the estimation of fracture intensity at this site, each pair of average S-wave velocities (radial-S and transverse-S)

calculated for each source-receiver combination were used as input for Equation 3.1. The resulting estimates of S-wave anisotropy are displayed as Figures 3.13 and 3.14. Except for a narrow azimuth corridor of approximately 60 degrees in the northwest azimuth quadrant, these VSP estimates of S-wave anisotropy are less than 3-percent. This result coincides with the low S-wave anisotropy obtained with dipole sonic logs (Fig. 3.4d) even though the log estimate was made along a short vertical path through the Marcellus interval and the VSP estimate was made along a much longer and slanted path across the Marcellus interval. This close agreement between dipole sonic log results and results provided by vertical-vibrator VSP data is offered as confirmation that: (1) direct-S modes are produced by vertical vibrators, and (2) these direct-S modes can be used to provide valuable estimates of fracture intensity around a VSP well.

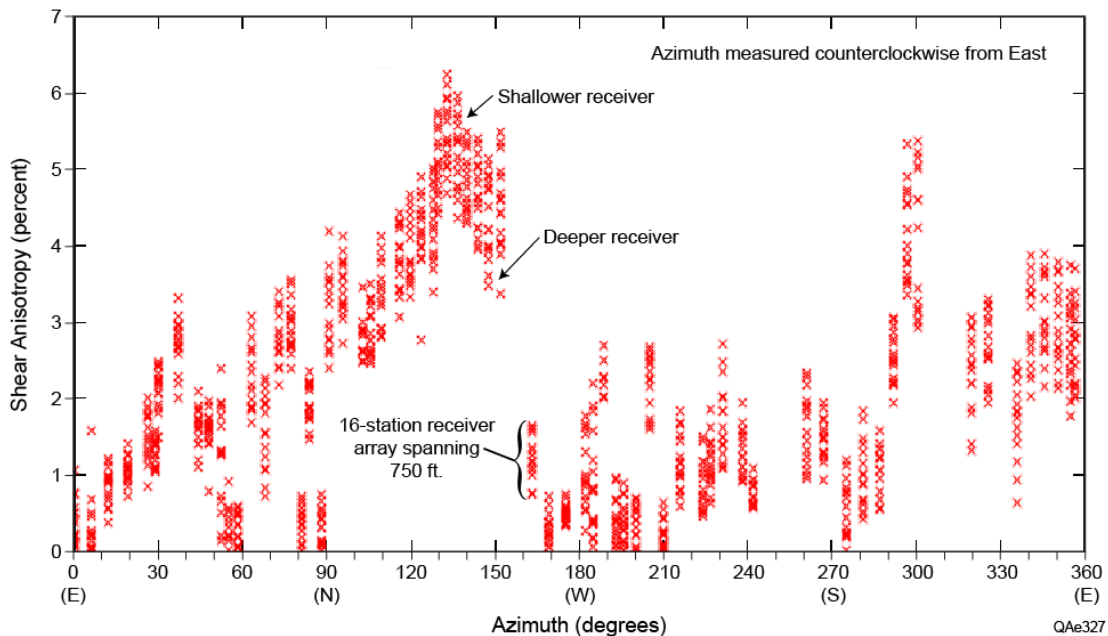


Figure 3.13. S-wave anisotropy calculated from the direct-S velocities plotted on Figure 3.12.

It should be emphasized that S-wave anisotropy is only a qualitative indicator, not a quantitative estimate, of fracture density. It is not possible to relate a numerical value of S-wave anisotropy to a specific number of fractures per unit length or to a certain number of fractures per unit volume within a rock interval. Several measurements of fracture sizes and counts of fracture populations must be made within a seismic propagation medium to establish a numerical relationship between S-wave anisotropy and fracture intensity. Such rock measurements are impossible to make, so S-wave anisotropy is used only in a qualitative way to indicate where fracture population increases and decreases along S-wave travel paths.

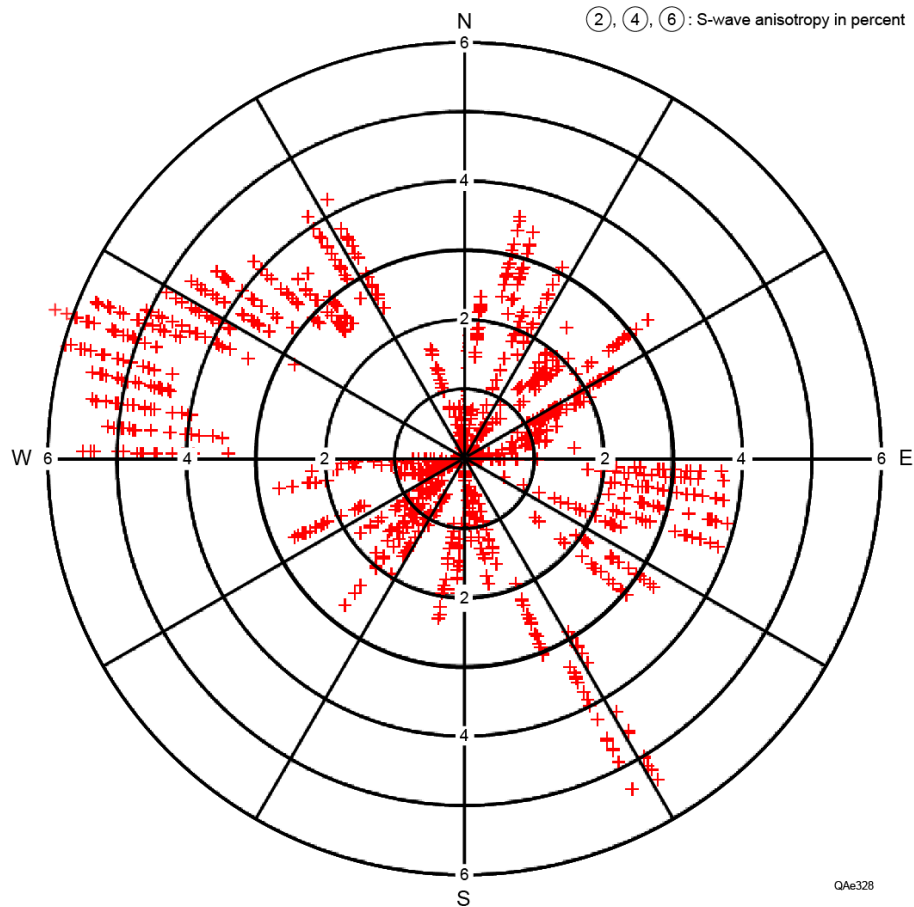


Figure 3.14. Polar-grid plot of S-wave anisotropy.

Direct-Mode Velocities and Stress Directions

Our research team had access to a small 3C3D seismic survey that was centered on the receiver well where these WAR VSP data were acquired. Our interpretation of the 3D image volumes created from these data showed that the Marcellus Shale interval across this prospect had a folded structure manifested by a series of linear ridges oriented west to east. The structural configurations of the Marcellus Shale expressed by P-P and P-SV data are shown on Figure 3.15. Comparing these structural maps with the azimuth distributions of average V_P and V_S velocities (Figs. 3.10 and 3.11) shows that each velocity has its maximum value in a westward azimuth, the same azimuth as the axes of the linear folds.

A common interpretation of azimuth-dependent velocity behavior is that the fastest value of a wave-mode velocity aligns with the direction of maximum horizontal stress. A conundrum is introduced if this velocity interpretation is applied to this situation because an equally popular interpretation principle of structural geology is that maximum horizontal stress is oriented perpendicular to

a structural fold, not along the axis of a fold as our velocity analyses indicate. Thus there is some uncertainty about the relationship between the azimuth of fast-mode velocity and the azimuth of maximum horizontal stress that should be adopted for the Marcellus Shale at this site. This is the first opportunity our research team has had to interpret seismic modes that propagate in media having orthogonal joint sets such as the Marcellus Shale. We feel we have more to learn about velocity behavior in such media. In some cases, stress-induced effects on velocity may dominate fracture-induced effects. In other instances, the opposite may be true, and fractures can influence the direction of fast-mode azimuth more than do stress conditions.

One conclusion that is obvious when azimuth-dependent velocities are compared against these structural folds is that a fast mode propagates in the azimuth of one natural coordinate axis of the Marcellus Shale and a slower mode propagates in the azimuth of the companion (and orthogonal) natural coordinate axis. The only confusion is to determine which of these natural coordinate axes corresponds to the azimuth of maximum horizontal stress and which corresponds to the azimuth of minimum horizontal stress.

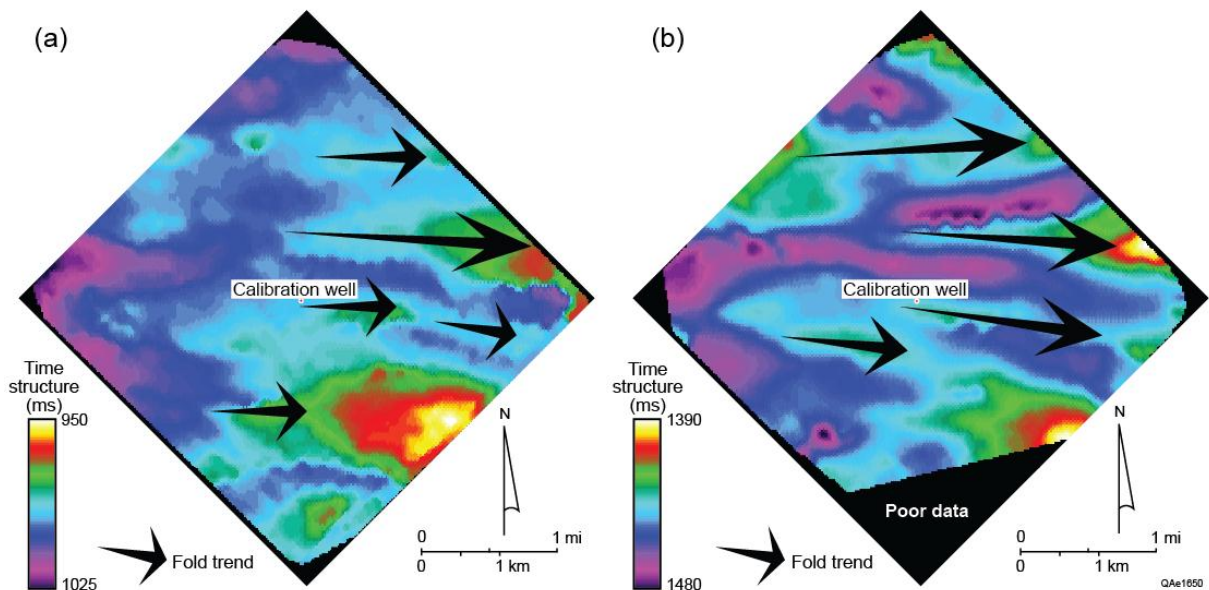


Figure 3.15 (a) Structural map of the Marcellus Shale constructed from P-P data. The Marcellus is deformed into a series of folded ridges oriented west to east. (b) Structural map of the Marcellus Shale constructed from P-SV data. These converted-S data show the same folded-ridge structure as do P-P data, with some minor variations in detail.

Conclusions

The fundamental objective of this project was to present conclusive proof that vertical vibrators produce direct-S modes and that these direct-S modes increase the value of VSP data for evaluating unconventional reservoirs. The 70 vertical-vibrator source stations utilized in this Marcellus Shale WAR VSP study produced data that showed convincing proof that direct-S modes were produced at each source station and allowed the velocities of these direct-S modes and their companion direct-P mode to be calculated in a full-azimuth circle around the VSP well. The resulting average velocities were used to calculate S-wave anisotropy so spatial variations in fracture density could be predicted in all azimuths away from the receiver well. These seismic-based estimates of S-wave anisotropy agreed with S-wave anisotropy values determined from a dipole sonic log acquired in the VSP well. This agreement between VSP data and log data was a valuable confirmation that direct-S modes produced by a vertical vibrator can be used in fracture applications that to date have been attempted using only direct-S modes produced by horizontal vibrators.

An important aspect of this study site was that we had access to seismic-based structure maps of the Marcellus Shale which showed the Marcellus was distorted into a series of linear folds oriented approximately west to east. Average V_P and V_S velocities calculated from the direct-P and direct-S modes produced by the WAR VSP vertical-vibrator sources showed that a fast-P and a fast-S wave mode propagated in the azimuth of the long axis of the folds, and a slow mode propagated in a perpendicular azimuth. Direct-S modes produced by a vertical vibrator thus define the azimuths of natural coordinate axes local to a VSP well. These natural coordinate axes can be associated with azimuths of horizontal stresses or with azimuths of vertical fractures and joints, depending on which of these two geologic properties (tectonic stress or fractures) is the more dominate.

Chapter 4

VSP Analysis 2 – Tight Sandstone Prospect

Introduction

The VSP data analyzed in this chapter were acquired in a well that penetrated approximately 4000 ft of tight sandstone. The specific data coordinates and well name will not be stated to protect the interests of the operator who provided the data for our analysis. The general location of the well in western Colorado is shown on the map displayed as Figure 1.2 of Chapter 1.

VSP Source-Receiver Geometry

The vertical-vibrator source geometry involved in the walkaround (WAR) VSP survey acquired in this tight-sandstone well is illustrated on the map displayed as Figure 4.1. The VSP receiver well was approximately 12,000 ft (3660 m) deep. The wellbore had a modest deviation with the well head positioned at the solid circle at the map origin coordinates, and the deepest depth point located at the solid square approximately 1000 ft (305 m) southwest of the well head. Because of the simple quasi-vertical nature of the receiver well, a well diagram will not be shown.

It is important to note the large offset distances of the vertical-vibrator source stations in this VSP data acquisition. Source-to-receiver offsets range from approximately 10,000 ft (3050 m) to approximately 15,000 ft (4570 m). These offsets are severe violations of the common practice of utilizing a zero-offset source-to-receiver geometry to perform Alford rotation analysis (Chapter 2). Our labeling system for the walkaround source stations starts with station A south of the VSP well and increases alphabetically in a clockwise manner to station E southeast of the well.

A thick stack of thin shale beds alternating with thin tight-sandstone units forms the bottom 4,000 ft (1220 m) of drilled section. Most, and probably all, of the thin tight-sandstone beds in this deepest portion of the well are fractured. This deep 4000-ft (1220 m) fractured interval will be referred to as the *reservoir interval* in this report. When recording WAR VSP data at this site, 80 receiver stations were positioned at depth increments of 50-ft (15 m) across this targeted reservoir interval.

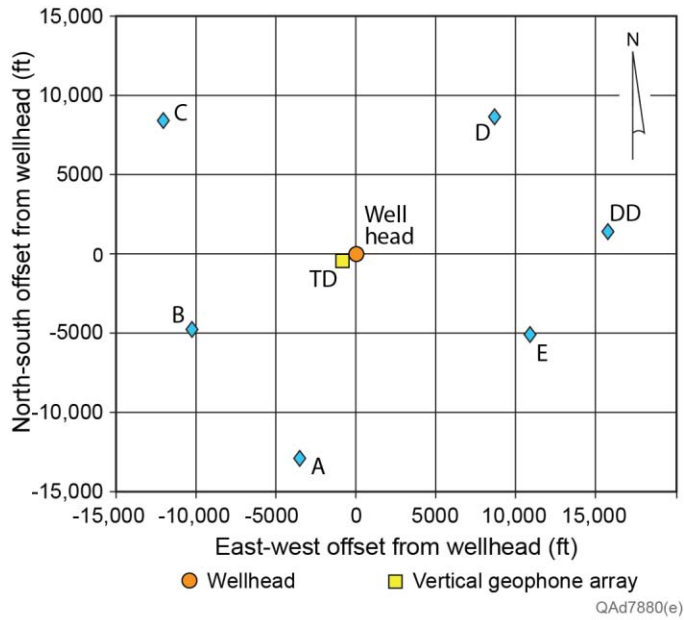


Figure 4.1. (a) Map view of vertical-vibrator source stations positioned around the VSP well at study site 2.

Stratigraphic Column

The stratigraphic sequence and rock types penetrated by this VSP receiver well are illustrated on Figure 4.2. We will not divert into a detailed description of the geology local to this study well. Our objectives are only to show the general nature of the Mesaverde tight-sandstone units that form this particular unconventional reservoir target and to emphasize the considerable thickness of the reservoir target (approximately 4000 ft [1220 m]). The information illustrated on Figure 4.2 describes the general stratigraphy and bedding across the Piceance Basin, not the stratigraphy and bedding local to this particular VSP well.

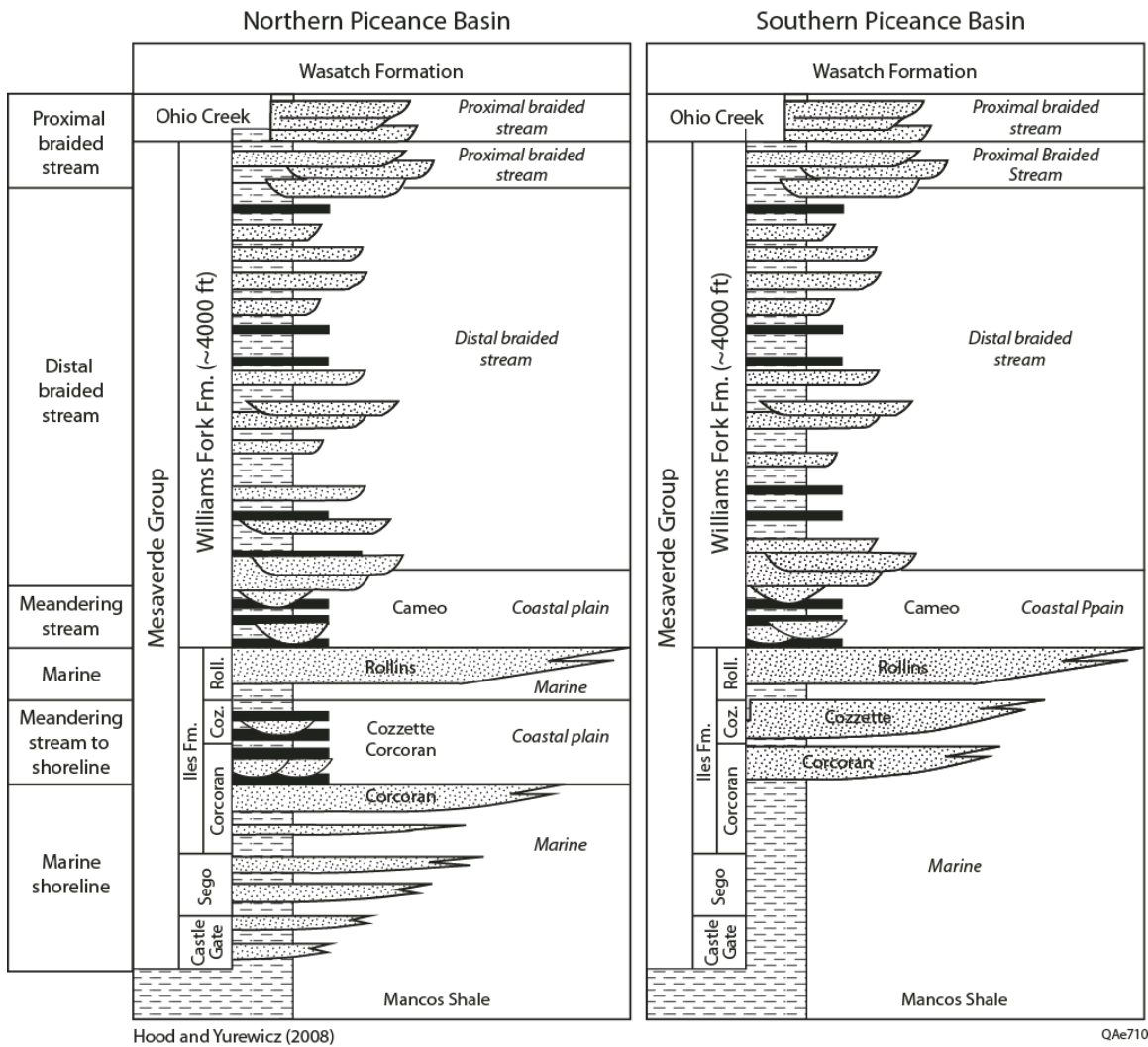


Figure 4.2. Formation nomenclature and general stratigraphy in the area of this VSP study well. Modified from Hood and Yurewicz, (2008)

Calibration Database

The key subsurface calibration data that will be shown in this report are S-wave VSP data generated by horizontal vibrators. These horizontal vibrators were positioned at a zero-offset location to generate the crossed-dipole type of VSP S-wave data that are ideal for Alford rotation analysis as described in Chapter 2 (Figs. 2.3 and 2.5). A commercial VSP contractor processed these horizontal-vibrator data to determine fracture orientation and slow-S time delays for the entire stratigraphic section over which receivers were deployed. These horizontal-vibrator VSP data-processing results will be compared with our vertical-vibrator VSP data-processing efforts in a later section of this chapter.

Examples of Raw Unprocessed VSP Data

Examples of VSP wavefields produced by a vertical vibrator positioned at one of the offset source stations are shown on Figure 4.3. These data have been transformed to radial/transverse coordinate space (Figures 2.1 and 2.3, Chapter 2) to better illustrate direct-S modes embedded in the VSP wavefields. Direct-S data windows are identified by the green box outlines on these displays. Direct radial-S data are labeled SR, and direct transverse-S data are labeled ST. These data are representative of the direct-S data quality generated at all vertical-vibrator source stations.

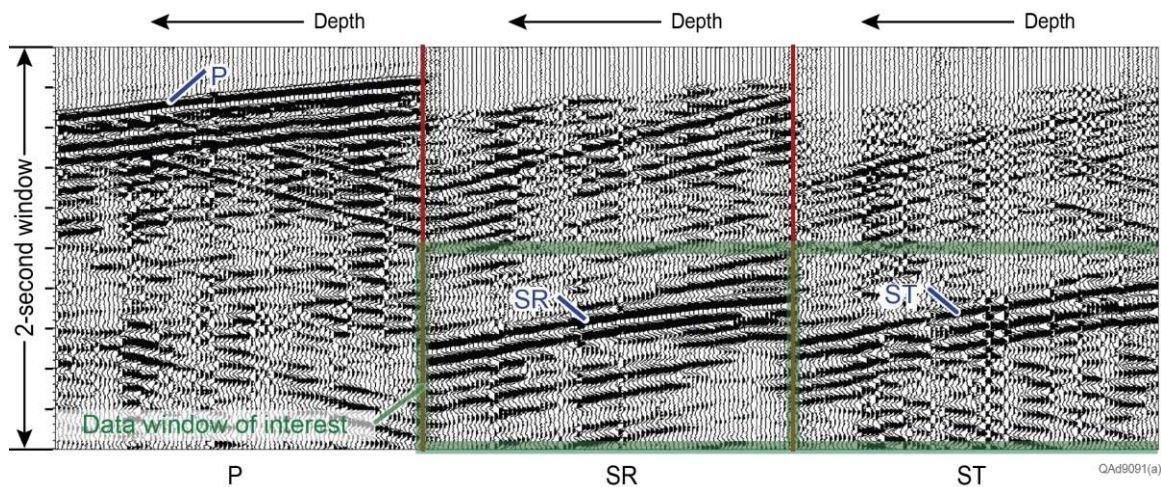


Figure 4.3. Example of VSP data produced at WAR source stations. The data are shown after wavefields have been rotated to radial-transverse data space. The outlined windows define direct-S modes used in Alford rotation analysis for this particular source station. These data, and their associated direct-S analysis windows, are similar to direct-S data generated at all vertical-vibrator walkaround source stations at this study site.

The radial/transverse orientation of wavefields produced at two source stations remote from each other requires that the output of an Alford rotation be interpreted differently than is an Alford rotation result calculated from data produced by two crossed-dipole sources (horizontal vibrators) positioned at a single source station. The latter condition is the source assumption embedded in the theory of Alford rotation. Basically, when one vertical-vibrator source station is selected as the reference location where two orthogonal S-wave vectors are assumed to have originated, the radial-receiver data from the second vertical-vibrator source station, which is remote from the first station, have to be used as if they were transverse-receiver data propagating from the first source location. Similarly, the transverse-receiver data from the second vertical-source source have to be interpreted as being radial-receiver data produced at the first source station. This exchange of radial-receiver and transverse-receiver data at the second source station will be important when Alford rotation results are described later.

Examples of Processed VSP Data

To interpret results produced by an Alford rotation analysis, it is essential to define the orientations of VSP receivers when direct-S wavelets are mathematically transformed onto rotated-axis coordinate systems created by the Alford rotation procedure. The orientations of the downhole radial and transverse horizontal geophones used to analyze orthogonal-azimuth S-wave source data generated at source stations A and E are illustrated on Figure 4.4. Data from these two vertical-vibrator source stations are used in Figures 2.10 through 2.18 of Chapter 2 using the same source station nomenclature (A and E). Rather than having redundant displays in this chapter of the analysis of direct-S modes produced at these two source stations, we will refer back to these figures in Chapter 2 when necessary.

At each receiver depth, the Alford rotation calculation begins with VSP radial and transverse geophones oriented as shown by the diagram labeled “*Starting rotation.*” Note that at this starting calculation, radial and transverse receivers must be oriented in the same azimuths whether data are generated at source-station A or at source-station E. These horizontal geophones are then mathematically rotated counterclockwise in small azimuth increments of $\Delta\theta$ to create new azimuths for the data space in which direct-S wavelets can be described (Figures 2.2 and 2.3, Chapter 2). In the Alford rotation analyses shown in this report, $\Delta\theta = 10$ degrees. This receiver orientation and sensor-rotation notation is used on subsequent figures displaying Alford rotation results for data generated at source-station A and source-station E. Reference back to this initial orientation of VSP horizontal geophones allows interpreted azimuths of natural coordinate axes to be defined relative to a vertical plane passing through a receiver station and any one of the two quasi-orthogonal source stations used in this first analysis. Relative to the VSP receiver well, the azimuth for source-station E is 112 degrees from north (Fig. 4.4a). The corresponding azimuth for source-station A is 192 degrees from north (Fig. 4.4b). The azimuth angle between these two source stations is 80 degrees, not 90 degrees.

The phase-change azimuths labeled on Figures 2.12 through 2.15 of Chapter 2 are measured counterclockwise from the vertical plane passing through the receiver well and source station A. This reference azimuth causes the azimuths of natural coordinate axes N1 and N2 to be approximately 22 degrees and 112 degrees, respectively.

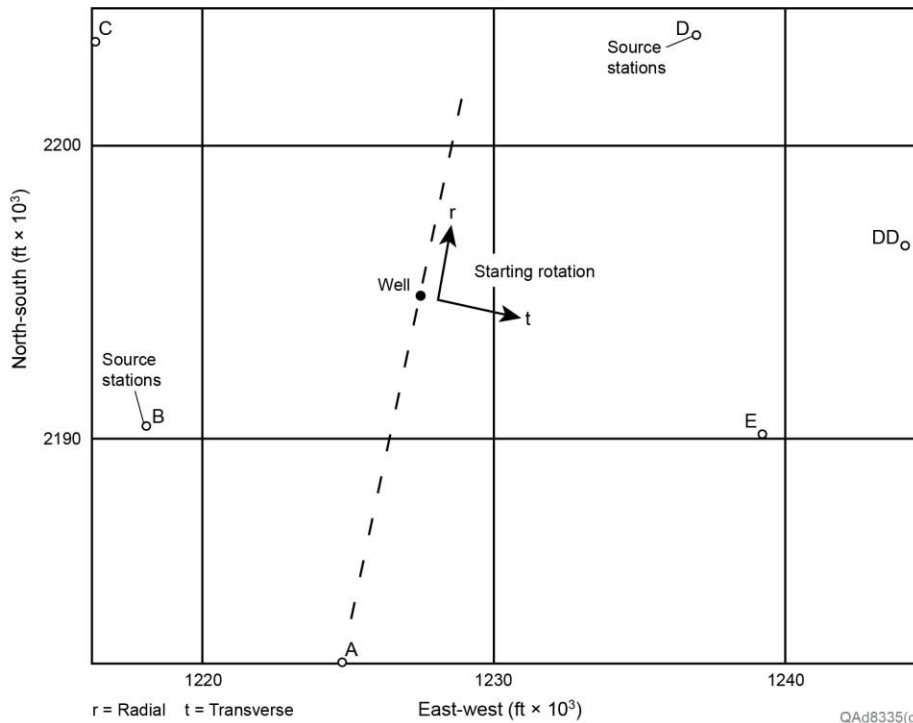
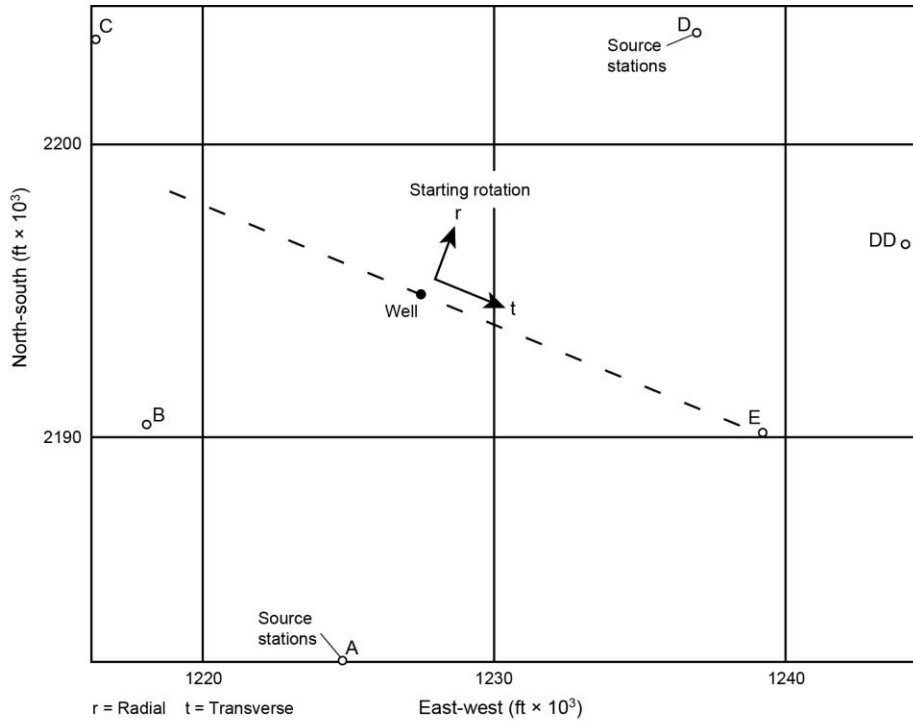


Figure 4.4. Notation used to define receiver orientations during Alford rotation calculations for (a) source station E, and (b) source station A. r indicates a radial VSP geophone, and t defines a transverse VSP geophone. Receiver rotations are done in a counterclockwise direction over an azimuth range of 0 to 360 degrees. Azimuths of natural coordinate axes can now be defined relative to the known azimuth of the vertical plane passing through the receiver station and either of the source stations.

Redundancy Check

The data presented in Chapter 2 as Figures 2.12 through 2.18 introduce the concept that direct-S modes produced by vertical vibrators may be as valuable as direct-S modes produced by horizontal vibrators for determining fracture attributes. To confirm this orthogonal-azimuth-source VSP application of vertical vibrators, a redundancy check was done to determine if different pairs of vertical vibrators produce S-wave results equivalent to those achieved with vibrators at source stations A and E.

In this redundancy test, data generated by vertical vibrators positioned at orthogonal-azimuth stations C and D are compared with data generated by orthogonal-azimuth vibrator pair A and E to determine if direct-S wave results are source-station dependent. For general application of the principles emphasized in this report, it is important to demonstrate that consistent S-wave attributes can be achieved using data produced by orthogonal-azimuth pairs of vertical vibrators having arbitrary positions relative to a VSP receiver well. The map on Figure 4.5 defines the locations of source stations C and D and the starting orientation of VSP receivers when analyzing S-wave data at each downhole receiver station. The direct-S modes propagating away from source stations C and D are displayed on Figure 4.6.

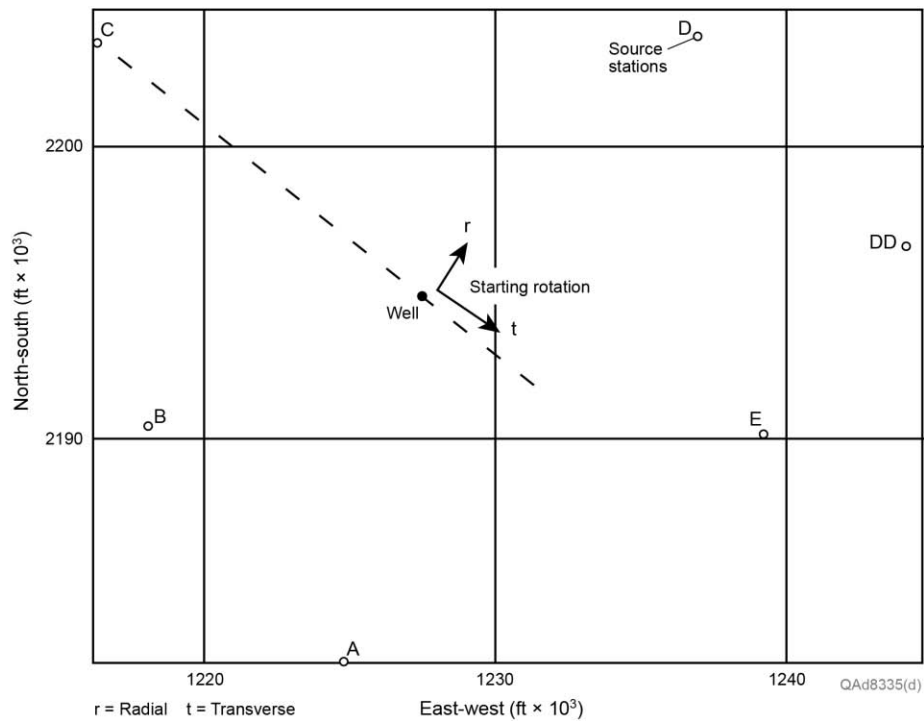
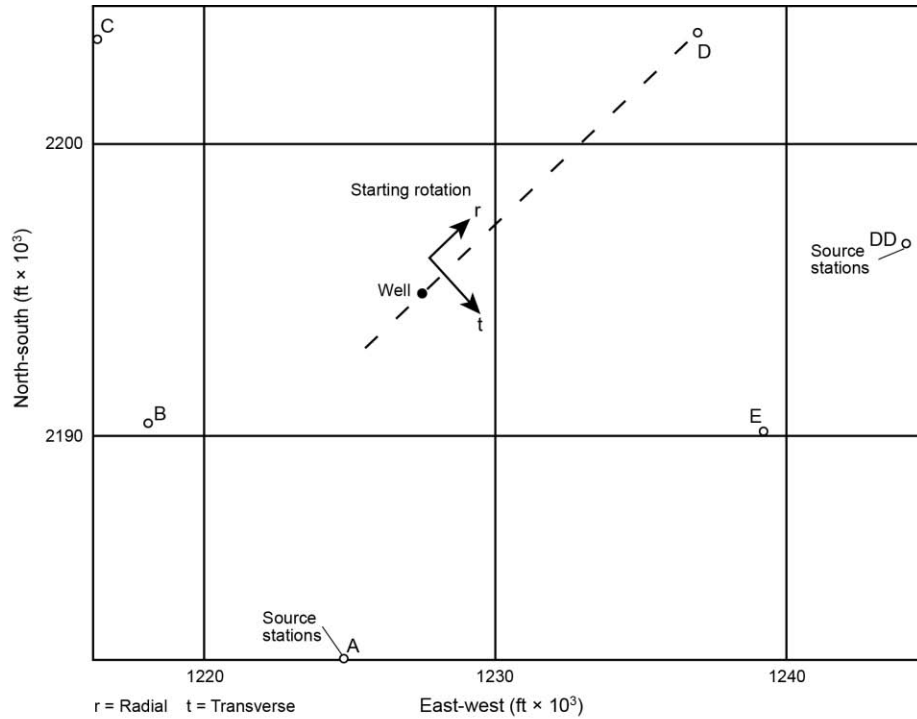


Figure 4.5. Notation used to define receiver orientations during Alford rotation calculations for (a) source station D, and (b) source station C. r indicates a radial VSP geophone, and t defines a transverse VSP geophone. Receiver rotations are done in a counterclockwise direction over an azimuth range of 0 to 360 degrees. Azimuths of natural coordinate axes can now be defined relative to the known azimuth of the vertical plane passing through the receiver station and either of the source stations.

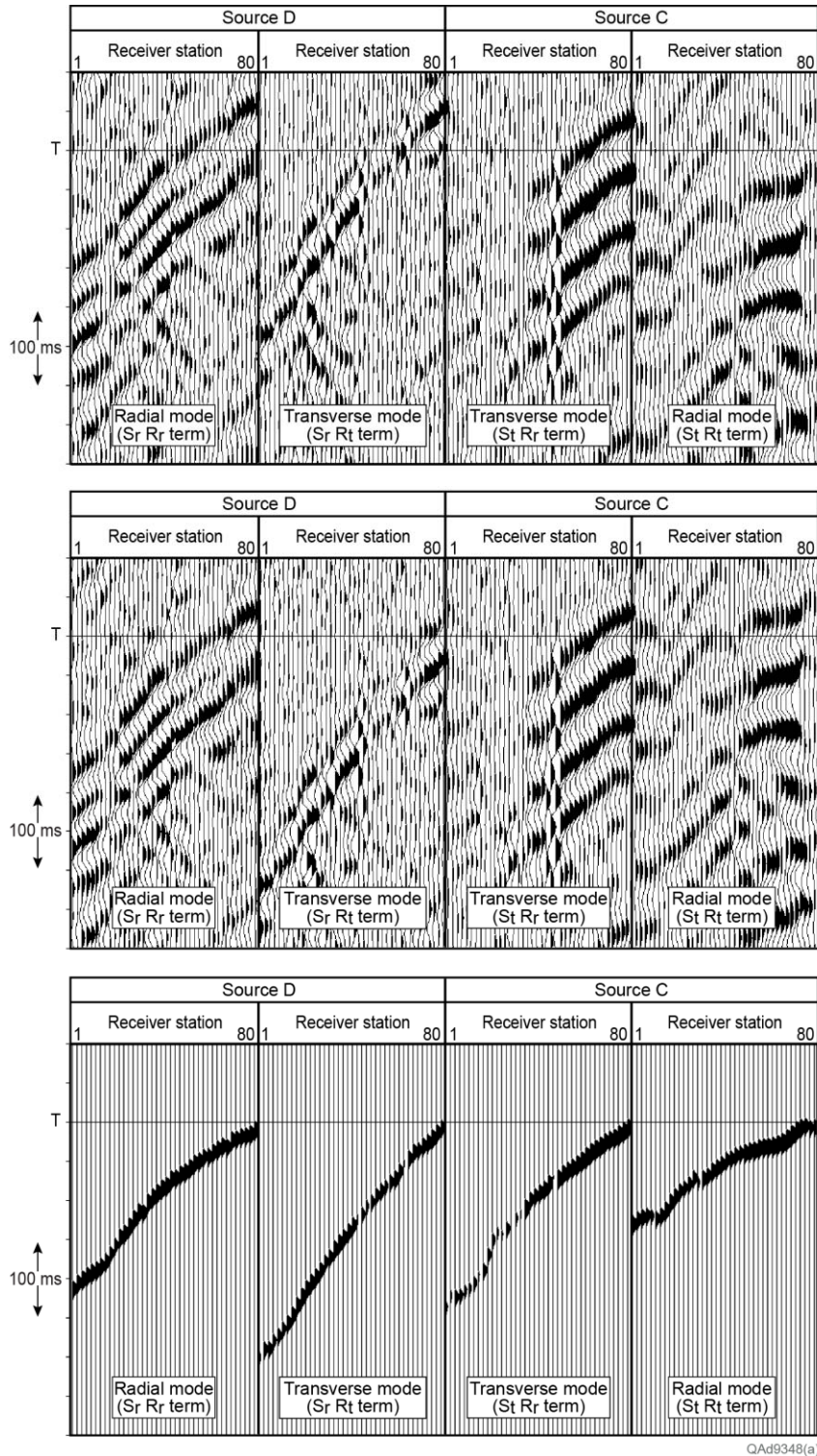


Figure 4.6. (a) Radial and transverse direct-S wavefields from orthogonal-azimuth vertical-vibrator source stations C and D. (b) Wavefields after shifting the arrival times at receiver station 80 to time datum T to remove the effects of traveltime differences through the overburden. (c) Replacement Gaussian wavelets used for first-arrivals in Alford Rotation analysis. Labels S_rR_r , S_rR_t , S_tR_r , S_tR_t placed on the data panels correspond to matrix element terms used in the right-hand-side matrix of the Alford rotation equation (Fig. 2.2, Chapter 2).

Figures 4.7 through 4.11 illustrate Alford rotation analyses of direct-S modes produced by vibrators at stations C and D. These figures replicate data examples from vibrators A and E illustrated on Figures 2.12 through 2.16 of Chapter 2.

Azimuths of the N1 and N2 natural coordinate axes within the reservoir interval as predicted by vertical-vibrator source pair C and D are 136 degrees and 46 degrees from North, respectively. These estimated azimuths differ by 25 degrees from those estimated by source pair A and E. Estimates of fracture orientations for these two source pairs (pair A and E and pair C and D) differ more than desired. This finding is important and introduces some caution about the accuracy of fracture-orientation information provided by direct-S waves produced by vertical vibrators.

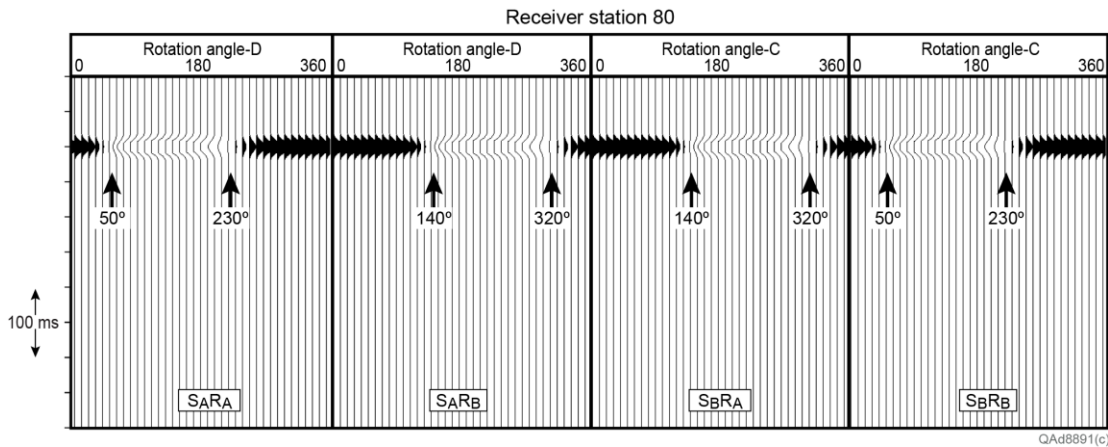


Figure 4.7. Alford rotation of direct-S wavelets generated at source stations C and D recorded at receiver station 80. At this receiver depth, S wavefields are just emerging from the overburden and beginning to enter the fractured reservoir interval. Alford rotation analysis implies the natural earth coordinates in the overburden above receiver station 80 are oriented 50 degrees and 140 degrees counterclockwise from source station 2, which would be 94 degrees and 184 degrees from North. These azimuths differ by 33 degrees from the estimates calculated from data generated at source stations A and E (Fig. 2.12, Chapter 2).

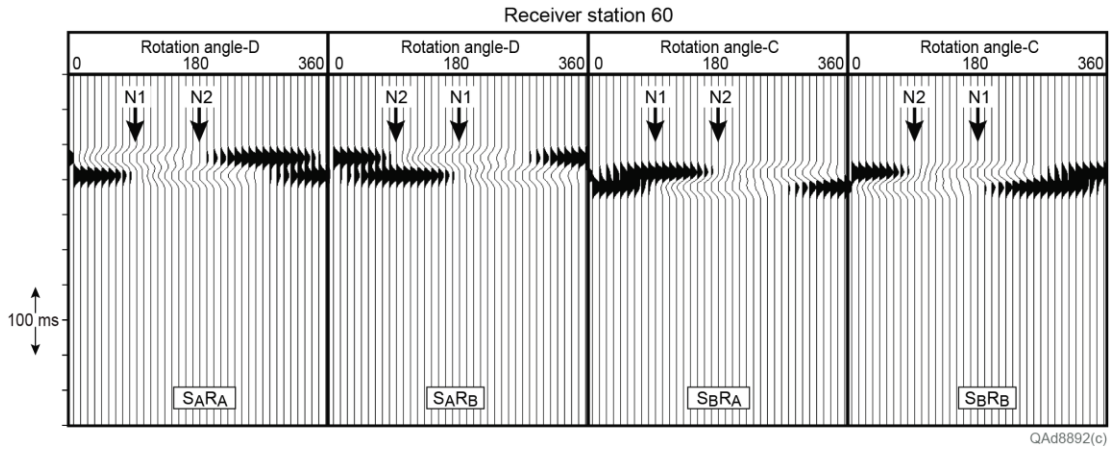


Figure 4.8. Alford rotation at receiver station 60 (1000 ft [305 m] below receiver 80 of Figure 4.7) using direct-S wavelets propagating from source stations C and D. N1 and N2 = azimuths of natural coordinate axes measured counterclockwise from source station D.

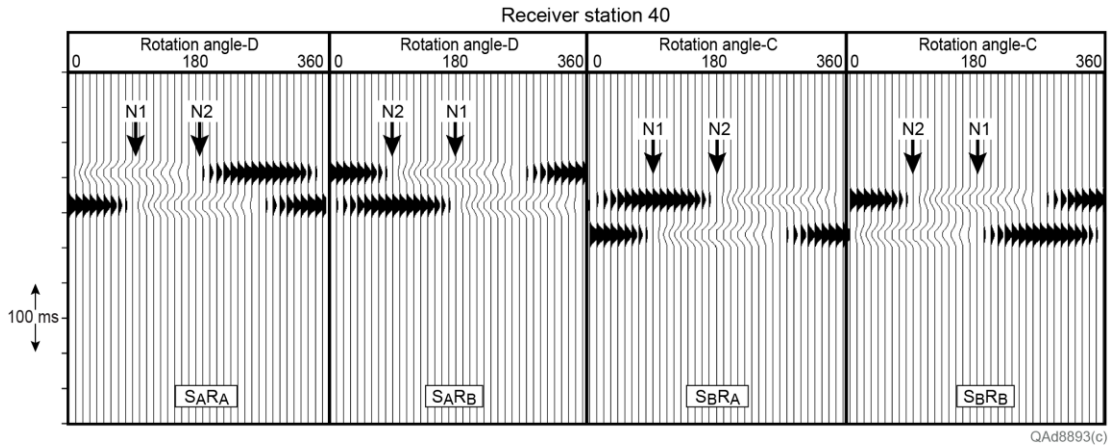


Figure 4.9. Alford rotation at receiver station 40 (1000 ft [305 m] below receiver 60 of Figure 4.8) using direct-S wavelets propagating from source stations 2 and 3. N1 and N2 = azimuths of natural coordinate axes measured counterclockwise from source station D.

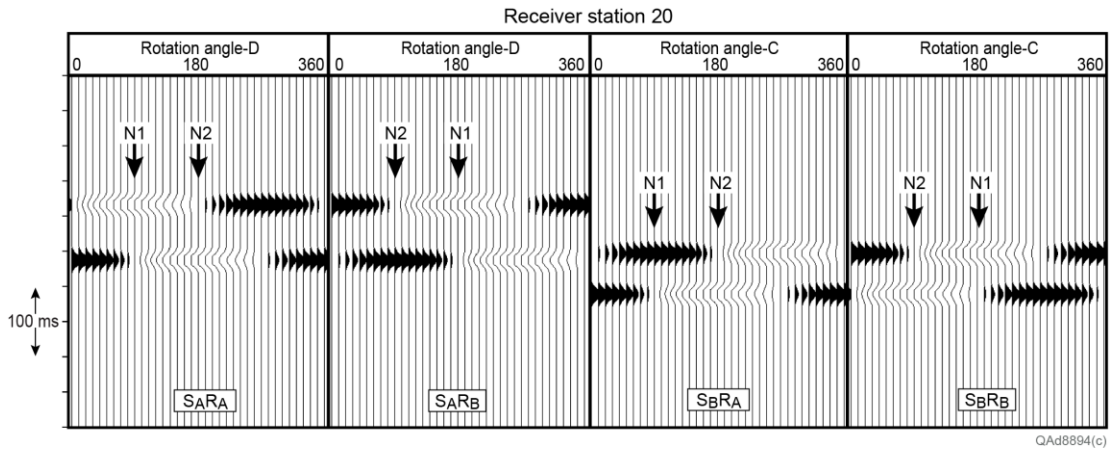


Figure 4.10. Alford rotation at receiver station 20 (1000 ft [305 m] below receiver 40 of Figure 4.10) using direct-S wavelets propagating from source stations C and D. N1 and N2 = azimuths of natural coordinate axes measured counterclockwise from source station D.

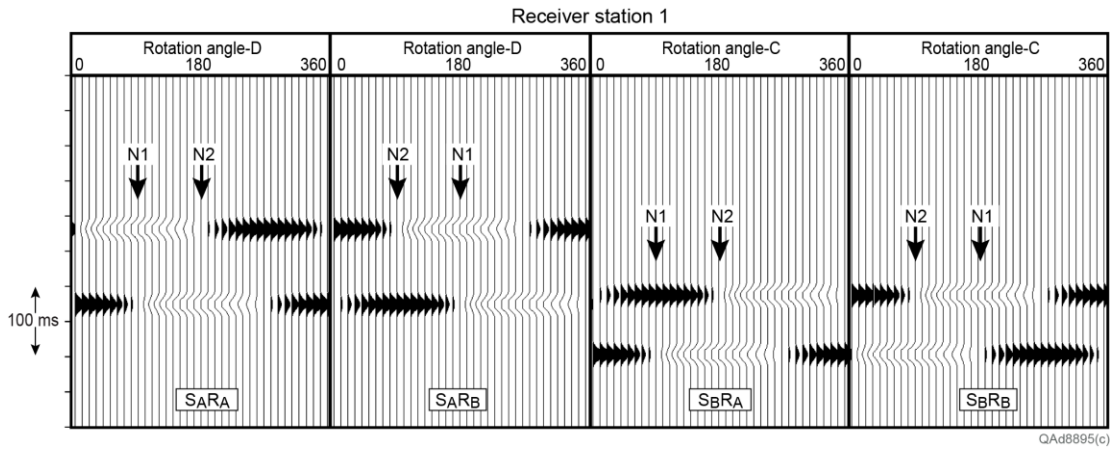


Figure 4.11. Alford rotation at receiver station 1 (1000 ft [305 m] below receiver 20 of Figure 4.10) using direct-S wavelets propagating from source stations C and D. N1 and N2 = azimuths of natural coordinate axes measured counterclockwise from source station D.

Arrival times of S_1 and S_2 modes from source pair C and D at all 80 VSP receiver stations are illustrated on Figure 4.12. This display format is the same as that used for source pair A and E (Fig. 2.16, Chapter 2). An important application of this technology is again demonstrated – that being S_2 time delays determined from one source station differ from S_2 time delays calculated for a second source station. These slow-S time delays are essential for estimating fracture density around a VSP well.

The distinctions between these S-wave anisotropy calculations occur because slant travel paths to VSP receivers differ for each source station and measure S_1 and S_2 velocity behavior in different earth volumes around a VSP well. By combining S-wave anisotropy estimates along travel paths from each source station around a VSP well, it is possible to construct a volumetric picture of fracture intensity around a vertical receiver array, as demonstrated by the display on Figure 4.13.

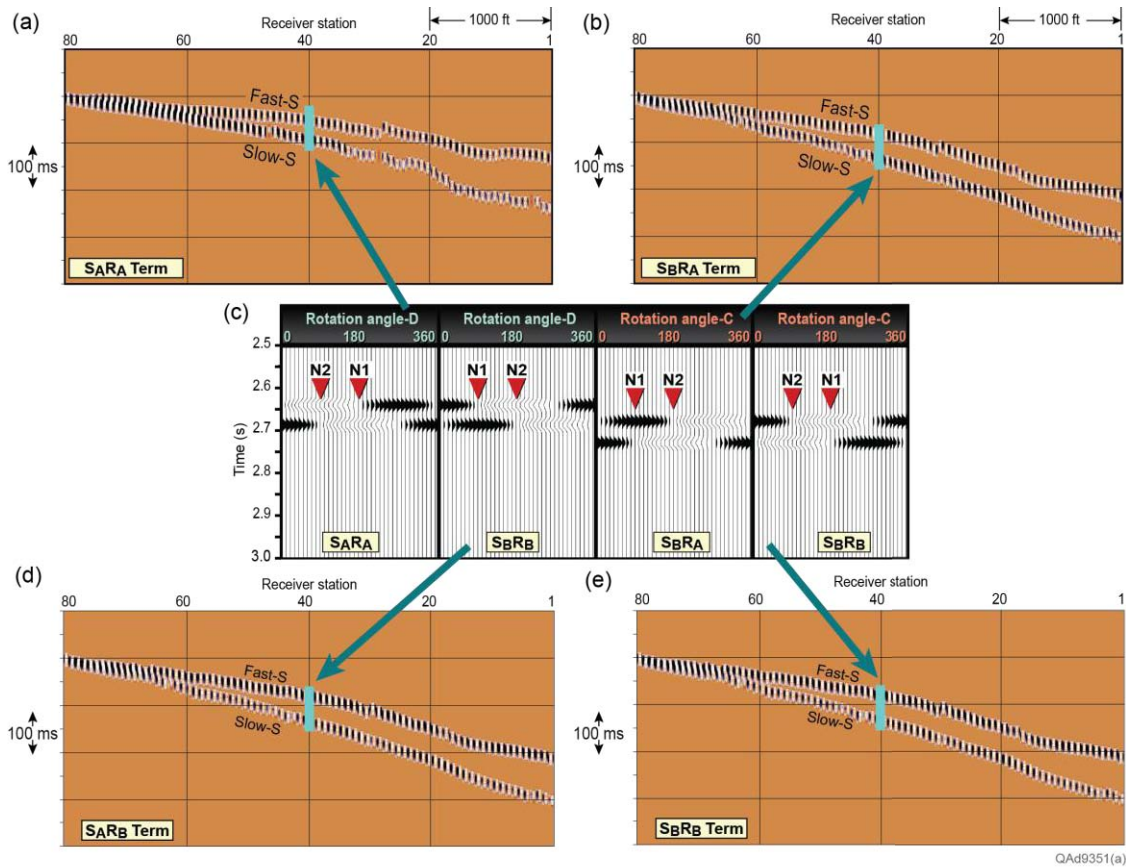


Figure 4.12. S_1 and S_2 arrival times calculated from direct-S modes produced by vertical vibrators at source stations C and D.

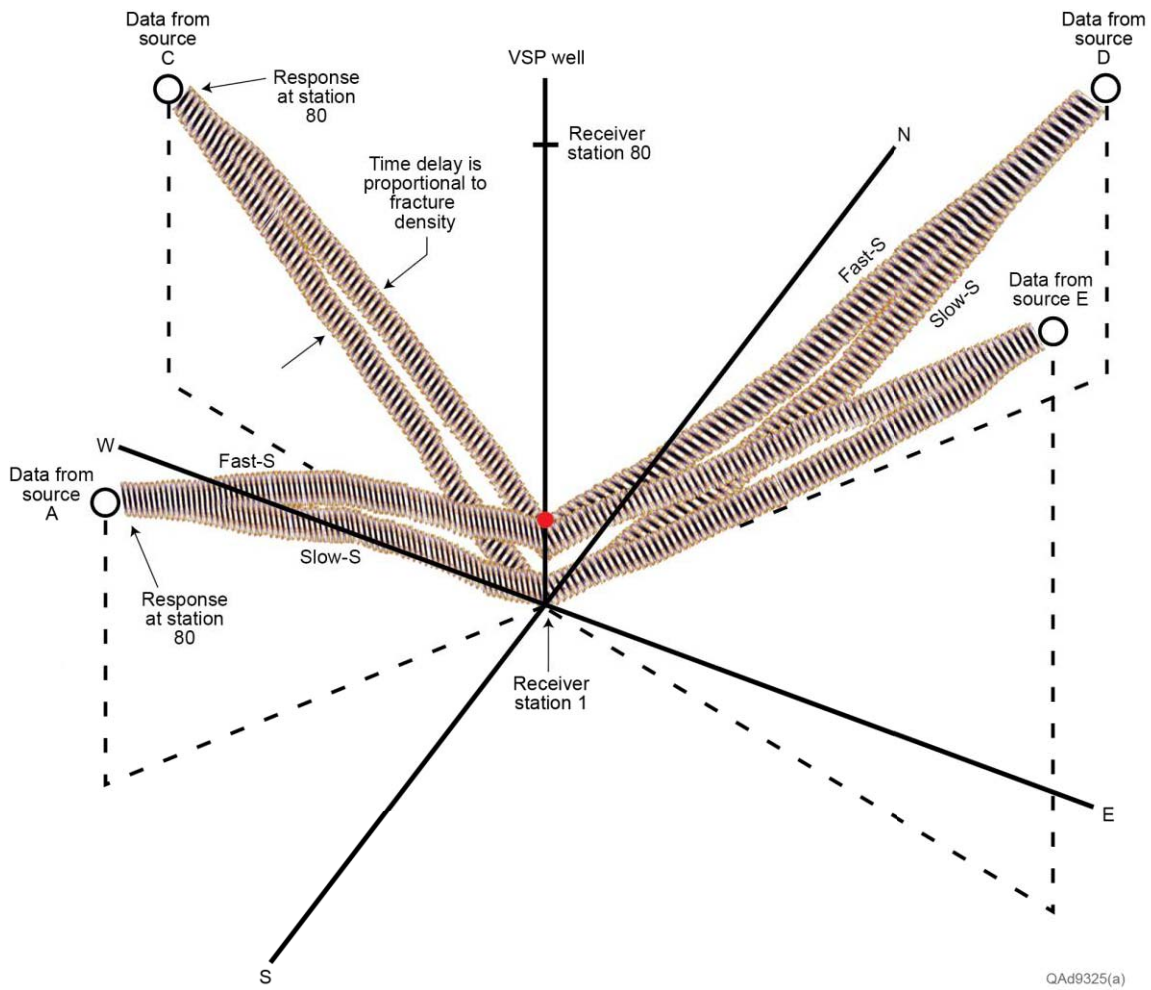


Figure 4.13. Partial construction of a volumetric picture of S-wave anisotropy around this VSP well using Alford rotation results from orthogonal-azimuth source-station pairs. Only S_2 time delays from source stations A, C, D, and E are shown.

Non-Orthogonal Source Stations

Analyses done to this point have utilized direct-S data generated by vertical vibrators positioned at azimuths that are approximately orthogonal relative to the VSP receiver well. We now utilize direct-S data generated by vertical vibrators stationed at azimuths that differ significantly from 90 degrees. Data are considered from source station B and source station DD, whose azimuths differ by 162 degrees.

These source-receiver azimuth angles imitate source-receiver geometries that can be encountered when processing surface-based 3D multicomponent seismic data. Analysis of VSP data that provide S-wave vectors having both small differences and large differences in azimuth orientation should help establish the level of confidence that can be assumed when Alford rotation procedures are applied to surface-recorded, full-azimuth 3D S-wave data. If inconsistent fast-S and slow-S azimuths occur at the same subsurface point when direct-S VSP data from variable-azimuth source pairs are processed by Alford rotation principles, that same inconsistency can occur when analyzing data acquired with surface-based 3D sources and receivers deployed over a wide range of azimuths. If inconsistent slow-S time delays are found at a VSP receiver station when direct-S modes propagate from source stations having different azimuths, that same inconsistent slow-S time delay should occur when 3D surface-based S-wave data using the same source stations and the same source-to-receiver azimuths..

Downgoing radial-S and transverse-S modes produced by source pair B and DD are exhibited on Figure 4.14a after first-arrival times at receiver station 80 are adjusted to time datum T. The first-arrival wavelets are replaced with Gaussian wavelets on Figure 4.14b. The amplitudes of these Gaussian wavelets are scaled to match the relative amplitudes of the direct-S first-arrival wavelets. Alford rotations of the Gaussian wavelet data at receiver station 1, the deepest receiver station, are displayed as Figure 4.15. Azimuths of the N1 and N2 natural coordinate axes estimated from this calculation are 174 degrees and 84 degrees from North, respectively. These estimates differ from log-measured azimuths of fracture orientation by 62 degrees. The implication is that data generated by vertical-vibrator stations positioned at azimuths that differ significantly from 90 degrees will not provide reliable estimates of fracture azimuth.

The magnitudes of the depth-dependent S_2 time delays calculated from source pair B and DD are displayed on Figure 4.16. Although we now question the reliability of fracture azimuth estimates calculated from direct-S modes produced by vertical vibrators, we conclude Alford rotation results calculated from data generated by a non-orthogonal-azimuth vertical-vibrator source pair provide reliable estimates of differences in S_1 and S_2 arrival times and create reliable estimates of S-wave anisotropy along each of the two source-to-receiver travel paths used in an Alford rotation calculation. Thus the S-wave anisotropy behaviors exhibited on Figure 4.16 should provide qualitative estimates of fracture intensity along travel paths from vertical-vibrator source stations that are not positioned at orthogonal azimuths from a VSP well.

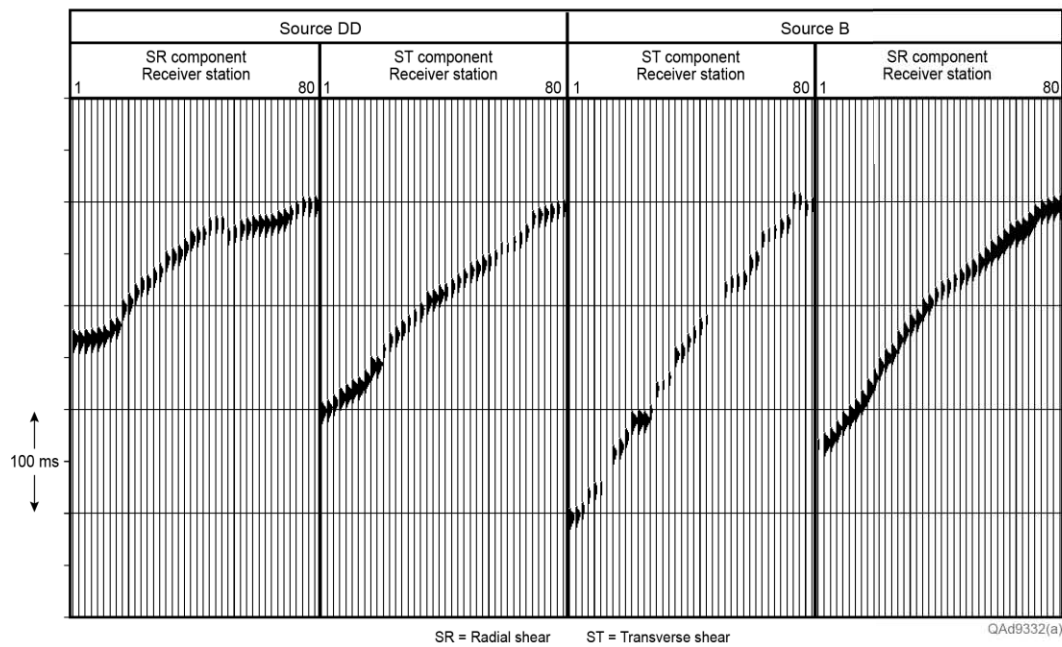
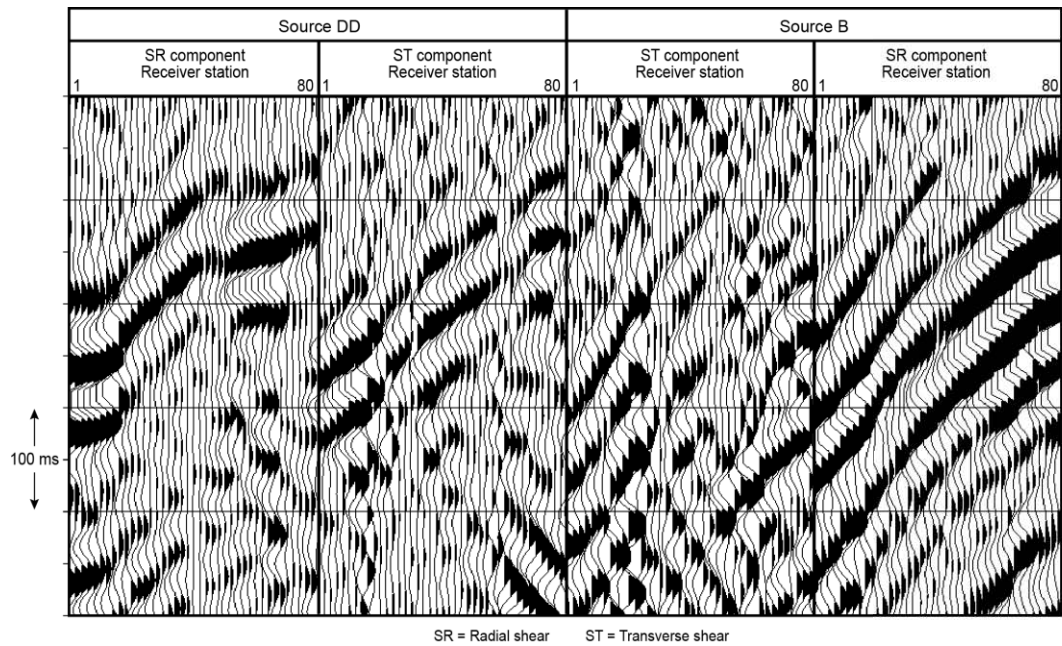


Figure 4.14. (a) Direct radial-S and transverse-S wavefields from orthogonal-azimuth vertical-vibrator source stations B and DD after shifting the arrival times at receiver station 80 to time datum T to remove the effects of travel time differences through the overburden. (b) Relative-amplitude Gaussian wavelets centered on first-arrival times.

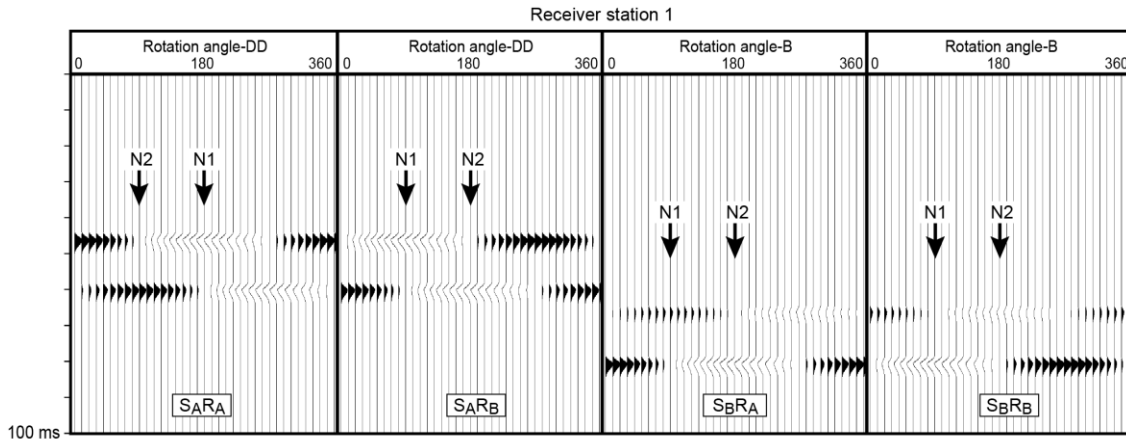


Figure 4.15. Alford rotation at receiver station 1 using direct-S wavelets propagating from vertical-vibrator source stations B and DD. N1 and N2 = azimuths of natural coordinate axes measured counterclockwise from source station B.

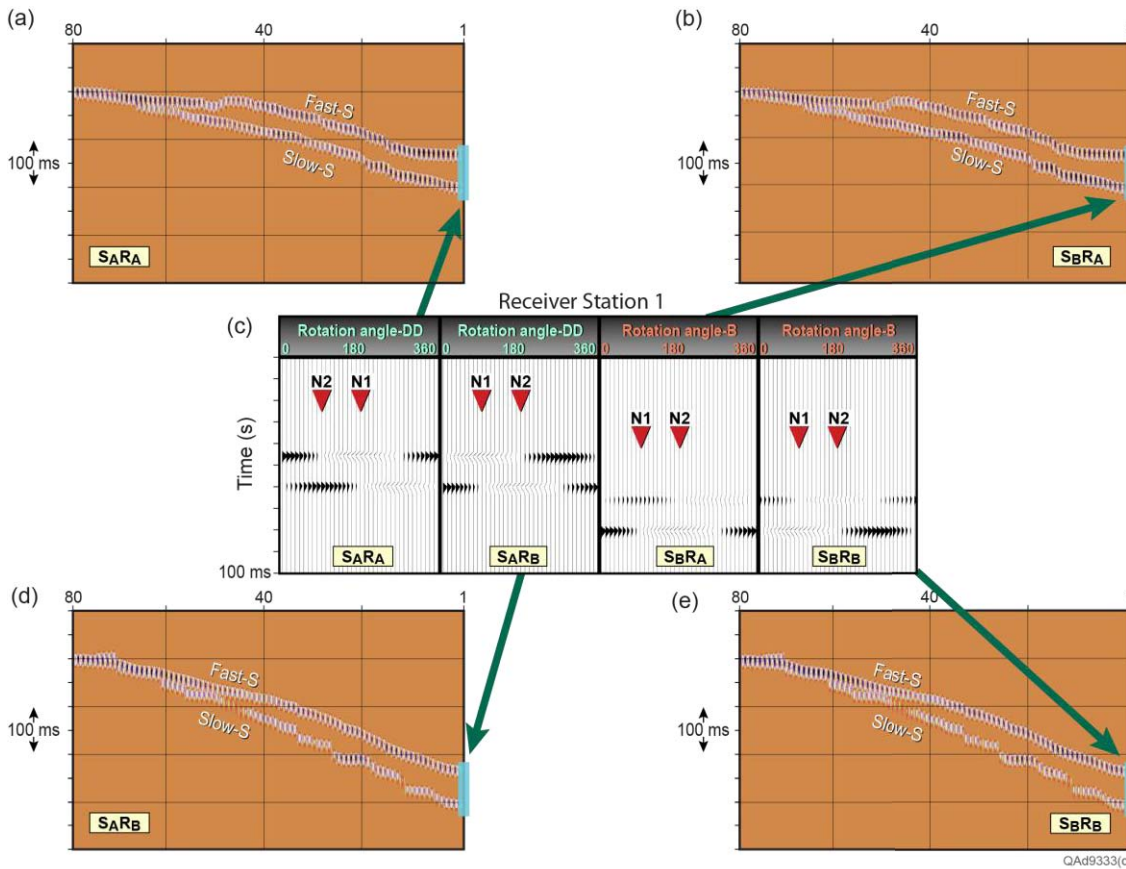


Figure 4.16. S_1 and S_2 arrival times calculated from direct-S modes produced at vertical-vibrator source stations B and DD.

Comparison with Calibration Data

S-wave anisotropy values estimated from direct-S modes produced by horizontal vibrators are plotted on Figure 4.17. These S-wave anisotropy values were calculated by a commercial VSP data processing company, not by our research team. S-wave anisotropy values calculated along slant paths from far-offset source stations A and E are added to the plot as open circles spanning the reservoir interval from 8,000 to 12,000 ft [2440 to 3660 m]. These open-circle data points represent the slow-S time delay depicted by Alford rotation matrix term S_1R_1 from Figure 2.17a (Chapter 2). Because slant-paths from far-offset source stations A and E to VSP receiver stations are longer than vertical travel paths from zero-offset stations to those same receiver stations, larger S_2 time-delays are measured for the far-offset vertical-vibrator data. These slant-path estimates of S-wave anisotropy should be more representative of what occurs when large-offset 2D and 3D S-wave surveys are acquired with surface-based sensors.

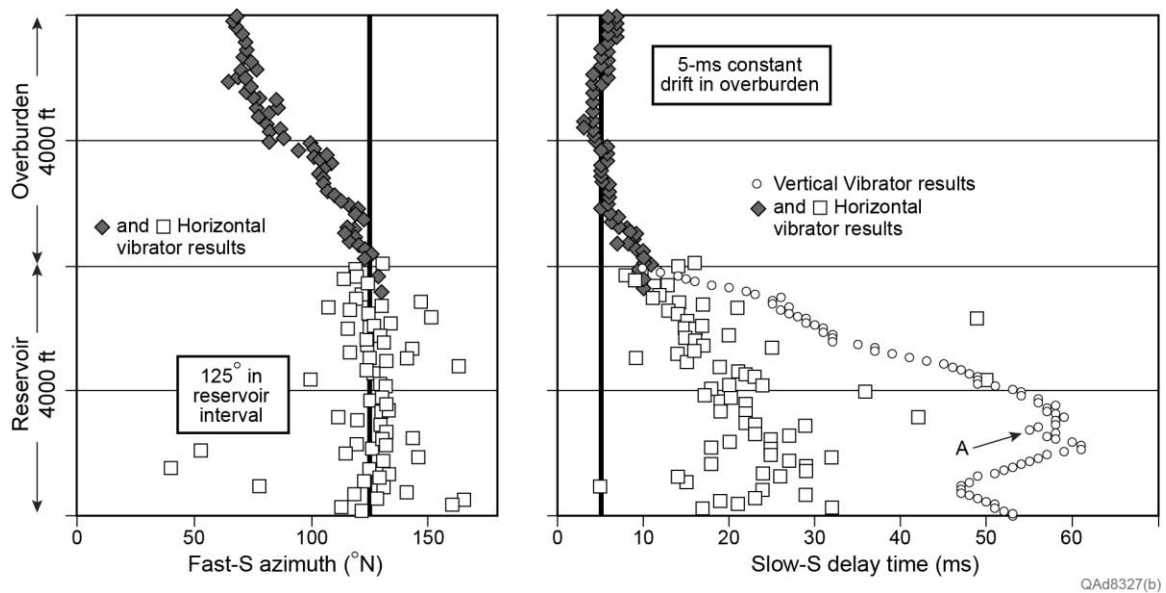


Figure 4.17. Comparisons between S_2 time delays estimated from data generated by zero-offset horizontal S-wave vibrators (data shown as diamonds and squares) and equivalent estimates made at thin depth increments of 50-ft using data generated by vertical vibrators at source stations A and E (data shown as open circles).

The smooth, consistent, depth behavior of S_2 time delays calculated from vertical-vibrator direct-S modes is impressive and quite a contrast to the noisy, erratic trend calculated with horizontal-vibrator data. The reversal in the vertical-vibrator time-delay curve starting at depth A is assumed to be caused by overpressure. Production engineers who operate wells in this field have documented overpressure conditions in the deepest reservoir units in several wells (private communication from operator). The horizontal-vibrator and vertical-vibrator data comparisons on Figure 4.17 show that direct-S wavefields produced by vertical vibrators provide valuable fracture-sensitive data, just as do S waves produced by horizontal vibrators. In particular, vertical-vibrator wavefields produce estimates of fracture intensity over intervals as thin as 50 ft, and appear to do so with an accuracy equivalent to, and perhaps superior to, that achieved with horizontal vibrators.

Conclusions

The data analyzed in this chapter allowed us to combine the concept of direct-S modes produced by vertical vibrators with the concept of positioning vertical vibrators at orthogonal-azimuth source stations to analyze fracture orientation and fracture density within a thick stack of fractured tight gas sandstones. We conclude that estimations of fracture orientation calculated from direct-S modes produced by orthogonal-azimuth vertical vibrators are not stable, but vary unacceptably when different options of orthogonal-azimuth source pairs are selected. It is appropriate to mention that when horizontal vibrators are arranged in orthogonal azimuths at a zero-offset station to generate direct-S mode data for estimating fracture orientation that no redundancy check has ever been made, to our knowledge, by using a second pair of horizontal vibrators at another source station as we did with vertical vibrators at this test site. It would be interesting to know if redundant horizontal-vibrator data would be stable or would exhibit variations in estimated fracture azimuths of the same magnitude we observed for direct-S modes from vertical vibrators.

We conclude the estimates of S-wave anisotropy provided by direct-S vertical vibrators are reliable. We propose that the estimates of S-wave anisotropy we produce along slant-paths from far-offset vertical-vibrator source stations to a VSP receiver are more valuable for depicting fracture density around a VSP well than are the vertical-path estimates made by zero-offset horizontal vibrators. Our logic is that slant-path estimates provide estimates of fracture density at large distances from a VSP well and in many azimuth directions. Direct-S modes produced by zero-offset horizontal vibrators provide estimates of S-wave anisotropy in only a slim cylinder of rocks immediately around a VSP well, whereas in contrast, direct-S modes from far-offset vertical vibrators allow fracture density to be mapped in a large volume of rocks that extends large radial distances and in many azimuth directions away from a WAR VSP well.

Chapter 5

Concluding Remarks and Recommendations

Introduction

VSP data that illuminate unconventional reservoirs in two diverse geological settings have been analyzed to demonstrate that the use of direct-S modes produced by vertical vibrators at orthogonal-azimuth source stations is a valuable way to evaluate fracture systems and anisotropic properties of unconventional reservoir systems. This investigation establishes important principles of elastic wavefield physics, with key findings being:

1. SV shear wavefields are produced directly at the point where a vertical vibrator applies its vertical force vector to the earth.
2. These direct-SV wavefields are robust and can be used to estimate S-wave anisotropy in the same manner as S wavefields produced by horizontal vibrators. In any fracture-prone reservoir, S-wave anisotropy indicates fracture intensity, with increases in anisotropy implying higher fracture densities. We used direct-SV modes generated by vertical vibrators to create S-wave anisotropy profiles at two unconventional reservoir prospects and compared these seismic estimates with S-wave anisotropy values calculated from downhole data. In our study at a Marcellus Shale prospect, we compared S-wave anisotropy estimates determined from vertical-vibrator direct-S data with values determined from a dipole sonic log. The seismic estimates were essentially identical to the dipole-sonic values. Both types of data predicted low anisotropy values of the order of 2-percent. At our tight sandstone study site, we compared S-wave anisotropy determined from vertical-vibrator data with values determined from direct-S waves produced by horizontal vibrators. The vertical-vibrator estimates yielded a smooth trend in which it was easy to see the onset of overpressure. In contrast, the horizontal-vibrator data exhibited a large scatter that did not allow the onset of overpressure to be recognized.
3. Unexpectedly, our methodology did not produce consistent estimates of fracture orientation. More work needs to be done to determine if fracture orientation is a fracture attribute that cannot be predicted with direct-S modes produced by vertical vibrators. Specifically, we obtained different estimates of fracture orientation when we used direct-S modes produced by different combinations of orthogonal-azimuth vertical vibrators. It is appropriate to observe that to the knowledge of this research team, no one has ever used VSP data produced by more than one pair of horizontal vibrators to estimate fracture orientation. Thus it is not known if inconsistent fracture orientations would also be obtained if two sets of

horizontal vibrators were used at different offsets and azimuths away from a VSP well as we did in this study with vertical vibrators.

4. When vertical-vibrator source stations are distributed in a circle around a VSP well, azimuth-dependent direct-S and direct-P average velocities can be calculated to allow natural-coordinate axes to be recognized. Using all available calibration data, the azimuths of these natural coordinate axes can then be associated with either the azimuths of vertical fractures or with the azimuths of maximum and minimum horizontal stresses.

Observations

The implications of the principles listed above can be significant in VSP data-acquisition. Specifically, the necessity to deploy horizontal vibrators in order to create S wavefields can be avoided in many VSP S-wave applications. The number of horizontal vibrators available worldwide has always been, and still is, a small number. In contrast, hundreds of vertical vibrators are used in seismic programs around the world. By reducing the requirement to deploy horizontal vibrators, VSP S-wave data acquisition can be expanded to more basins and prospect areas.

The implications in VSP data processing are equally significant. In particular, the limitation is removed that the only S mode that can be processed when a vertical-vibrator source is used is a P-to-SV converted mode created at subsurface interfaces. Instead, vertical-vibrator sources should be viewed as providing two S-wave modes for data processors: (1) the popular P-SV mode produced at remote interfaces, and (2) a direct S-S mode produced directly at the source station. The value of having two independent S-wave modes is that P-SV and S-S waves exhibit different reflectivities at interfaces and provide different information about rock and fluid properties within propagation media.

This study documents Alford rotation can be applied to a wider range of VSP data than some investigators have supposed. Examples from this study show Alford rotation concepts can be applied to VSP data that violate the following assumptions that many investigators impose on VSP data that are used to determine natural-coordinate axes.

1. VSP data can be used when source-receiver offsets exceed receiver depth, and when raypath arrival angles are 45° and larger. This use of Alford rotation contrasts with the common assumptions that source-to-receiver offsets for data used in Alford rotation procedures should be small and that raypath arrival angles of S-wave raypaths at VSP receiver stations should be close to vertical.

2. VSP S-wave data can be used when the radial and transverse S-wave displacement vectors used in Alford rotation are not oriented in orthogonal azimuths. In contrast, most data processors take great care to use S-wave data in Alford rotation analyses in which radial and transverse displacement vectors are as close to orthogonal as possible.
3. Vertical vibrators used in this analysis were positioned at widely separated source stations and raypaths from the sources traversed significantly different overburden conditions before reaching a targeted reservoir interval. In contrast, data preferred for Alford rotation are produced by orthogonal horizontal vibrators positioned at the same zero-offset source station so that source wavelets travel identical trajectory paths through identical overburden conditions to reach a fracture interval.

Recommendations

We do not encourage gross violations of zero-offset S-wave data, coincident S-wave source stations, and orthogonal S-wave source displacement vectors when applying Alford rotation concepts, but neither should Alford rotation be abandoned when S-wave data have been acquired that violate one or more of these conditions. The results achieved in this study confirm Alford rotation is a robust procedure that produces valuable results (i.e. S-wave anisotropy information) when S-wave data conditions depart from ideal.

When there is an interface above a fractured interval that produces a reasonable-quality P-to-SV converted mode, two sets of downgoing S-wave modes can be used to estimate fracture attributes when VSP data are acquired with orthogonal-azimuth vertical vibrators. Wave-mode pair 1 utilizes downgoing direct-S data, and wave-mode pair 2 uses downgoing P-SV converted-mode data. This S-wave redundancy can be useful because one mode (either converted-S or direct-S may have a better signal-to-noise ratio than the other. Also, converted-S data tend to have a wider frequency spectrum than direct-S data, and this broader P-SV frequency spectrum may allow converted-mode data to be used to study thinner fracture intervals than can be studied with lower-frequency direct-S data.

When all of these observations are combined, the result is that positioning vertical vibrators at quasi-orthogonal-azimuth VSP source stations allows valuable fracture attribute information to be acquired and analyzed. For the time being, standard Alford rotation procedures seem to be the most effective method for extracting fracture-sensitive information from the direct-S modes acquired with this distinctive source geometry.

In the VSP application described in this report, it is preferred to deploy vertical vibrators at source stations that have source-to-receiver azimuths that

differ by 90° in order to illuminate a fractured interval with orthogonal S-wave displacement vectors. However, when acquiring 2D and 3D reflection data with surface receivers, this orthogonal-azimuth source-station geometry has to be abandoned. The next phase of developing vertical-vibrator S-wave technology will be to expand the direct-S methodology described here away from VSP applications to surface-recorded data. Concepts are usually more difficult to demonstrate and verify with surface-positioned sensors than with VSP receivers.

References

- Alford, R. M., 1986, Shear data in the presence of azimuthal anisotropy—Dilley, Texas: Paper S9.6, Expanded abstracts of 56th Annual Meeting of Society of Exploration Geophysicists, p. 476-479.
- Alford, R. M., H. B. Lynn, and L. A. Thomsen, 1989, Seismic surveying technique for the detection of azimuthal variations in the earth's subsurface: U.S. Patent 4,817,061.
- Alford, R.M., 1989, Multisource multireceiver method and system for geophysical exploration: U.S. Patent 4,803,666.
- Angerer, E., S. Crampin, X.Y. Li, and T.L. Davis, 2002, Processing, modeling, and predicting time-lapse effects of overpressured fluid-injection in a fractured reservoir: *Geophys. J. Int.*, v. 149, p. 276-280.
- Daley, P. F., 2002, S-shear energy from a P-wave source: CREWES Research Report, v. 14.
- Delinger, J.A., and B. Nolte, 1997, A crossed-dipole reciprocity paradox: *The Leading Edge*, v. 16, p. 1465-1471.
- Delinger, J.A., B. Nolte, and J.T. Etgen, 2001, Alford rotation, ray theory, and crossed-dipole geometry: *Geophysics*, v. 66, p. 637-647.
- Fertig, J., 1984, Shear waves by an explosive point-source – the Earth surface as a generator of converted P-S waves: *Geophysical Prospecting*, v. 32, p. 1-17.
- Geyer, R. L., and S. T. Martner, 1969, SH waves from explosive sources: *Geophysics*, v. 34, no. 6, p. 893-905.
- Hardage, B.A., 1983, *Vertical seismic profiling*: Geophysical Press, 450 pages.
- Hardage, B.A., 1985, *Vertical seismic profiling (second edition)*: Geophysical Press, 512 pages.
- Helbig, K., and C. S. Mesdag, 1982, The potential of shear-wave observations: *Geophysical Prospecting*, v. 30, p. 413-431.
- Hood, K. C., and D. A. Yurewica, 2008, Assessing the Mesaverde basin-center gas play, Piceance Basin Colorado: AAPG Hedberg Series No. 3, p. 87-104.
- Hou, A., and Marfurt, K.J., 2002, Multicomponent prestack depth migration by scalar wavefield extrapolation: *Geophysics*, v. 67, p. 1886-1894.
- Lash, G.C., 2007, Influence of basin dynamics on Upper Devonian Black Shale deposition, western New York state and northwest Pennsylvania: AAPG Search and Discovery Article #30050 (2007).
- Li, Y., P. Sun, D. Tang, Y. He, H. Chen, and Y. Yue, 2007, Imaging through gas-filled sediments with land 3C seismic data: EAGE 69th Conference and Exhibit, Expanded Abstract B022 (5 pages).

- Liu, Y., Q. Zhang, L. Bao, and X. Wei, 2007, Pure S-waves in land P-wave source VSP data: *Applied Geophysics*, v. 4, no. 3, p. 173-182.
- Luschen, E., 1994, Crustal bright spots and anisotropy from multicomponent P and S wave measurements in southern Germany: *Tectonophysics*, v. 232, p. 343-354, Elsevier Science Publishers.
- Lynn, H. B., 2004a, The winds of change: anisotropic rocks—their preferred direction of fluid flow and their associated seismic signatures, Part 1: The Leading Edge, v. 23, p. 1156-1162.
- Lynn, H. B., 2004b, The winds of change: anisotropic rocks—their preferred direction of fluid flow and their associated seismic signatures, Part 2: The Leading Edge, v. 23, p. 1258-1268.
- Mazzotti, A., R. G. Ferber, and R. Marschall, 1989, Two-component recording with a P-wave source to improve seismic resolution: *Surveys in Geophysics*, v. 10, p. 155-222, Kluwer Academic Publishers.
- Michaud, G., and R. Snieder, 2004, Error in shear-wave polarization and time splitting: *Geophy. Prospecting*, v. 52, p. 123-132.
- Miller, G., and H. Pursey, 1954, The field and radiation impedance of mechanical radiators on the free surface of a semi-infinite isotropic solid: *Proceedings of the Royal Society of London, Series A*, v. 223, 521-541.
- Mueller, M.C., 1991, Prediction of lateral variability in fracture intensity using multicomponent shear-wave surface seismic as a precursor to horizontal drilling in the Austin Chalk: *Geophys. J. Int.*, v. 107, p. 409-415.
- O'Brien, J., 1992, VSP measurement of shear-wave velocities in consolidated and poorly consolidated formations: *Geophysics*, v. 57, no. 12, p. 1583-1592.
- Sondergeld, C. H., and C. S. Rai, 1992, Laboratory observations of shear-wave propagation in anisotropic media: *The Leading Edge*, v. 11, 38-43.
- Sun, Z, and M. J. Jones, 1993, Seismic wavefields recorded at near-vertical incidence from a counterphase source: *CREWES Research Report*, v. 5, p. 7.1 – 7.12.
- Thomsen, L. 1995, Elastic anisotropy due to aligned cracks in porous rock: *Geophysical Prospecting*. v. 43, p. 805-829.
- White, J. E., 1983, *Underground sound—applications of seismic waves*: Elsevier Science Publishers.
- Winterstein, D.F., and M.A. Meadows, 1991, Changes in shear-wave polarization azimuth with depth in Cymric and Railroad Gap oil fields: *Geophysics*, v. 56, p. 1349-1364.
- Winterstein, D.F., and G.S. De, 2001, VTI Documented: *Geophysics*, v. 66, p. 237-245.
- Yang, L., Z. Qinghong, B. Leiyang, and W. Xiucheng, Pure S-waves in land P-wave source VSP data: *Appl. Geophys.*, v. 4, no. 3, p. 173-182.
- Yokoi, T., 1996, Numerical study on the generation of downgoing S-waves by a vertical force acting close to a step-like topography: *Geophysics*, v. 61, no. 1, p. 192-201.

- Zeng, X., and C. Macbeth, 1993, Algebraic processing techniques for estimating shear-wave splitting in near-offset VSP data – theory: *Geophys. Prospecting*, v. 41, p. 1033-1066.
- Zhao, X., R. Zhou, Y. Li, P. Janak, and D. Dushman, 2005, Shear waves from near-offset VSP survey and applications: SEG XXth Annual Meeting and Exhibition, Expanded Abstract VSP 1.6, p. 2629-2632.
- Zhou, R., X. Zhao, and D. Dushman, 2005, Shear-wave anisotropy from far-offset VSP: SEG XXth Annual Meeting and Exhibition, Expanded Abstract MC 4.2, p. 971-974.

Glossary

crossline: the direction normal to a receiver line. See **inline**.

direct-S: an S mode produced directly at the point where a vertical vibrator applies its force vector to the earth

inline: the direction in which a receiver line is deployed. See **crossline**.

natural coordinate axes: coordinate axes within the earth along which anisotropic earth conditions cause fast-velocity and slow-velocity seismic modes to propagate.

N1: one of the earth natural-coordinate axes

N2: one of the earth natural-coordinate axes

principal axes: a term sometimes used instead of “natural coordinate axes”. See **natural coordinate axes**.

radial: the azimuth direction from a source (receiver) station to a receiver (source) station. See **transverse**.

S1: fast S-wave mode

S2: slow S-wave mode

SH: transverse shear mode

SV: vertical shear mode

transverse: the azimuth direction orthogonal to the radial azimuth. See **radial**.

VSP: vertical seismic profile

WAR: walkaround

WAR VSP: walkaround vertical seismic profile

Appendix A

This appendix is a copy of a paper that is scheduled to be published in the April 2013 issue of the *Journal of Seismic Exploration*. The material in this journal paper is part of the PhD thesis deliverables required of Engin Alkan at The University of Texas at Austin. The data presented here are analyses of real-data direct-S modes produced by vertical and horizontal vibrators. The wave-mode comparisons that are presented provide additional proof that a vertical vibrator produces direct-S modes that appear to be equivalent to the direct-S modes produced by horizontal vibrators.

Direct-S Wave Modes Produced by Vertical and Horizontal Vibrators

Engin Alkan and Bob Hardage
Exploration Geophysics Laboratory
Bureau of Economic Geology
Austin, TX 78713-8924

Introduction

We present here an investigation of direct-S radiation patterns generated by vertical and horizontal vibrators. In our terminology, a direct-S mode is an S wave produced directly at the point where a seismic source applies its force vector to the Earth. We describe our field-test procedure and then analyze VSP data that describe downgoing direct-S wavefields generated by two types of vibratory seismic sources—a vertical vibrator that applies a vertical force to the Earth, and a horizontal vibrator that applies a horizontal force to the Earth. In the analyses presented here, we demonstrate that strong direct-S modes are produced by vertical vibrators and that these vertical-vibrator direct-S modes are reasonably equivalent to direct-S modes produced by horizontal vibrators, the latter being the sources most geophysicists prefer to use to generate direct-S modes.

At our test site, we found that the highest frequency in propagating direct-S modes was 50 to 55 percent of the highest frequency component of the vibrator sweep that generated each direct-S mode. Because vertical vibrators can be swept to higher frequencies than horizontal vibrators, direct-S modes produced by vertical vibrators have wider frequency spectra, and wavelets that provide better spatial resolution of geologic targets, than do direct-S modes produced by horizontal vibrators.

Devine Test Site

This field test was done at the Devine Test Site operated by the Bureau of Economic Geology, a research unit of The University of Texas at Austin. The Devine Test Site was constructed by Sohio southwest of San Antonio, Texas, near the town of Devine (Fig. 1a) in the 1980's. Sohio used the site to develop crosswell seismic and electromagnetic profiling technologies. After Sohio and BP merged, BP transferred the test site to The University of Texas at Austin so that the property could be managed by the University as a public test site. An aerial photo showing the distribution of test wells across the property is included as Figure 1b.

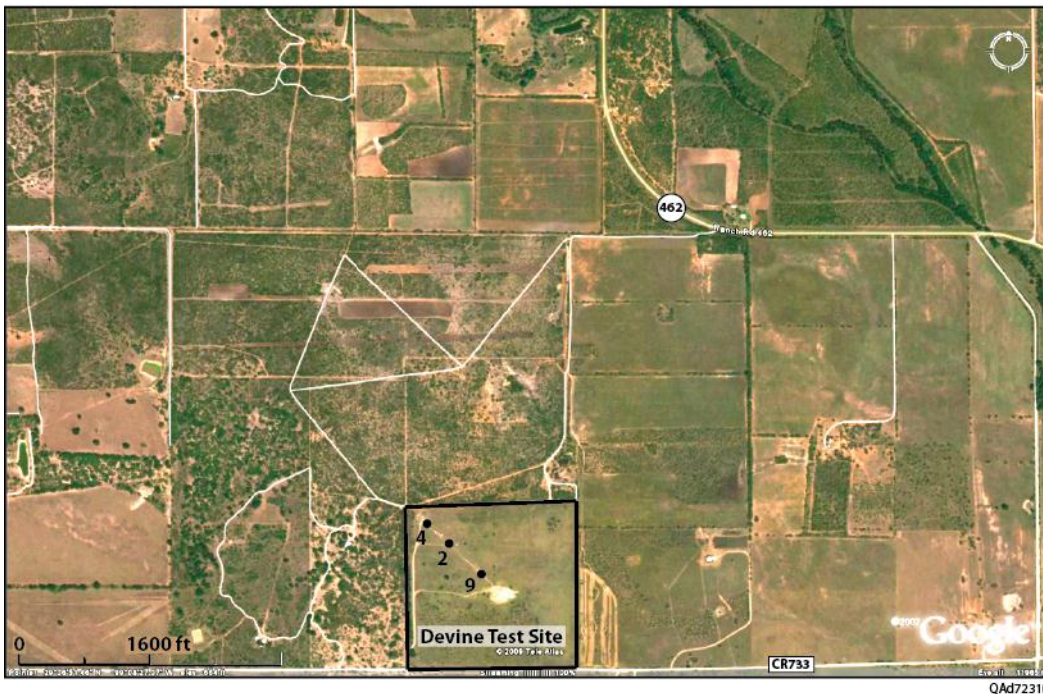
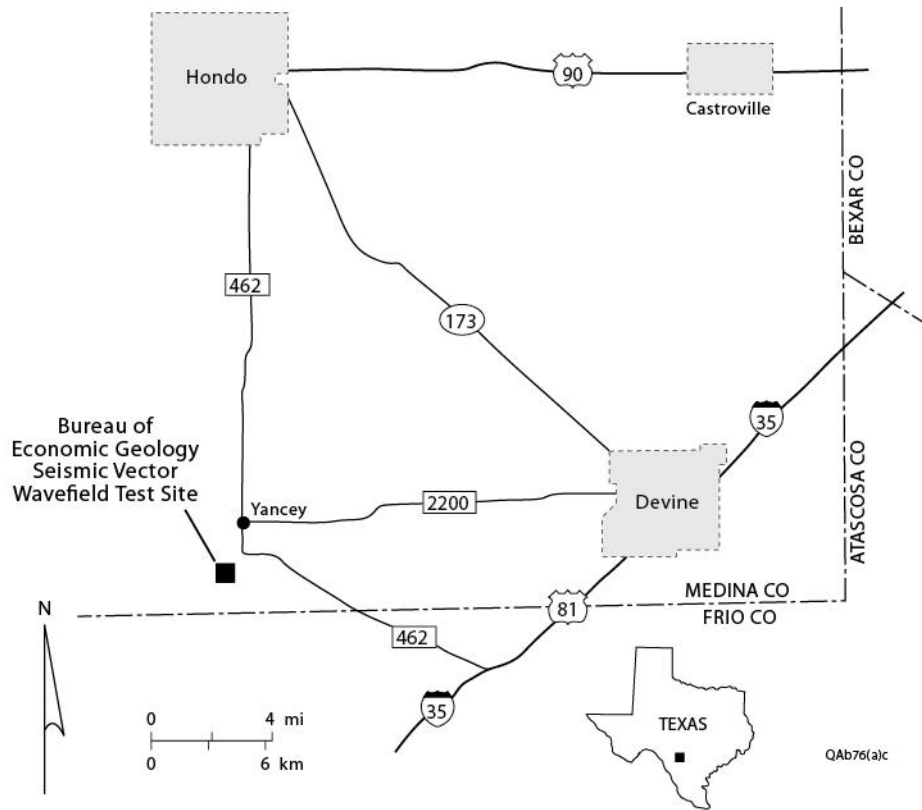


Figure 1. (a) Location of the 100-acre Devine Test Site in Medina County, Texas. The city of San Antonio is approximately 50 km east of the town of Hondo shown on this map. (b) Photo showing the positions of test wells 4, 2, and 9 across the test-site property. These wells were constructed for the purpose of deploying downhole instrumentation, particularly seismic sources and receivers and logging tools. All wells are 3000 ft (914 m) deep.

The stratigraphy penetrated by the test wells is labeled on the well log curves displayed as Figure 2. These logs were recorded in well 4 (Fig. 1b) and define V_P and V_S velocities and gamma-ray readings across the rock units that form the seismic propagation medium beneath the test-site property. These log measurements start immediately below the base of surface casing, which is at a depth of 532 ft (162 m) in well 4 where these logs were recorded.

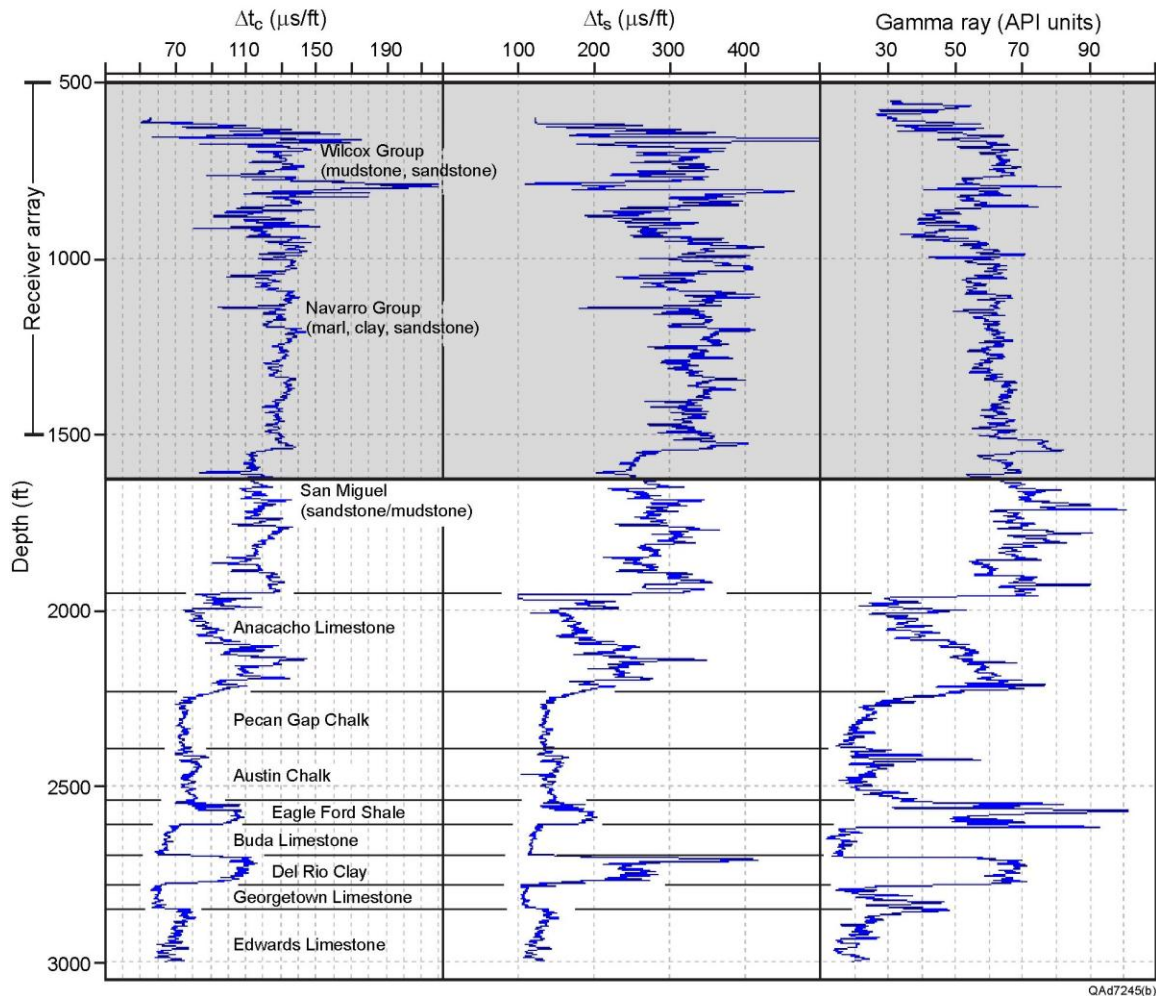


Figure 2. V_P and V_S velocity logs and gamma-ray log acquired in well 4 on the Devine Test Site. The shaded interval defines the depth range over which downhole geophones were deployed for the source tests described here.

Source-Receiver Geometry

The source-receiver geometry we utilized to evaluate surface-source P and S radiation patterns combined the concepts of horizontal wave testing (involving only a horizontal receiver array) and vertical wave testing (involving only a vertical receiver array) as described by Hardage (2009, 2010). Much of

our wave-test philosophy was inspired by the field technique published by Robertson and Corrigan (1983). These researchers used a single subsurface 3C geophone to quantify SH and SV radiation patterns produced by a horizontal vibrator. We expanded their methodology by using a vertical array of twenty-four 3C geophones, deploying vertical-force, inclined-force, and horizontal-force sources, and analyzing P-wave radiation patterns produced by these sources in addition to S-wave radiation patterns. Although we generated a comprehensive source-test database, only analyses of direct-S waves produced by vertical and horizontal vibrators and recorded by a downhole vertical array of receivers will be presented in this paper.

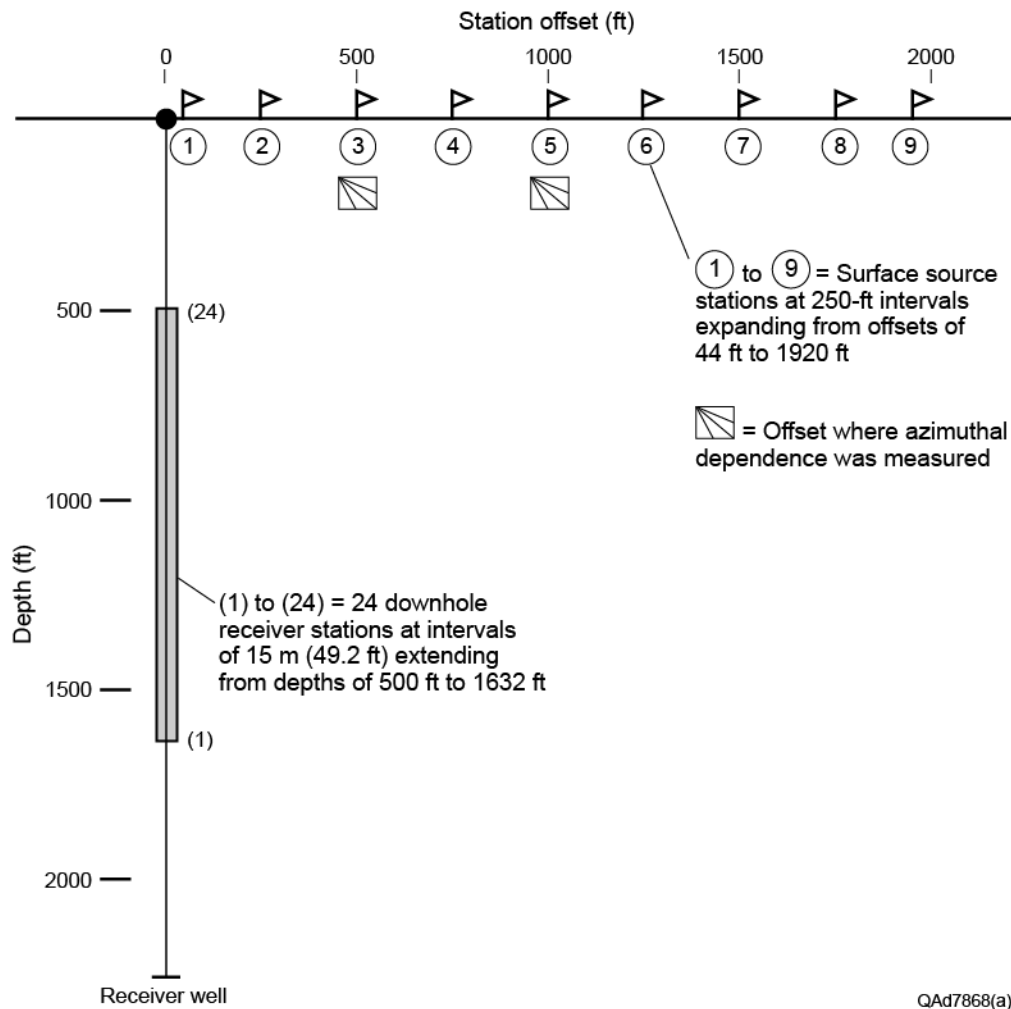


Figure 3. Source-receiver geometry used to analyze P and S radiation patterns emitted by surface-based seismic sources. A 24-station vertical array of 3C geophones spaced at intervals of 15 m (49.2 ft) spanned the depth interval from 500 to 1632 ft in well 4. Source stations were offset from the test well at intervals of 250 ft (76 m). Horizontal-force sources were activated at several different azimuth orientations relative to the line of profile at source stations 3 and 5, as shown by the special labels at these stations.

Well 4 on the Devine Test Site property was chosen for the location of the vertical receiver array. A 24-station receiver system was deployed in this well. Receiver stations spanned a depth interval extending from 500 to 1632 ft (Fig. 3). The velocity layering and lithology variations local to this vertical sensor array are defined by the log character inside the shaded interval shown on Figure 2.

In this source test, we defined the inline (radial) direction as the azimuth of the straight-line profile that passed through the nine source stations and the receiver well (Fig. 3). The crossline (transverse) direction was perpendicular to the vertical plane of this profile. At inline source stations 3 and 5 (offset 500 and 1000 ft (305 m) from the receiver well), a horizontal vibrator was positioned at several azimuth orientations relative to the line of profile to generate data describing the azimuth-dependent character of S-wave radiation patterns produced by a horizontal-vibrator source. The azimuth directions in which each horizontal force was applied to the Earth surface at these two offset stations are illustrated on Figure 4. This diagram describes how the horizontal vibrator was positioned in 10° azimuth increments to transition from a crossline baseplate orientation (0° azimuth of vehicle headlights in our notation on Figure 4) to an inline baseplate orientation (90° azimuth of vehicle headlights). In this diagram, line AB is the inline (radial) direction. A photo of a horizontal vibrator generating azimuth-dependent data at source station 3 is shown as Figure 5.

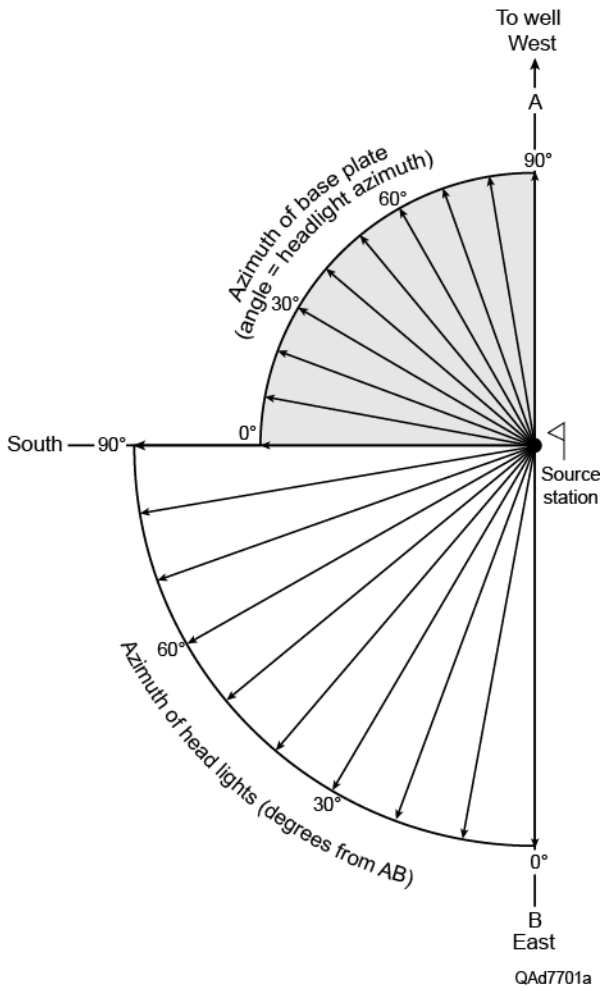


Figure 4. Map view of azimuth directions in which horizontal forces were applied at source stations 3 and 5. The diagram is drawn to describe the azimuth positions assumed by a horizontal vibrator (bottom) and its base plate (top).

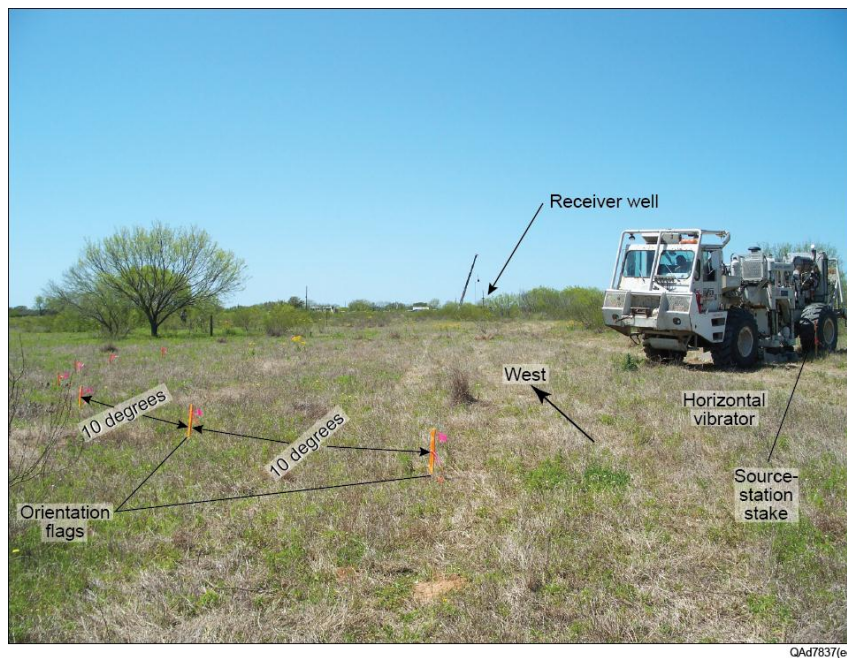


Figure 5. Horizontal vibrator executing a sequence of 10° azimuth positions at source station 3.

Vertical-Force Sources and Direct-S Modes

A robust amount of SV shear energy is produced by a vertical-force seismic source. This principle is illustrated on Figure 6 which shows the geometrical shapes and relative strengths of P and SV energy propagating away from the point where a vertical-force source applies its force vector to a homogeneous Earth. The P and SV radiation patterns shown by this figure are replications of analyses published by Miller and Pursey (1954) and White (1983). Both P and SV modes are generated directly at the point where vertical force vector F contacts the Earth surface. The relative strengths of P and SV modes propagating at any take-off angle from the source station are indicated by the radial distances from the origin point to the outer edges of the P and SV radiation patterns. For example, in Figure 6a the magnitude of the SV mode propagating at an angle of 30-degrees from vertical is approximately 8 times greater than the magnitude of the P mode propagating in that same take-off direction.

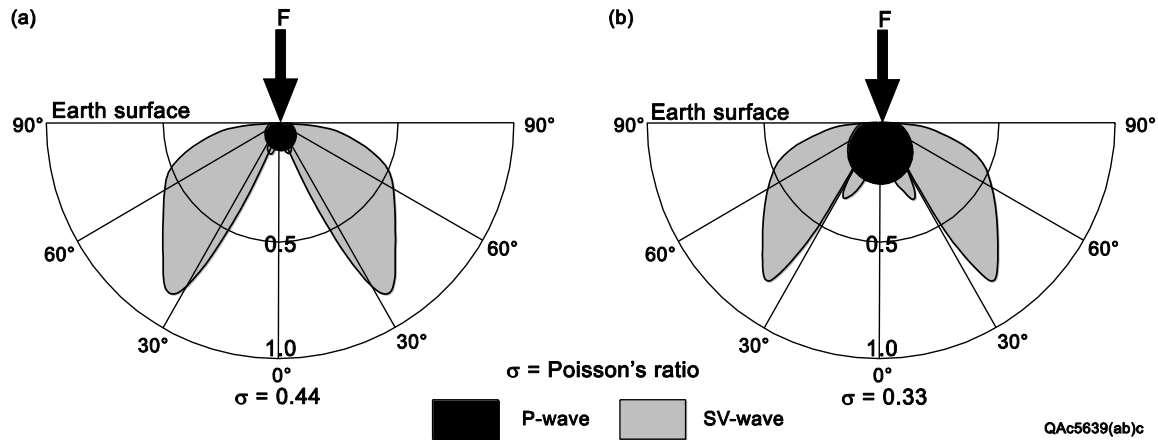


Figure 6. P and SV radiation patterns produced when a vertical force is applied to the surface of a homogeneous Earth. (a) A soft Earth surface. (b) A hard Earth surface. In both cases more SV energy radiates from the source station than does P energy.

Previous researchers have used this model as the starting point for investigations into direct-S illumination of geologic targets by vertical-force sources. Edelmann (1981) analyzed S displacement vectors associated with raypaths slanted at arbitrary takeoff angles in the SV lobes of Figure 6 to conclude that a vertical vibrator should create SH illumination in addition to SV illumination. Fertig and Krajewski (1989) used the same radiation diagram in their study and made the important declaration that not only does a vertical vibrator produce direct-S modes, but so does a shot-hole explosive and an air gun in a pit. Lynn and McCardle (1990) also state direct-S waves are produced by air guns operating in rectangular pits and show direct-S modes labeled as SV and SH produced by vertical vibrators.

The radiation of direct-S modes from shot-hole explosives has been documented by Wright and Carpenter (1962) following investigations to determine how to detect tests of buried nuclear devices. They made plaster casts of shot-hole cavities that showed asymmetric deformation generated by explosive detonations. They state that “on no occasion has an underground firing failed to give rise to significant transverse seismic waves”. Fertig (1984) also concludes a shot-hole explosive generates direct-S modes but associates the generation of these modes to P-to-SV conversion at the Earth-air interface above a shot. Zhou et al. (2005) show VSP data in which they propose azimuthal anisotropy local to a source station as being the reason they observe both direct SH and qSV modes propagating away from vertical-vibrator stations. Yang et al. (2007) present excellent data examples of direct-S modes produced by both vertical vibrators and shot-hole explosives and refer to pure-S (SH) modes radiating from these vertical-force sources in addition to SV modes.

We emphasize the P and SV radiation patterns on Figure 6 apply for wave propagation in a homogeneous elastic half space. When azimuthal anisotropy exists in shallow Earth layers, wave propagation needs to be described in terms of natural coordinate axes. Others have analyzed VSP data acquired at the Devine Test Site where our data originate and concluded a weak S-wave anisotropy is present in the local rock layering. Raikes (1991) used an inclined-impact source to produce horizontal-force source VSP data and concluded S-wave anisotropy was less than 3-percent. She found a time delay of 12 ms between fast and slow modes at the deepest geophones, and estimated cracks were oriented at an azimuth of 10 degrees from North. The same data were later studied by Li et al. (1998) who confirmed S-wave anisotropy was less than 3-percent, calculated fast and slow modes travel times differed by 10 ms at deep receiver stations, and estimated one natural coordinate axis was oriented 60 degrees from North.

The important distinction between our study and all of these cited studies is that none of the above studies used a combination of vertical-force and horizontal-force sources in the same test so direct-S modes produced by both sources types could be directly compared. Our approach was to deploy vertical vibrators and horizontal vibrators at the same test site, generate direct-S modes with each source type, and record downgoing direct-S modes with the same vertical receiver array. We do not delve into the effects of azimuthal anisotropy on P and SV radiation in the data analyses we show. We describe only this simple field experiment in which we positioned a vertical vibrator and a horizontal vibrator at the same source station and recorded the direct-S wavefields produced by each vibrator with a vertical array of downhole 3C geophones. We ignore the issue of whether the downgoing direct-S wavefields do or do not propagate in an azimuthally anisotropic medium and simply compare the character of the direct-S wavefields recorded by radial geophones and transverse geophones for each type of vibrator source. The end result is that

we observe a strong similarity between direct-S modes produced by vertical and horizontal vibrators at this one test site.

Transforming VSP Test Data to Wave-Mode Data

In a vertical receiver well, azimuth orientations of X,Y horizontal geophones differ at each downhole station because sensor packages are deployed on twisted-wire cable that rotates as it spools off a cable reel. As a result, sensors rotate by different amounts when they reach different deployment depths. Phase shifts and amplitude variations introduced into horizontal-sensor data by station-to-station variations in receiver orientation do not allow individual events or distinct wave modes to be recognized, particularly S-wave events that dominate horizontal-sensor response. Receivers must be mathematically oriented to consistent azimuths and to proper inclinations to define downgoing and upgoing P and S modes.

Transformations of borehole receivers from in situ X, Y, Z orientations to a data space where receivers are oriented to emphasize P, radial-shear (SR), and transverse-shear (ST) events have been practiced in VSP technology for several decades (DiSiena, et al., 1981; Hardage, 2000). A graphical description of the transformation of receivers from X, Y, Z data space to P, SR, ST data space is shown on Figure 7. Azimuth rotation angle θ and inclination angle Φ are calculated by analyzing downgoing P-wave first-arrival wavelets at each receiver station so that P-wave displacement vectors are aligned along raypath RS. Radial-S displacement vector SR is then assumed to be orthogonal to RS and to be in vertical plane ROS. Transverse-S displacement vector ST is assumed to be orthogonal to plane ROS.

Wavefield Separation

In our analysis, we examine multicomponent data generated by vertical and horizontal vibrators using all sensor components of the 3C geophones that were deployed as a downhole receiver array. Figure 8 illustrates downgoing illuminating VSP wavefields produced by vertical, inline-horizontal, and crossline-horizontal vibrators after downhole geophones have been rotated in azimuth and then in inclination to align sensors as illustrated on Figure 7. Visual inspection of the data shows there is an undesirable amount of high-amplitude reverberation and wavelet distortion in the data recorded by the top-most 5 or 6 receiver stations. The logs on Figure 2 indicate there is significant variation in stratigraphic layering in this interval of the receiver well. Below a receiver station depth of 800 ft (244 m), S-event waveshapes are stable and direct-S modes produced by vertical and horizontal vibrators have essentially the same arrival times at each downhole receiver station. However, visual examination shows the range of frequencies recorded on radial and transverse component sensors are different for vertical and horizontal vibrators.

It is important to recognize the differences in the radial and transverse wavefields produced by the vertical vibrator. The radial-S component of the vertical-vibrator direct-S mode (Fig. 8d) shows a prominent downgoing P-SV event generated not far below a depth of 500 ft (152 m). In contrast, the transverse-S component (Fig. 8g) shows is no evidence of P-SV converted events. We have not observed converted-shear events on any transverse-S data produced by the several vertical-force source data sets we have examined.

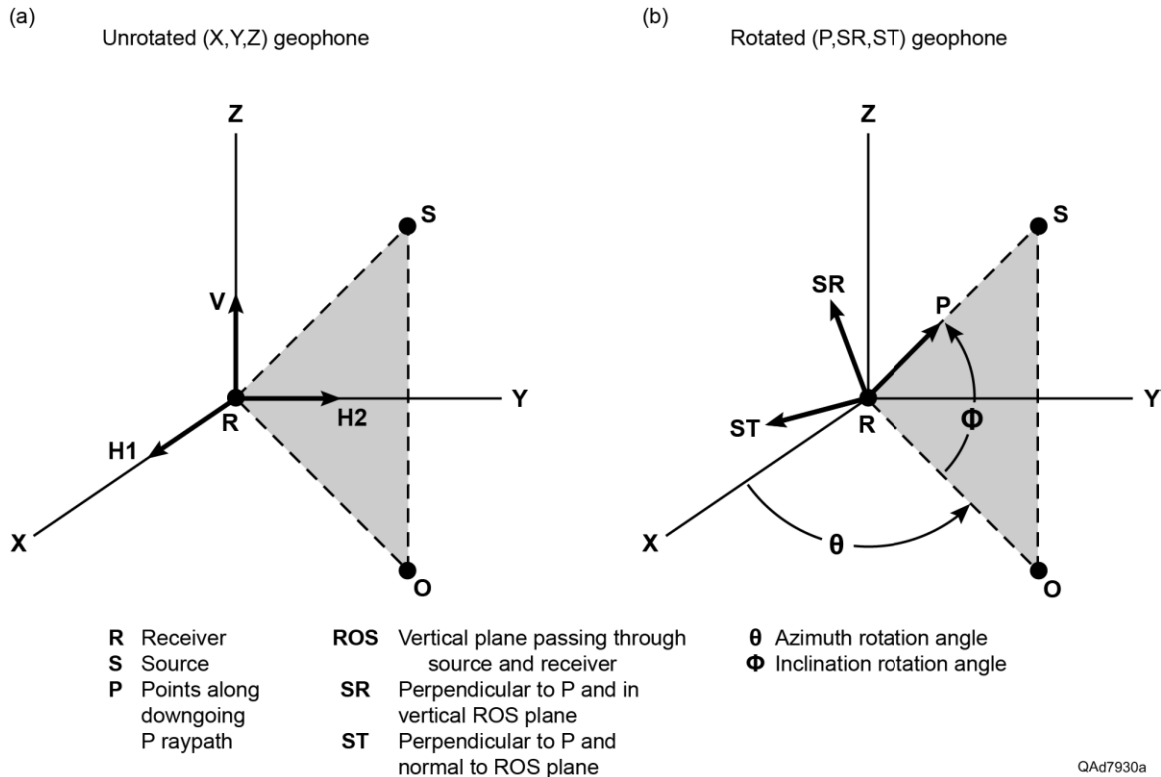


Figure 7. Reorientation of X, Y, Z receivers to P, SR, and ST receivers.

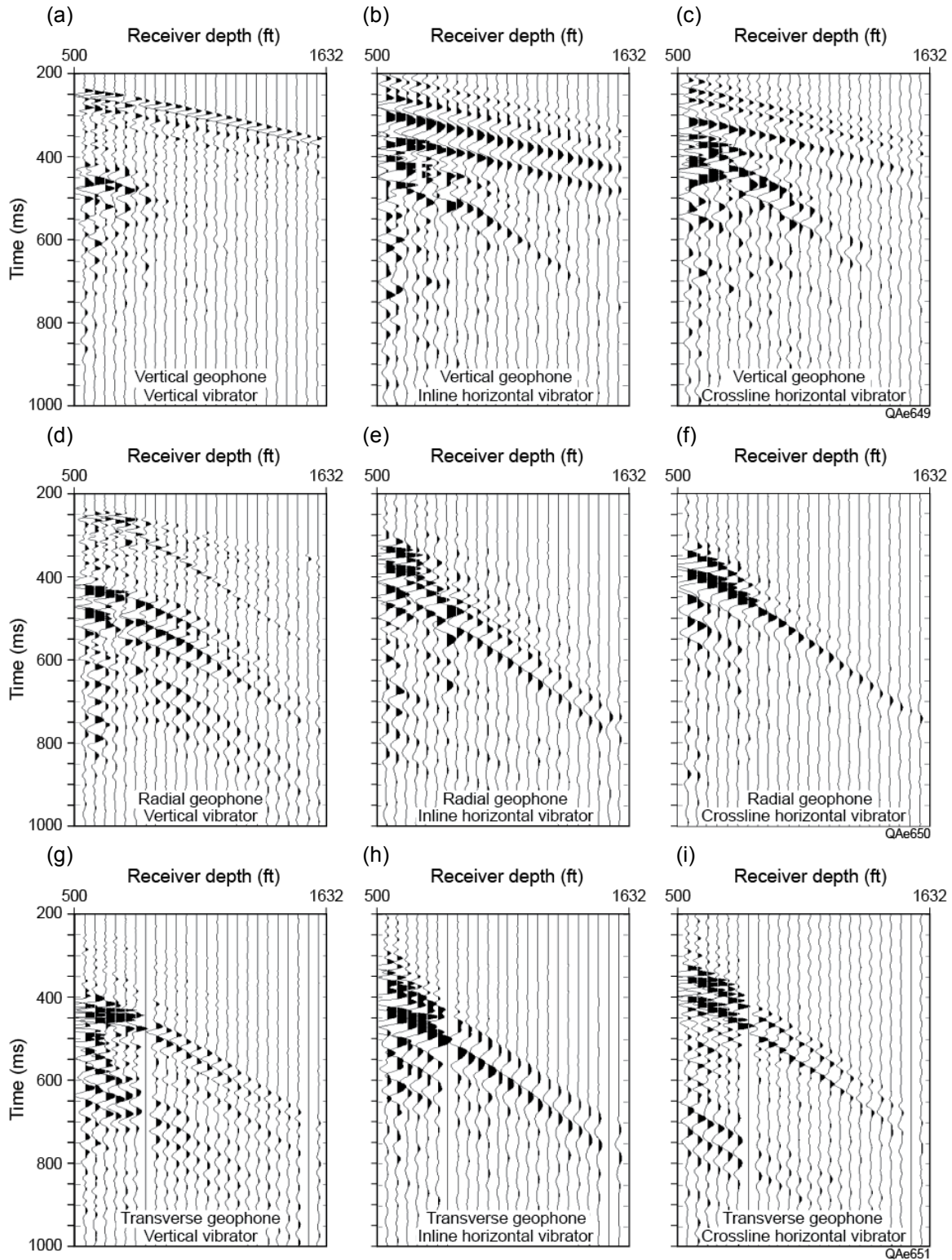


Figure 8. Comparisons of data recorded by vertical (a,b,c), radial (d,e,f), and transverse (g,h,i) sensors after rotations of 3C VSP geophones. The wavefields were generated by vertical (a,d,g), inline-horizontal (b,e,h), and crossline-horizontal (c,f,i) vibrators positioned at the same source station. Orientations and couplings of receivers were not altered during the data recording. Data above 800 ft (243.8 m) are distorted by critical refractions and interbed reverberations.

Comparing Frequency Content of Direct-S modes

Prudent field practice is to limit the highest frequency of a horizontal-vibrator sweep to approximately 50 Hz. Horizontal vibrators can sweep to frequencies higher than 50 Hz, but tend to have an unacceptable number of mechanical problems when forced to operate at high frequencies because of undue stress on hydraulic systems and structural supports. It is also challenging to maintain proper phase locking of horizontal vibrators at high frequencies. For these reasons, the sweep range of the horizontal vibrators used in our field tests was constrained to a bandwidth of 4 to 50 Hz, which is a common sweep range people use when deploying horizontal vibrators in exploration programs. In contrast, vertical vibrators can sweep to frequencies well above 100 Hz without undue mechanical problems or phase-locking issues. In our field experiment, the sweep range of the vertical vibrators was set at a modest interval of 8 to 96 Hz. When utilizing vertical and horizontal vibrators in data-acquisition projects, it is common practice to set sweep parameters so that the start and stop frequencies and frequency bandwidths used for vertical vibrators are a factor of 2 greater than the equivalent sweep parameters used for horizontal vibrators. We followed this common field practice in our field tests.

Quantifications of the differences in frequency content of direct-S modes produced by vertical-force and horizontal-force sources are illustrated on Figures 9 and 10. The radial component of the direct-S mode generated by a vertical vibrator is compared with the radial component of the direct-S mode produced by a horizontal vibrator on Figure 9; the transverse components of direct-S modes radiating from these two vibratory sources are compared on Figure 10. Some important wave physics principles are exhibited by these data:

1. For both vertical and horizontal vibrators, the highest frequency in the propagating direct-S wavelet observed at our test-site geology was 50 percent to 55 percent of the highest frequency used in the vibrator sweep. For example, a 50-Hz upper sweep limit for the horizontal vibrator resulted in an upper frequency of approximately 28 Hz in the downgoing direct-S wavelet for that source, and a 96-Hz upper sweep limit for the vertical vibrator created an upper frequency of 50 to 55 Hz in the direct-S illuminating wavelet for that vertical-force source.
2. In terms of octaves, the bandwidths of direct-S wavelets propagating from both horizontal and vertical vibrators are approximately the same, with wavelets from each source spanning slightly less than three octaves (4 to 28 Hz for the horizontal vibrator, and 8 to 55 Hz for the vertical vibrator).
3. Because the bandwidth of the direct-S wavelet generated by a vertical vibrator spans higher frequencies than does the bandwidth of the direct-S wavelet produced by a horizontal vibrator, a vertical vibrator should

provide better S-wave resolution of geologic targets than can a horizontal vibrator.

Item 3 of this list is particularly important and may result in wider use of vertical-force-source direct-S wavefields in future seismic evaluations of prospect areas.

We illustrate the similarity between direct-S modes produced by horizontal vibrators and vertical vibrators by overlaying the downgoing illuminating direct-S modes produced by each source so the arrival times and wavelet attributes of these modes can be more easily compared. These wavefield comparisons are displayed on Figure 11. The direct-S radial wavefield propagating from the horizontal vibrator (Fig. 11a) has a polarity opposite to that of the radial direct-S mode produced by the vertical vibrator because the horizontal vibrator was oriented North, causing the first motion of its baseplate (the direction of its radial-S polarity) to be away from the receiver well. In contrast, the radial-S vector produced by the vertical vibrator was oriented toward the receiver well. Rather than reverse the polarity of one of the wavefields displayed on Figure 11a, we left them as shown because this dual-color display of opposite-polarity data helps some people better judge the equivalence of the two modes. The polarities of the transverse component of the vertical-vibrator and horizontal-vibrator direct-S wavefields are identical (Fig. 11b) and are essentially exact copies of each other when data above 800 ft (243.8 m) are ignored.

The comments above focus only on data within the outlined windows on each display, which define the downgoing direct-S modes produced by each vibrator. When data character outside these direct-S data windows are considered, there are several downgoing P-to-SV converted events in the vertical vibrator data that are absent in the horizontal-vibrator data. The most obvious downgoing converted-SV mode is the event that originates near a depth of 500 ft (152 m) that precedes the direct-S data window (Fig. 11a). These downgoing converted-S events contribute noise in radial-S data produced by a vertical vibrator that does not have to be dealt with when a horizontal vibrator is used. No downgoing converted modes exist in transverse-S data produced by a vertical vibrator (Fig. 11b).

Visual examination of both of these dual-wavefield displays causes us to conclude that at this test site, except for the different frequency bandwidths documented on Figures 9 and 10, the downgoing direct-S wavefields produced by a vertical vibrator are reasonably equivalent to the downgoing direct-S modes produced by a horizontal vibrator. We plan to continue field tests to confirm if there are geologic conditions where direct-S modes produced by vertical vibrators strongly differ from direct-S modes produced by horizontal vibrators. The close equivalence of direct-S wavefields produced by vertical and horizontal vibrators is an important principle that has not to our knowledge been documented in geophysical literature.

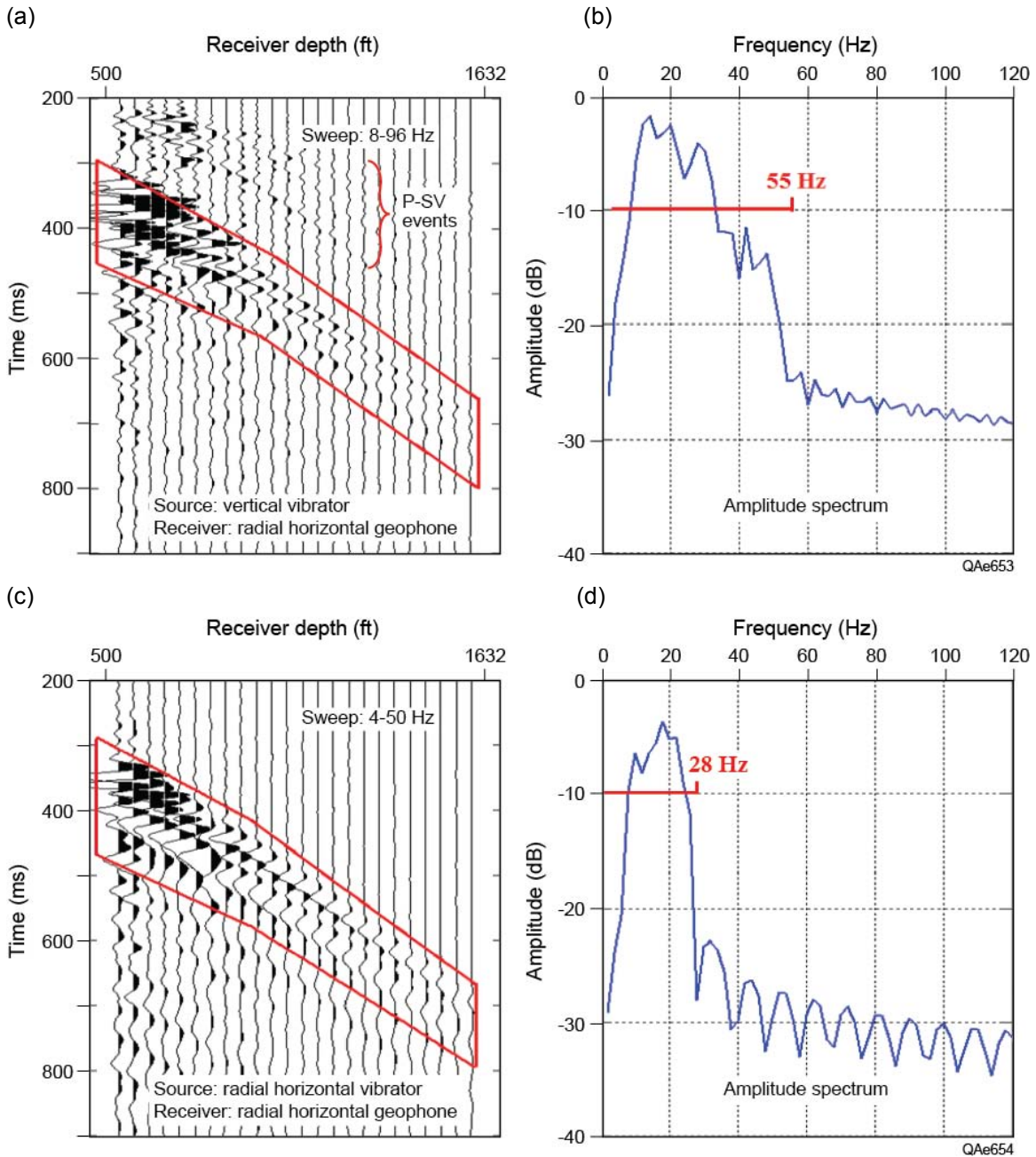


Figure 9. Comparison of radial-S data generated by (a) a vertical vibrator and (c) an inline horizontal vibrator. Data were recorded by the same vertical receiver array without altering receiver orientations or couplings. The amplitude spectrum of these direct-S wavefields are shown as (b) and (d). Data recorded at receiver stations above 800 ft (243.8 m) are distorted by critical refractions and interbed reverberations.

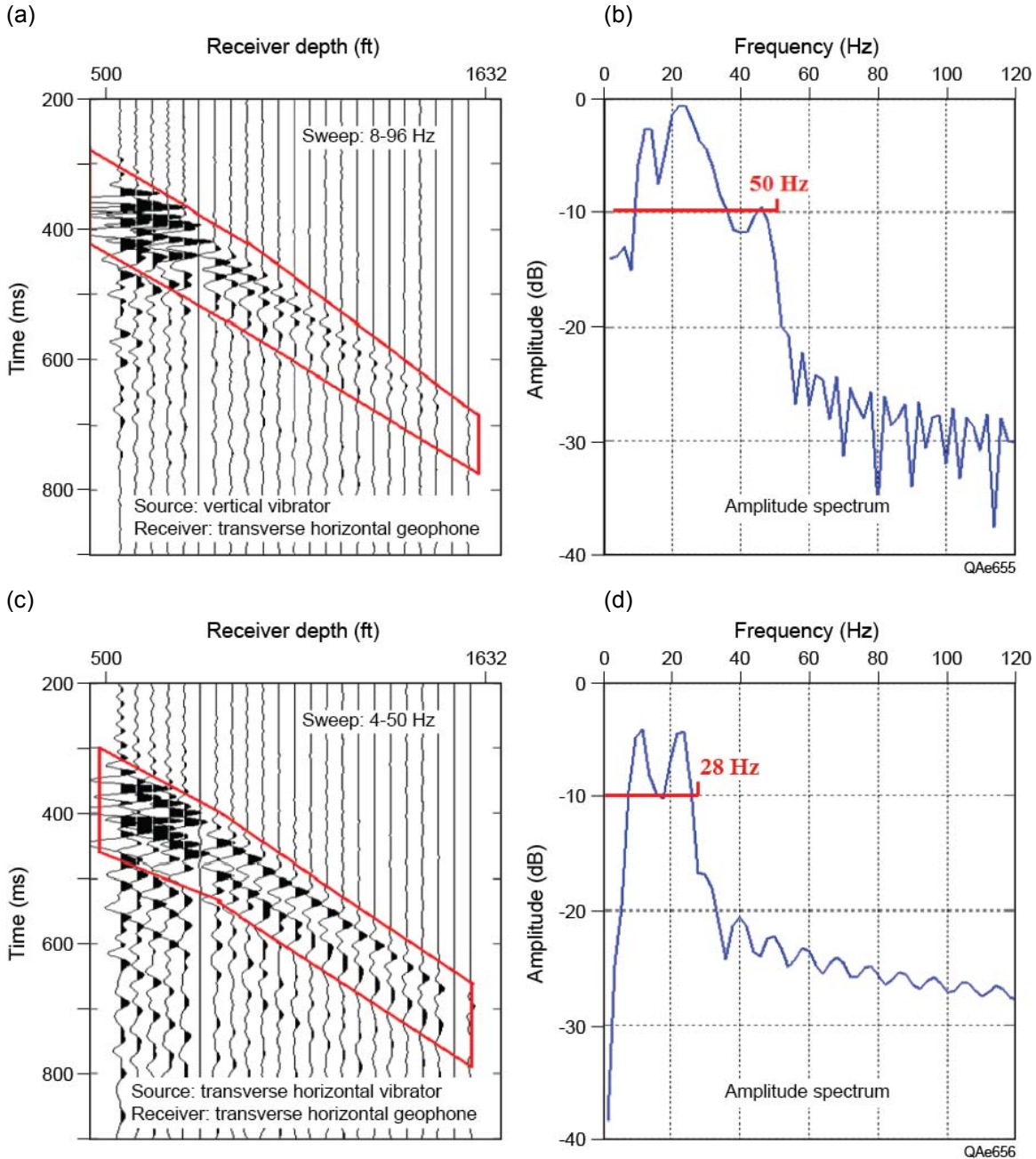


Figure 10. Comparison of transverse-S data generated by (a) a vertical vibrator and (c) a crossline horizontal vibrator positioned at the same surface station. Data were recorded by the same vertical receiver array without altering receiver orientations or couplings. The amplitude spectrum of each direct-S illuminating wavelet is shown as (b) and (d). Data recorded at receiver stations above 800 ft (243.8 m) are distorted by critical refractions and interbed reverberations.

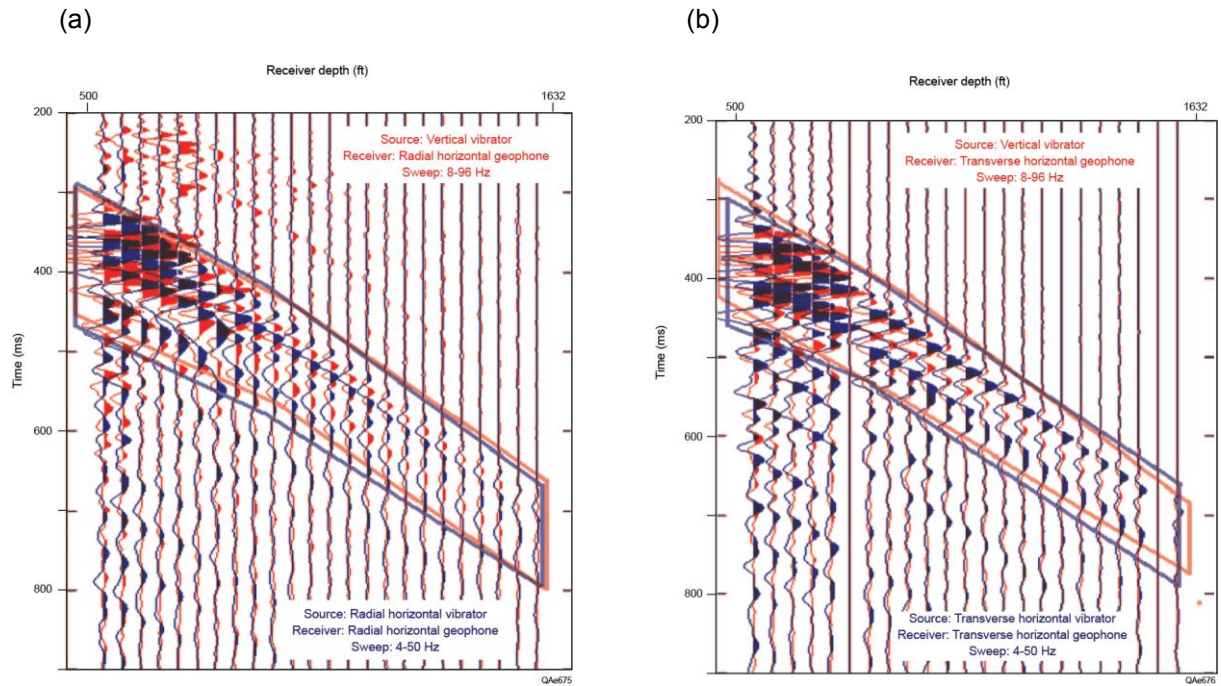


Figure 11. (a) Radial direct-S wavefield produced by a vertical vibrator (red traces) overlain by the radial direct-S wavefield produced by a radial horizontal vibrator (blue traces). (b) Transverse direct-S wavefield produced by a vertical vibrator (red traces) overlain by the transverse direct-S wavefield produced by a transverse horizontal vibrator (blue traces). Vibrators were positioned at the same surface source station. Data were recorded by the same vertical receiver array without altering receiver orientations or couplings. Data recorded at receiver stations above 800 ft (243.8 m) are distorted by critical refractions and interbed reverberations.

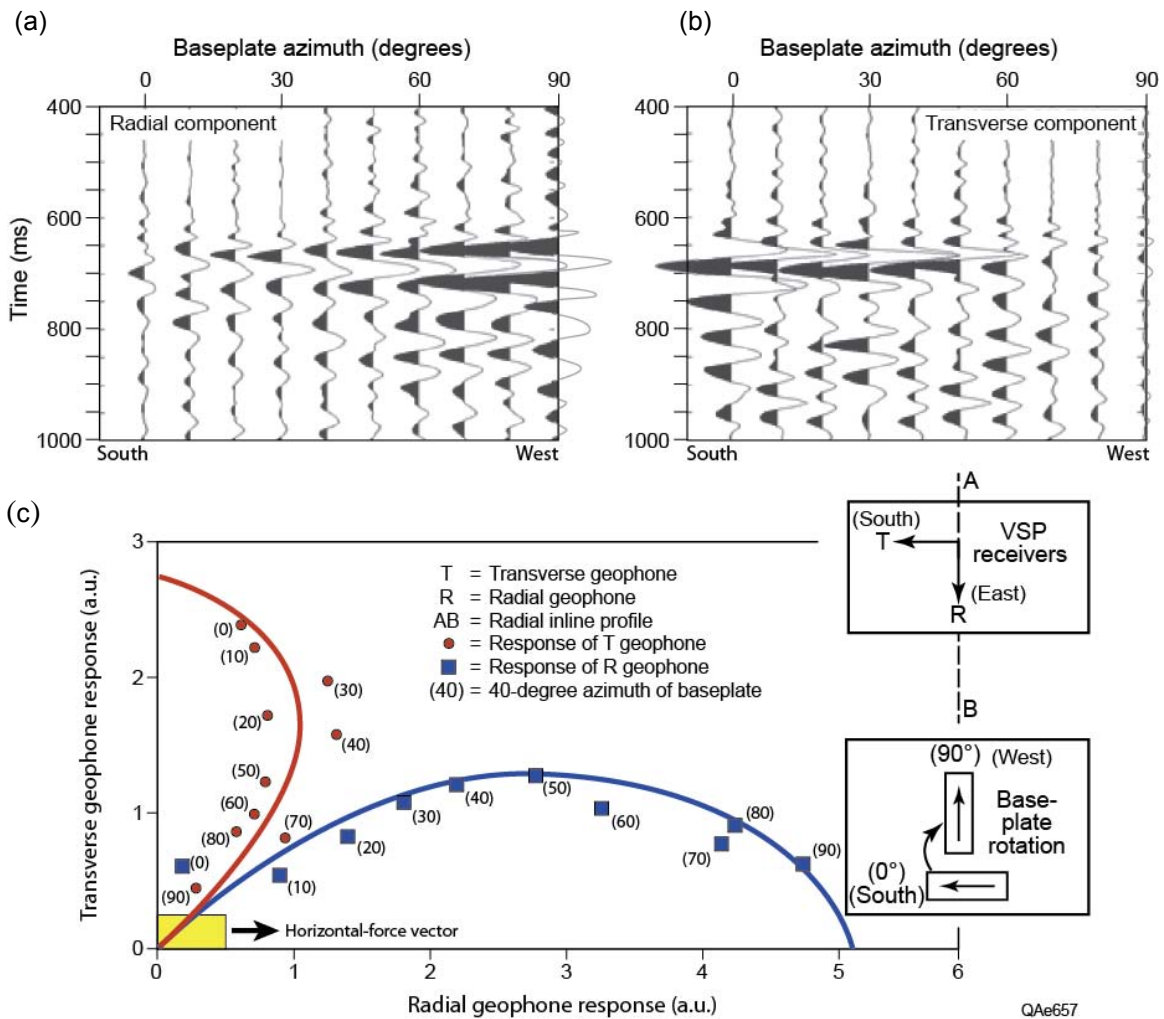


Figure 12. (a) Azimuth-dependent radial-S data produced by a horizontal vibrator oriented in azimuth increments of 10° at source station 3 (Fig. 3). (b) Azimuth-dependent transverse-S data produced by the same horizontal vibrator. The sequential azimuth orientations of the vibrator base plate is described on Figures 4 and 5. The receiver was positioned at station 19 at a depth of 1386 ft (422 m) as shown in Figures. 2 and 3. (c) A map view of radial-S and transverse-S amplitude strengths from (a) and (b) showing the geometrical spreading of radial-S (solid square data points) and transverse-S (solid circle data points) modes from this horizontal-force source station.

We close this analysis of vibrator-generated direct-S modes by presenting data that illustrate map views of the radial-S and transverse-S radiation lobes that propagated away from the horizontal-vibrator source we positioned at source station 3 (Fig. 3). An equivalent analysis has been published by Robertson and Corrigan (1983), and we wished to repeat their analysis procedure because our test data were collected over a different type of near-surface layer than what existed at the site used by these earlier investigators, and our wavefields propagated through a geologic section that had a higher degree of stratigraphic layering. As shown on Figure 3, we deployed a horizontal vibrator at source stations 3 and 5 so that its base plate was positioned at azimuths ranging from 0° to 90° relative to inline profile AB passing through source and receiver stations (Figs. 4 and 5). Data recorded by the downhole vertical array of 3C geophones could then be analyzed in the manner used by Robertson and Corrigan (1983). Our results are presented as Figure 12; the corresponding radial-S and transverse-S radiation pattern published by Robertson and Corrigan (1983) is shown on Figure 13 for comparison.

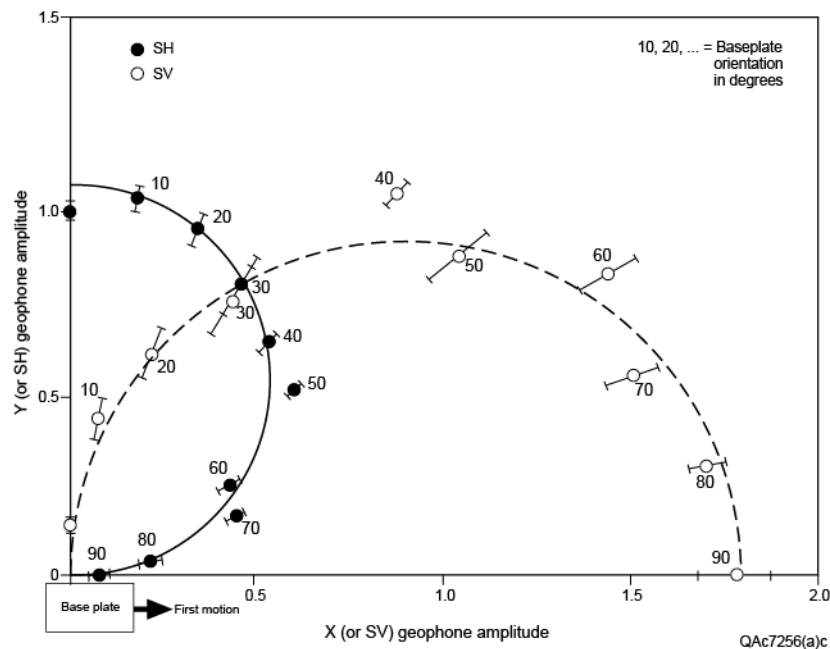


Figure 13. Radial-S and Transverse-S radiation patterns published by Robertson and Corrigan (1983).

There are strong similarities in the radiation patterns exhibited in these two figures. In each test, radial-S and transverse-S modes spread away from the source station in orthogonal directions, and radial-S energy is stronger than transverse-S energy. In our analysis (Fig. 12c), the ratio of radial-S to transverse-S energy is higher than what Robertson and Corrigan observed (Fig. 13). We made no attempt to calibrate the responses of the two horizontal geophones in

our test so we do not know if equal impulses on our radial and transverse geophones produce equivalent outputs. If the radial and transverse geophones produce data with different amplitude strengths, the radial-S and transverse-S amplitudes plotted on Figure 12c could be biased. Neither did we attempt to determine if our wall-locked radial and transverse geophones were equally coupled to the formation. In the test conducted by Robertson and Corrigan (1983), their downhole geophone was cemented in place and probably had excellent coupling of all three sensing elements. Perhaps most importantly, we did not verify that the base plate of the horizontal vibrator was uniformly coupled to the Earth at each vehicle orientation so that a constant horizontal force was generated in each azimuth direction. For two base-plate orientations (40° and 70°), there was an unexplained increase in amplitude on radial and transverse geophones. We assumed these anomalous amplitudes were caused by a different base-plate coupling for these vibrator orientations. We had to decide whether to delete the data for these two base-plate orientations or to apply a scaling factor that forced the data into the range of the companion data observed for all other base-plate positions. We elected to scale the data so that trace amplitudes agreed with the amplitude trends observed for the family of traces exhibited on Figures 12a and 12b. The resulting positions of the 40° and 70° azimuth data points on Figure 12c appear reasonable but could be eliminated without altering the transverse-S and radial-S radiation patterns that are shown.

One difference in the two test sites represented by the data exhibited on Figures 12 and 13 is that Robertson and Corrigan positioned a single 3C geophone at a shallow depth of 430 ft in a reasonably uniform shale layer; whereas, our receiver was 1386 ft (422 m) deep in stratified layering (Fig. 2). Our measurement may be more representative of the attributes of radial-S and transverse-S modes that propagate in layered media. Robertson and Corrigan recorded several individual vibrator sweeps at each base-plate orientation and established error bars on their measurements presented as Figure 13. In contrast, we summed two vibrator sweeps at each base-plate orientation and did not repeat measurements at any vehicle orientation. Thus we show no error bars on our data.

Conclusions

The analysis of VSP test data acquired at the Devine Test Site confirmed that direct-S modes are produced by vertical vibrators and suggests these modes can be substituted for direct-S modes produced by horizontal vibrators in some instances. An appealing aspect of direct-S modes produced by vertical vibrators is that they have a higher range of frequencies than do direct-S modes produced by horizontal vibrators, and thus vertical-vibrator direct-S modes should produce better S-wave resolution of geologic targets.

Numerous tests remain to be done. For example, our test data were generated using a single vertical vibrator at all source stations. How will direct-S modes be affected if arrays of 2, 3, or 4 vertical vibrators are used? Investigations also need to be done to determine how attributes of direct-S modes produced at a vertical-force station are affected by the elastic properties of the top surface layer across a prospect area. Are there some Earth surface conditions in which ineffective direct-S modes will be produced by vertical vibrators? Some of these tests are under way. Our ultimate goal is to perform analyses of direct-S wave modes generated by all types of vertical-force sources deployed in different array geometries and compare these results with direct-S radiation generated by horizontal-force sources

This research is significant because one implication is that direct-S data acquisition can be done in some instances with only vertical vibrator sources without the necessity of deploying horizontal vibrators. Because vertical vibrators are widespread but horizontal vibrators are not, a second implication is that direct-S data acquisition can be considered across many areas where S-wave technology may otherwise not be done. These research results thus impact seismic imaging technology, the fundamental theme of this journal.

Perhaps the most important consideration is that the cost of acquiring multicomponent seismic data can be reduced by using vertical-force sources to generate direct-S waves. Because of the potential commercial value of using vertical-force sources to generate direct-S modes, the concepts illustrated in this paper have been patented by the Board of Regents of The University of Texas System (Hardage, 2011).

Acknowledgments

These source tests could not have been done without the assistance of sponsors of the Exploration Geophysics Laboratory. Mitcham Industries provided the MaxiWave system used for the vertical array as well as surface 3C geophones and DSU3 sensors, a recording truck, and field technicians. Halliburton provided wireline services and engineers, Dawson Geophysical provided vibrators, vibrator support personnel, and transportation for other sources, Sercel provided a 428 recorder, support personnel, and Unite cable-free boxes. Seismic Source and i-Seis combined to provide Sigma cable-free boxes, a Universal Encorder, and engineering staff. Austin Powder provided explosives and a certified shooter. United Services Alliance and Vecta Technology provided their accelerated-weight (nitrogen-spring) source and source operators. OyoGeospace provided a variety of special geophones, GSR cable-free boxes, and field personnel.

References

- DiSiena, J.P., Gaiser, J.E., and Corrigan, D., 1981. Three-component vertical seismic profiles – orientation for shear wave analysis. Tech. Paper S5.4, 1990-2011, Expanded Abstracts, 51st Annual International Meeting of SEG.
- Edelmann, H.A.K., 1981. Shover shear-wave generation by vibration orthogonal to the polarization. *Geophy. Prospect.*, 29, 541-549.
- Fertig, J., 1984. Shear waves by an explosive point-source – the Earth surface as a generator of converted P-S waves. *Geophy. Prospect.*, 32, 1-17.
- Fertig, J., and Krajewski, P., 1989. Acquisition and processing of pure and converted shear waves generated by compressional wave sources: Surveys in Geophysics, 1p0, 103-132.
- Hardage, B.A., 2000. Vertical seismic profiling – principles. Third updated and revised edition, Pergamon, 552 pages (Editions 1 and 2 published in 1983 and 1985 by other publishing houses)
- Hardage, B.A., 2009, Horizontal wave testing. *AAPG Explorer*, v. 30, no. 12, p. 26–27.
- Hardage, B.A. 2010. Vertical wave testing. *AAPG Explorer*, v. 31, no. 1, p. 32–33.
- Hardage, B. A., 2011. System and method for acquisition and processing of elastic wavefield data. U.S. Patent 8,040,754 B1.

Li, X.Y., C. MacBeth, and Crampin, S., 1998. Interpreting non-orthogonal split shear waves for seismic anisotropy in multicomponent VSPs. *Geophy. Prospect.*, 46, 1-27.

Lynn, H.B., and McCardle, M., 1990. Four 3-component VSPs from South Texas onshore – S-wave velocities for AVO and discussion of acquisition parameters. Paper BG3.2, *SEG Expanded Abstracts*, 9, 52-55.

Miller, G. and Pursey H., 1954. The field and radiation impedance of mechanical vibrators on the free surface of a semi-infinite isotropic solid. *Proceedings of the Royal Society of London, Series A*, 223, no. 1155, 521–541.

Raikes, S., 1991. Shear-wave characterization of the BP Devine test site. Paper BG2.8, *SEG Expanded Abstracts*, 10, 65-68.

Robertson, J.D. and Corrigan, D., 1983. Radiation patterns of a shear-wave vibrator in near-surface shale. *Geophysics*, 48, 19–26.

White, J. E., 1983. *Underground sound—applications of seismic waves*. Elsevier Science Publishers.

Wright, J.K., and Carpenter, E.W., 1962. The generation of horizontally polarized shear waves by underground explosions. *J. Geophy. Res.*, 67, no. 5, 1957-1963.

Yang, L., Zhang, Q., Bao, L., and Wei, X., 2007. Pure S-waves in land P-wave source VSP data. *Applied Geophy.* 4, no. 3, 173-182.

Zhou, R., Zhao, X., and Dushman, D., 2005. Shear-wave anisotropy from far-offset VSP. Paper MC4.2, *SEG Expanded Abstracts*, 971-974.

Appendix B

S-S Imaging with Vertical Vibrators

The purpose of this appendix is to illustrate that S-S images can be constructed from direct-S modes produced by vertical vibrators. The data used in these illustrations were acquired at the Marcellus Shale study site described in Chapter 3. Referring to the map on Figure 3.1 of Chapter 3, the data used in this appendix were generated by a vertical vibrator positioned near source station D southwest of the VSP well. The data were recorded by an extensive vertical array of receivers starting at a depth of 6770 ft and extending up to 600 ft below KB.

The raw data are exhibited on Figure 1. After implementing the receiver rotation described in Chapter 2 (Fig. 2.8), these data were transformed into the radial-transverse data domain. We will consider only the transverse-S data produced by this receiver rotation, which are exhibited on Figure 2. In this new data domain, the direct-S mode can be readily recognized and is labeled on Figure 2. Velocity filtering and deconvolution of these data created the upgoing transverse-S wavefield and primary transverse-S reflections shown on Figure 3a and 3b, respectively.

The transverse-S data from Figure 3b were converted into an S-S image using standard VSP-CDP binning procedures similar to that practiced by VSP contractors. The resulting image is displayed as Figure 4. This sequence of figures demonstrates that direct-S data produced by vertical vibrators are capable of producing high-quality VSP S-S images. Unfortunately a horizontal vibrator was not used in this particular VSP program, and it is not possible to compare this vertical-vibrator S-S image with an image produced by a horizontal vibrator. Such a side-by-side comparison of vertical-vibrator and horizontal-vibrator S-S images will have to be done in subsequent studies.

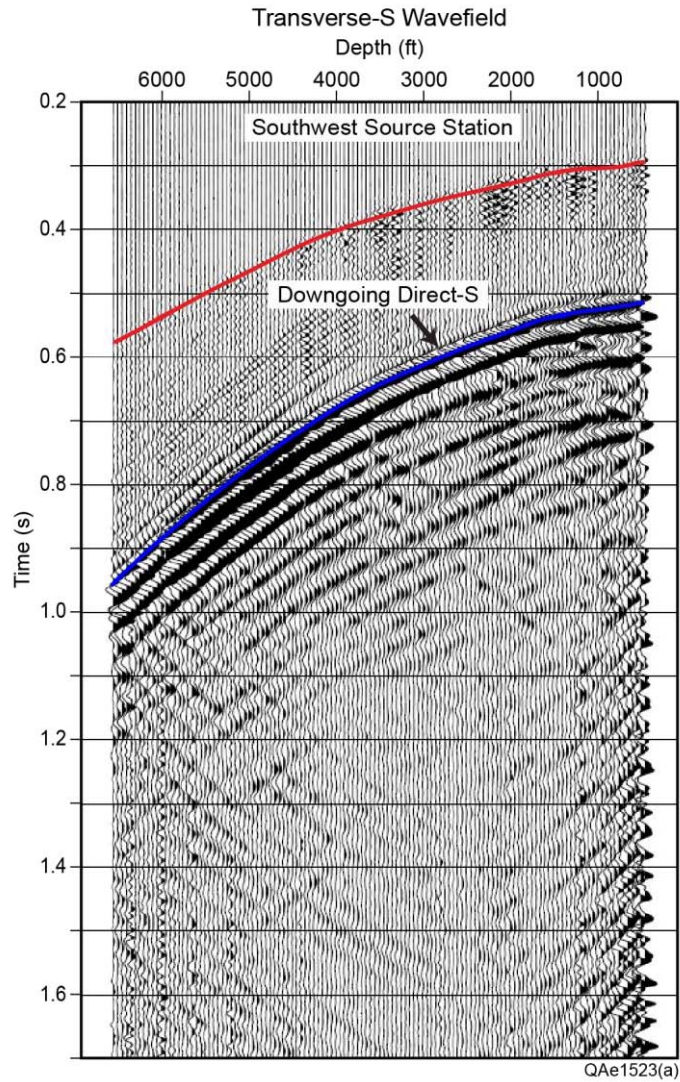


Figure 2. Transverse-S wavefield extracted from the data shown on Figure 1. These data are the total wavefield consisting of the downgoing wavefield (events that slope down to the left) and the upgoing wavefield (weaker events that slope down to the right).

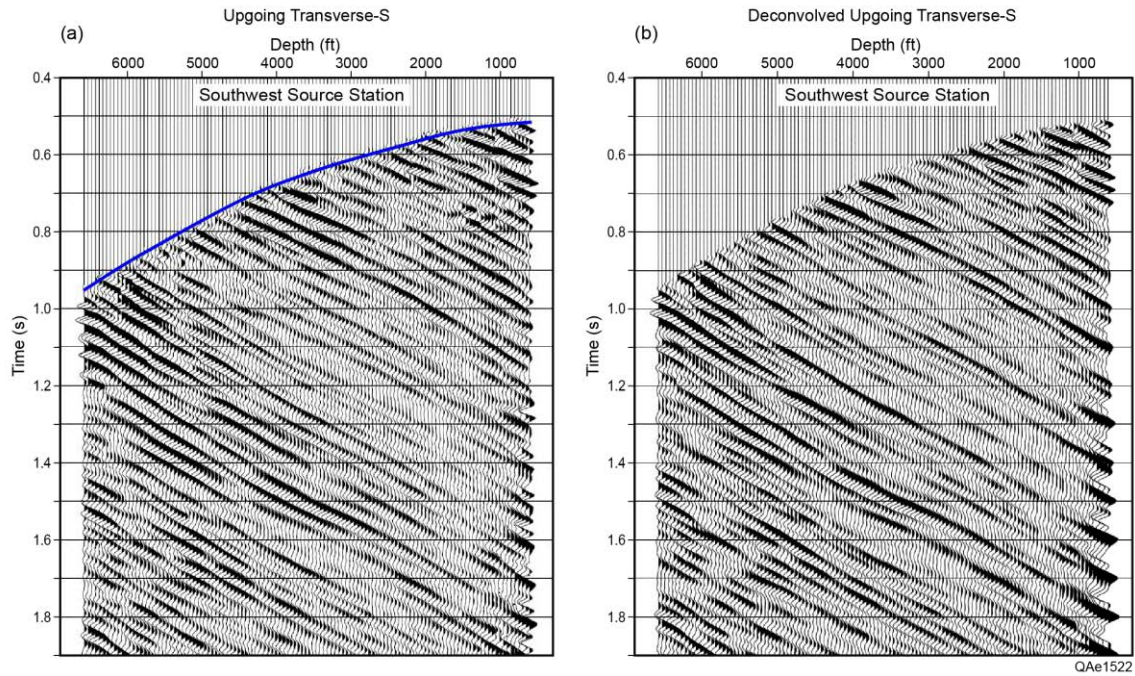


Figure 3. (a) Upgoing transverse-S wavefield extracted from the data shown on Figure 2. (b) Upgoing transverse-S primary reflections extracted from the total upgoing wavefield in (a).

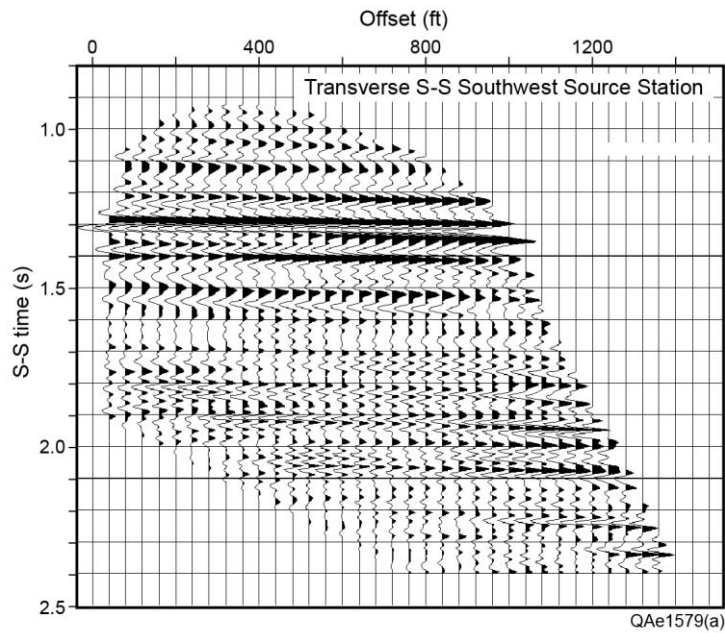


Figure 4. Transverse-S image constructed by VSP-CDP binning procedures. A reliable image begins at the receiver well and extends approximately 1000 ft (300 m) toward the vertical-vibrator source station.

National Energy Technology Laboratory

626 Cochrans Mill Road
P.O. Box 10940
Pittsburgh, PA 15236-0940

3610 Collins Ferry Road
P.O. Box 880
Morgantown, WV 26507-0880

13131 Dairy Ashford Road, Suite 225
Sugar Land, TX 77478

1450 Queen Avenue SW
Albany, OR 97321-2198

Arctic Energy Office
420 L Street, Suite 305
Anchorage, AK 99501

Visit the NETL website at:
www.netl.doe.gov

Customer Service Line:
1-800-553-7681

